4942:1

RF Project 1864
Technical 1

THE OHIO STATE UNIVERSITY

RESEARCH FOUNDATION

1314 KINNEAR ROAD COLUMBUS, OHIO 43212

AN EXPERIMENTAL INVESTIGATION OF THE INFLUENCE OF ELECTROSTATIC FIELDS ON FLOW ATTACHMENT

Gary P. Eiler

CLEARINGHOUSE
FOR FEDERAL SCIENTIFIC AND
TECHNICAL INFORMATION
Hardcopy Microfiche
$3.00 $.65 98 pp as
ARCHIVE COPY

U.S. Army Research Office - Durham
Box CM, Duke Station
Durham, North Carolina

Contract DA-31-124-ARO-D-246

DDC
RECEIVED
DEC 7 1966
D

Distribution of this document is unlimited.

The findings in this report are not to be construed as an official Department of the Army position, unless so designated by other authorized documents.

RF Project 1864

Report No. ~~4~~ one (1). art

TECHNICAL

REPORT

By

THE OHIO STATE UNIVERSITY
RESEARCH FOUNDATION

1314 KINNEAR RD.
COLUMBUS, OHIO 43212

To U. S. ARMY RESEARCH OFFICE - DURHAM
Box CM, Duke Station
Durham, North Carolina 27706
Project Nos. 20010501B700, 1D12140A142
Contract No. DA-31-124-ARO-D-246

On AN EXPERIMENTAL INVESTIGATION OF THE INFLUENCE OF ELECTROSTATIC FIELDS ON FLOW ATTACHMENT

Submitted by G. P. Eiler and Henry R. Velkoff
Department of Mechanical Engineering

Date 15 August 1966

Distribution of this document is unlimited.

The findings in this report are not to be construed as an official Department of the Army position, unless so designated by other authorized documents.

FOREWORD

This report presents essentially the same material as the Master's Thesis, "An Experimental Investigation of the Influence of Electrostatic Fields on Ion Flow Attachment," by G. P. Eiler. The thesis was presented in partial fulfillment of the requirements for the Master of Science degree in Mechanical Engineering at The Ohio State University.

The author wishes to thank Dr. Henry R. Velkoff, The Ohio State University Mechanical Engineering Department, for suggesting this topic and for his continued help and guidance throughout the course of the study.

ABSTRACT

An experimental investigation was conducted to determine whether an electrostatic field could be used to affect the attachment of an air stream to a flat surface. Tests were run using a fluid-amplifier type device in which corona wind was fed through the control ports of the device. It was found that the fluid stream could be made to detach from one wall, flip over to the opposite wall, and attach to that wall. The air stream could then be flipped back to the original wall by activating the opposite corona wind control port. Pressure distribution and velocity profile data were taken which indicated that by suitable design symmetric flip-flop of the fluid stream in the device could be achieved.

TABLE OF CONTENTS

	Page
List of Symbols	ix
SECTION I - INTRODUCTION	1
General Objective	1
Historical Review	1
Electrostatic Forces	2
SECTION II - EXPERIMENTAL APPROACH	5
Experimental Apparatus	5
Experimental Procedure	8
Experimental Calculations	9
SECTION III - RESULTS OF EXPERIMENTAL INVESTIGATION	13
Selection of Channel	13
Electrode Geometry	13
Current-Voltage Relationship	14
Current Required to Flip Flow	14
Velocity Profiles	16
Static Pressure Drop	17
SECTION IV - ANALYTICAL STUDY OF THE EFFECTS OF CORONA WIND ON THE JET	19
Analytical Solution	19
SECTION V - CONCLUSIONS AND RECOMMENDATIONS	25
SECTION VI	27
Illustrations	27
Sample Calculations	89
List of Equipment	95
SECTION VII - REFERENCES	97

LIST OF ILLUSTRATIONS

Fig. No.		Page
1	Typical fluid jet amplifier in unstable position	29
2	Fluid jet amplifier with flow attached to right wall, with schematic and logic of system	30
3	Corona wind from a charged wire	31
4	Over-all view of test setup. Sorensen high power supply, lower left, Singer electrostatic volmeter, upper left	32
5	Diagram of original test setup	33
6	Close-up view of settling chamber, settling screen and nozzle outlet	34
7	Diagrammatic sketch of nozzle showing its relative position with respect to the channel inlet and electrodes	35
8	Front view of test setup showing relative position of nozzle with respect to the channel, top and bottom air inlets, micrometer traverse, and glass total pressure probe	36
9	Close-up view of high voltage positive and negative connections, and pressure taps for measuring pressure drop across nozzle	37
10	Top view of channel showing top air inlet, center and micrometer traverse, upper right	38
11	Diagram of test setup with control nozzle	39
12	View of test setup with top and bottom control nozzles installed	40
13	Close-up view of nozzle outlet, channel inlet and control nozzles	41
14	Top view of test setup with control nozzle	42
15	Electrode configurations tested	43
16	Reynolds number for various pressure drops across a standard ASME orifice	44
17	Pressure drop across nozzle for various pressure drops across orifice	45

LIST OF ILLUSTRATIONS (Continued)

Fig. No.		Page
18	Schematic of channel flow and diffusion of attached jet	46
19	Schematic of flow in control nozzle	47
20	Description of Test 1	48
21	Current-voltage relationship for an 0.004-inch wire 0.30-inch above an 0.08-inch copper wire	49
22	Current required to flip flow from top plate to bottom plate at various Reynolds numbers	50
23	Velocity profiles before and after flipping	51
24	Description of Test 2	52
25	Current-voltage relationship. 0.004-inch wire 0.75-inch above 0.08-inch copper wire	53
26	Current required to flip flow from top plate to bottom plate with various Reynolds numbers	54
27	Velocity profile before and after flipping	55
28	Static pressure drop along plate with flow attached to it	56
29	Description of Test 3	57
30	Current-voltage relationship. 0.004-inch wire 0.75-inch above 0.08-inch copper wire	58
31	Current required to flip flow from top plate to bottom plate at various Reynolds numbers	59
32	Velocity profile before and after flipping	60
33	Static pressure drop along bottom plate with flow attached to it	61
34	Description of Test 4	62
35	Current-voltage relationship. 0.004-inch wire 0.75-inch above 0.08-inch copper wire	63
36	Current required to flip flow from top plate to bottom plate at various Reynolds numbers	64

LIST OF ILLUSTRATIONS (Continued)

Fig. No.		Page
37	Velocity profile before and after flipping	65
38	Static pressure drop along bottom plate with flow attached to it	66
39	Description of Tests 5, 6, 7	67
40	Current-voltage relationship for control nozzle. 0.004-inch wire 0.75-inch above nozzle outlet. Nozzle height 0.32 inch	68
41	Current required to flip flow up to top plate and down to bottom plate at various Reynolds numbers. Channel tilted up 2 degrees	69
42	Power and current required to flip flow both ways at various Reynolds numbers. Channel tilted up 2 degrees	70
43	Velocity profiles before and after flipping both ways. Channel tilted up 2 degrees	71
44	Current required to flip flow both ways at various Reynolds number. Tilted up 4 degrees	72
45	Power and current to flip flow both ways at various Reynolds numbers. Channel tilted up 4 degrees	73
46	Velocity profiles before and after flipping both ways. Channel tilted up 4 degrees	74
47	Current required to flip flow both ways at various Reynolds numbers. Channel tilted down 2 degrees	75
48	Power and current to flip flow both ways at various Reynolds numbers. Channel tilted down 2 degrees	76
49	Velocity profiles before and after flipping both ways. Channel tilted down 2 degrees	77
50	Static pressure drop along bottom plate with flow attached to it. Channel tilted up 2, 4 degrees, and down 2 degrees	78
51	Static pressure along control nozzle for various currents	79

LIST OF ILLUSTRATIONS (Continued)

Fig. No.		Page
52	Total and static pressure variation along control nozzle for 10 and 20 microamps	80
53	Total and static pressure variation along control nozzle for 30 microamps	81
54	Velocity along control nozzle at various currents	82
55	Control nozzle exit velocity at various currents	83
56	Suction developed by corona wind at a point just before positive wire	84
57	Total pressure increase at nozzle exit for various currents	85
58	Theoretical angle of primary jet deflection for various primary jet velocities and control jet currents	86
59	Angle of primary jet deflection for various currents at a Reynolds number of 1325, and velocity of 23.3 ft/sec	87
60	Ratio of control jet to primary jet mass flow rate required to flip flow at various Reynolds numbers	88

List of Symbols

Symbol		Units
A	distance from nozzle outlet to electrodes	in.
a	y intercept current-Reynolds number plot	microamp
A_1	area orifice	in.^{2}
A_n	area nozzle outlet	in.^{2}
B	distance from nozzle outlet to top air inlet	in.
b	y intercept power-Reynolds number plot	watts
C	distance from nozzle outlet to channel inlet	in.
c	emperical constant	1/in.
d	orifice diameter	in.
E	electric field strength	volts/m
F	body force	lb/ft^3
H	height channel from divider to plate at point of total pressure measurement	in.
h	pressure drop across orifice	in. H_2O
I	current	microamp
K	orifice flow coefficient	dimensionless
K_o	positive ion mobility	in.^{2}/volt-sec
m	slope current-Reynolds number plot	dimensionless
n	slope power-Reynolds number plot	dimensionless
P	power	watts
p	pressure	lb/in.^{2}
p_1	pressure upstream of orifice	lb/in.^{2}
p_s	static pressure	lb/in.^{2}
p_t	total pressure	lb/in.^{2}
Q	flow rate through nozzle	lb_m/min

List of Symbols (Continued)

Symbol		Units
Q_c	flow rate through orifice at T_1 and p_1	ft^3/min
R	gas constant	lb_f-ft/lb_m-R^o
Re	Reynolds number based on nozzle height	dimensionless
T_1	temperature upstream of orifice	F^o
t	time	seconds
V	channel velocity	ft/sec
V_o	maximum channel velocity for a given geometry and flow	ft/sec
V_1	velocity before orifice	ft/sec
V_n	nozzle velocity	ft/sec
v	air velocity	ft/sec
v_i	velocity ions in the air	ft/sec
v_t	total ion velocity	ft/sec
w	nozzle height	in.
X	distance along bottom plate	in.
x	distance along control nozzle	in.
Y	vertical distance into channel, measured from divider	in.
y	orifice expansion factor	dimensionless
y_o	reference distance close to corona wire	in.
y_2	distance from y_o	in.
ϵ	permittivity	farads/m
μ	dynamic viscosity	lb/ft-hr
ρ_1	density upstream of orifice	lb_m/ft^3
ρ_n	density at nozzle outlet	lb_m/ft^3

List of Symbols (Continued)

Symbol		Units
ρ_c	charge density	coulombs/m^3
σ_c	electrical conductivity	1/ohms
α	angle primary jet deflection	degrees

SECTION I

INTRODUCTION

General Objectives

The primary purpose of this investigation is to study the effects of electrostatic action on the attachment of flow to a flat surface. Upon the basis of prior studies of electrostatic interactions with fluids, many possible mechanisms exist which could possibly be used to influence the attachment of a stream of air and a surface.[16]* Typical interactions are corona wind in air, electrophoresis and dielectrophoresis in liquids, and surface instabilities induced by fields. The specific work reported herein will be directed toward effects on air and specifically corona wind effects.

The actual study involved the flow of air from a two-dimensional nozzle onto a flat test plate. With a variable plate spacing, it was planned to try to obtain a configuration where the flow attachment against one wall or the other was just barely stable. With such a configuration it was considered that it might be possible to flip the flow from one wall to the other with a very small electrostatic force.

If it were found to be possible to flip the flow with some repeatability and reliability, then it might be possible to construct a fluid amplifier type of device in which the flow is flipped from one wall to the other electrostatically.

Historical Review

In 1933 Henry Coanda recognized a unique character of boundary layer flow; that a flow stream issuing from a jet would tend to attach itself to a wall.[1] Coanda recognized this as a means of fluid control with no moving parts. His discovery eventually became the basic principle of the digital fluid amplifier.

In 1938 McMahan[2] reported on a means of controlling fluid flow with no moving parts and in 1940 Todd[3] reported on "mechanical relay of the fluid jet type" using the interaction of fluid jets. J. m. Rhoades and D. E. Cain[4] carried out some preliminary work on a variable restrictor using a vortex for the control principle in the early 1950's. The field actually did not advance significantly until 1960 when the result of independent and concentrated work at the Harry Diamond Laboratory and at the Massachusetts Institute of Technology were announced. The former

*The superscript numbers denote references listed at the end of this report.

reported on work concerning stream interface principles, while the latter presented fluid logic concepts. At the present time 15 to 20 corporations have major development programs concerning fluid amplifiers.

To understand the switching behavior of the fluid amplifier, the actual physical phenomenon must be examined. It is pertinent to first describe why the jet attaches itself to one wall or the other. Figure 1 shows a fluid jet amplifier with the jet in an unstable position centered between the two walls. The jet will entrain fluid from the trapezoidal cavity and carry it downstream. The fluid thus carried away must be replenished by a flow down along the diverging walls in a direction opposite to that of the jet. This secondary flow is induced by a pressure gradient between the atmosphere and the base of the jet.

Assume that the jet bends because of some random disturbance a little to the right. The amount of flow entrained on either side will remain fairly constant. However, the area through which the secondary flow can pass to replenish the entrained flow will decrease on the right and increase on the left. Under such conditions, the average pressure on the right will decrease in order to maintain the same secondary flow through a more restricted passage. Conversely, the average pressure on the left will rise. Thus, a net force has been set up in the same direction as the original bending of the jet, so as to force the jet further to the right in an unstable manner. The jet will continue its motion to the right until it attaches itself to the wall and forms a separation bubble.

Figure 2 shows the jet attached to the right-hand wall. Some flow is coming in through the left-hand and right-hand control ports. As the flow from the right-hand control is increased, the separation bubble enlarges and the stagnation point P moves downstream. When the stagnation point finally reaches the end of the wall, the jet will separate from the wall and attach to the other side. The jet will switch because the right-hand control port is providing the entrained fluid demanded by the left-hand side than is supplied by the control port. Thus, as the jet shifts to the left, the pressure on the left drops and carries the jet over to the left wall. It will now remain in this position if the flow does or does not continue from the right-hand control port.

This type of element can be used for logic or flow amplification. The logic is shown in the table in Fig. 2. Flow in a particular port is indicated with an "X" and the absence of flow with an "O".

Electrostatic Forces

An electrical field can influence not only fluids containing charged particles and conducting fluids but also neutral nonconducting fluids as well. The wide range of action may provide controlled body forces within the fluid without the high degree of ionization customarily used in magnetohydrodynamics.[16,17]

Although these forces are relatively small, they may be sufficient to affect the attachment of the flow, when acting at the surface-stream interface.

One possible method of producing this electrostatic force is the so-called electric wind phenomenon[5,6,7], as shown in Fig. 3. It consists of the flow of air from a highly charged needle point or fine wire.

In the vicinity of the points or fine wire, a very intense electric field exists. In such a field, the surrounding gas is ionized to a high degree due primarily, to the collisions of ions and electrons with the neutral molecules. Stray ions or electrons within the gas may gain enough velocity between collisions to ionize the neutral molecules. The new ions are likewise accelerated by the field and tend to move away from the intense field, to a point where the field strength is lower (negative electrode). Here, elastic collisions occur with neutral molecules, which lead to a drifting motion of both the ions and the neutral molecules. On a macroscopic scale, this drifting is a local mass motion or wind.

When the ions and neutral molecules move away from the point of high charge, a change of momentum takes place and a reaction on the body results. This phenomenon can produce a low-velocity flow of a mass of gas by using sufficient points or a grid of fine wires. The fundamental limitations to this type of device are the power requirements to achieve mass flow and the potential that can be applied before break-down (sparking).

It appears that the mass motion produced by the intense electric field could replace the flow from the control parts, as used in the typical fluid amplifier.[18]

SECTION II

EXPERIMENTAL APPROACH

Experimental Apparatus

In order to study the effects of electrostatic fields on flow attachment, an experimental setup as shown in Figs. 4 and 5 was used. The apparatus consists of a plexiglas nozzle and settling chamber and a flow channel

Nozzle and Settling Chamber

The nozzle and settling chamber, as shown in Figs. 6 and 7, is made of one-half-inch plexiglas. It consists of a one-half-inch air inlet, plenum settling chamber, and nozzle outlet. The settling screen is made of one-inch steel wool, meshed between 1/4-inch hardware cloth wire screen. Two nozzle top and bottom plates were made, one of plexiglas and the other of sheet steel, both 0.05 inch thick. Both gave a nozzle outlet five inches wide and 0.1095 inch high.

Flow Channel

The flow channel consists of two flat plates hald in position by half-inch plexiglas sides. A number of side plates were constructed so that the vertical spacing between the plates could be varied along with the angle of divergence. Three of the side plates had parallel walls of 1, 1.5, and 2 inches, respectively; while three others had divergent side walls with inlet widths of 1/2, 1/2, and 1 inch and outlet widths of 2.5, 5, and 4 inches. All channels were 12 inches long. The bottom plate of the channel has static pressure taps along its center line at 1/2-inch spacings. The top plate has openings for a total pressure probe.

The spacing of the nozzle with respect to the channel can be varied either horizontally or vertically. The two are held in position by means of a plexiglas bottom and two plexiglas side support plates.

A divider was also constructed for the channel, so that the flipping from one plate to the other was more apparent. It was nine inches long, the first six inches of which tapered from zero to one inch. The remainder was one inch wide.

Electrode Configuration

The electrode configuration consists of a positive corona wire, made of 0.004- or 0.006-inch steel wire mounted above an 0.08-inch copper wire. The electrodes are placed between the nozzle outlet

and the channel inlet, Fig. 7, and are centered vertically on the nozzle centerline.

The corona wire is held in place at the front supporting plate by a small piece of wire insulation slipped through a loop in the wire. The back end of the wire is connected to a bolt threaded into the rear side supporting plate. The bolt also serves as a high-voltage connection, Fig. 9. The negative electrode extends through the back of the plate and is connected directly to a microammeter, which in turn is connected directly to ground. A shorting switch across the meter prevents damage to the meter when breakdown occurs across the electrodes.

In later tests, a different configuration, described under control nozzles, was used.

Power Supply

The high voltage to the positive corona wire was supplied by a Sorensen high-voltage power supply, Fig. 4, and a Peschel high-voltage power supply.

The Sorensen power supply was a compact unit containing a built-in filter that produced a relatively ripple-free output voltage. Its major drawback was the scale selector, which was switched from position to position, starting at 5,000 volts. Each position had a range of 3,000 volts, that was adjusted by a separate dial. When switching from one scale setting to another, the voltage would have to be turned back to the low reading on the scale. This prevented a smooth, steady increase in the voltage output.

The Peschel unit was much bulkier than the Sorensen unit, since it contained an external transformer. It also had a very ripply output, which made an external filter necessary. Its control was much simpler than the Sorensen unit, in that the output voltage could be adjusted from 0 to 50,000 volts by simply turning one dial.

Air Inlets

Air inlets were provided on the top and bottom of the gap between the nozzle outlet and channel inlet, Fig. 10. The air inlets were made of plexiglas plates slid back and forth over the opening. These inlets controlled the air flow onto the top and bottom of the jet. The bottom inlet was set in the middle position and the top inlet was used to adjust the air flow. When the top inlet was opened, the increased amount of air coming in from the top caused the flow to flip from the top plate to the bottom plate. When closed, the air coming in from the bottom flipped the flow to the top plate.

Flow Measurement

The flow into the nozzle settling chamber was measured by a standard ASME flanged tap orifice with sharp edges. It was 0.4375 inch in diameter, mounted in an 0.963-inch pipe upstream of the settling chamber. The flow was regulated by a valve mounted underneath the table, Fig. 4.

Total Pressure Probe

The total pressure of the air flow in the channel was measured by means of a vertical traversing total pressure probe, Fig. 8. Because of the high electrical fields used in this study, a non-conducting probe was required. A glass probe was used with an external diameter of 0.06 inch and an internal diameter of 0.03 inch. The probe was positioned vertically by means of a micrometer traverse to which the probe was attached. The total pressure was actually measured by an inclined manometer. The static pressure of the tap directly beneath the probe was used in velocity calculations.

Static Pressure Measurement

The static pressure drop along the bottom plate of the channel was measured with an inclined manometer. The reference pressure was the first static pressure tap along the bottom of the channel.

Control Nozzles

For later tests, two small variable height nozzles were constructed of one-fourth inch plexiglas, Figs. 11, 12, 13, and 14. They were two inches long, the last one inch of which was a constant cross section. This cross section was five inches wide and could be varied from one-eighth inch to three-fourths inch in height. The nozzle outlet had two 0.05-inch flat plates, 0.15 inch wide, contoured into its sides, which served as negative electrodes (Fig. 19).

A positive corona wire, 0.004 inch in diameter, was run along the center of the nozzle. Its distance from the top side of the copper plates could be varied from 0.6 inch to 1.2 inches. The purpose of this nozzle was to direct the mass flow from the corona wind into the air exiting from the primary nozzle at right angles.

Experimental Procedure

The first step in the experimental procedure was to select a channel geometry in which the flow was just barely stable when attached to one plate or the other. Six sets of channel sides were prepared for this test, three of which had parallel sides and three of which had diverging sides.

During the test, the top air inlet was slid from the closed position to the wide open position as air flowed through the channel. The total pressure near the top and bottom plates was recorded. If the geometry is such that the flow will flip from one plate to the other, then the total pressure near the bottom plate should be high when the top air inlet is open, and the total pressure near the top plate should be high when the top air inlet is closed. In this manner the channel which was most suited for flipping the flow was selected.

Next, a suitable electrode geometry had to be constructed to give some sort of electrostatic force strong enough to flip the flow. To select a possible geometry, test runs were made with the configurations as shown in Fig. 15.

During each test run the air flow was kept constant and attached to one plate or the other. As the field was applied, the total pressure at different positions across the height of the channel was checked for any changes from that recorded with no field. A total pressure change would give some indication of some change in the flow attachment. If a particular geometry gave some indication of changing the attachment position, it was given further consideration and study.

After the channel geometry and electrode configuration were decided upon, a number of tests were run at varying nozzle Reynolds number, nozzle and channel placement, and top air inlet position.

For a given test run, the nozzle outlet and channel inlet would be placed at specified distances from the electrodes. The distance from the nozzle outlet to the electrodes was called distance A, Fig. 7. The distance from nozzle outlet to the front edge of the top air inlet was called B, and the distance from nozzle outlet to channel inlet was called C.

With the flow attached to the top plate, the top air inlet would be opened to let in enough air so that the flow was just barely attached to the top plate. The current, from the positive wire to ground wire, necessary to flip the flow from the top plate to the bottom plate was then recorded for different flow rates through the nozzle. The Reynolds number (Reynolds number in this report always refers to nozzle Reynolds number) was then plotted against the current required to flip the flow. The voltage across the electrodes was also plotted against the current flowing between the two electrodes.

Total pressure variation across the channel, with the air attached to the top plate before flipping, and attached to the bottom plate after flipping, was measured by the glass probe and micrometer traverse. From this data, velocity profiles before flipping and after flipping were plotted.

The static pressure drop along the bottom plate of the channel, with the flow attached to it, was recorded and plotted against channel length.

The final step in the series was to construct a model fluid amplifier in which the flow could be flipped both ways.

Those tests were run the same as the previous tests, except for the fact that the top and bottom air inlets were replaced by two variable height nozzles, with corona wind producing electrodes mounted in them.

In these tests, the current required to flip the flow to the top plate and to the bottom plate was plotted against Reynolds number. The velocity profiles and static pressure drop were plotted as before.

Experimental Calculations

Reynolds Number

The air flow into the settling chamber was measured by a standard ASME flanged tap orifice located upstream of the settling chamber. The piping before and after the orifice had an internal diameter of 0.963 inch, and the orifice itself had an interval diameter of 0.4375 inch.

The equation for the flow rate through the orifice[13] is given by

$$q = 7710\ Kyd^2\sqrt{h\ p_1/T_1} \qquad (1)$$

where

q is the flow rate in cubic feet per hour at T_1 and P_1,

K is the flow coefficient,

y is the expansion factor,

d is the orifice diameter in inches,

h is the pressure drop across the orifice in inches of water at 68°F,

p_1 is the pressure upstream of the orifice in pounds per square inch, and

T_1 is the temperature upstream of the orifice in degrees Rankine.

The Reynolds number at the nozzle exit, based on the nozzle height, w, and the mean velocity of flow at exit, V_n, is given by

$$Re = \frac{\rho_n V_n w}{\mu} \quad . \tag{2}$$

From the conservation of mass

$$\rho_1 V_1 A_1 = \rho_1 q = \rho_n V_n A_n$$

$$V_n = \frac{\rho_1 q}{\rho_n A_n} \quad . \tag{3}$$

From the equation of state

$$p_1 = \rho_1 R T_1$$

$$\rho_1 = \frac{p_1}{R T_1} \quad . \tag{4}$$

Substituting Eq. (1), (3), and (4) into Eq. (2)

$$Re = \frac{7710\ K y d^2 w \sqrt{h}}{R A_n \mu} (p_1/T_1)^{3/2} \quad . \tag{5}$$

A plot of the Reynolds number against the pressure drop across the orifice is shown in Fig. 16.

The pressure drop across the nozzle was calibrated against the pressure drop across the orifice, Fig. 17. From these two plots the Reynolds number can be found directly from the pressure drop across the nozzle.

Velocity

The total pressure at any point across the channel was measured by means of a glass probe positioned vertically by a micrometer traverse. The static pressure was measured at the static tap directly beneath the total pressure probe.

The velocity was then calculated from Bernoulli's equation

$$p_t - p_s = \frac{1}{2} \rho V^2 \quad . \tag{6}$$

Solving for the velocity

$$V = \sqrt{2(p_t - p_s)/\rho} \quad .$$

Plotting as a dimensionless parameter

$$\frac{V}{V_o} = \sqrt{\frac{p_t - p_s}{p_{to} - p_{so}}} \tag{7}$$

where

p_{to} is the total pressure corresponding to the maximum velocity, V_o, recorded across the channel, and

P_{so} is the static pressure corresponding to the maximum velocity, V_o, recorded across the channel.

SECTION III

RESULTS OF EXPERIMENTAL INVESTIGATION

Selection of Channel

The channel was tested with six different sets of sides, in the manner described in the experimental procedure. The channels with parallel sides showed no signs of flow attaching to one plate or the other. This was expected, since there was no room for any entrained fluid, Fig. 1, to be on either side of the jet; thus causing it to attach to one plate or the other.

All three of the divergent channels showed some signs of flow attachment. Both of the channels with one-half-inch inlet widths showed well-defined flow attachment, but there was also considerable flow in the other half of the channel.

The third divergent channel with a one-inch inlet and four-inch outlet, giving a divergence angle of five degrees, also showed well-defined signs of flow attachment and there was no sign of flow from the other side of the channel. In fact, there was flow into the side of the channel opposite to the plate to which the flow was attached, Fig. 18-a. This was caused by the pressure gradient between the atmosphere and the base of the jet.

Electrode Geometry

A number of electrode configurations were tested in order to select one which could produce a force strong enough to flip the flow.

The first configuration tested, Fig. 15-a, consisted of a positive wire mounted half-way through the nozzle on its centerline. The nozzle top and bottom plates were made of sheet steel and were connected to the ground. The bottom plate of the channel was also connected to ground. With this configuration, it was thought that some of the positive ions, produced by electron-molecule collisions near the positive wire, would be carried downstream and be attracted to the negative plate. These positive ions, having been attracted to the negative plate, could then transfer enough momentum to the neutral molecules of the air, in the direction of the plate, to cause the flow to attach to that plate. However, no change in the flow pattern could be measured when this configuration was tested. This was attributed to the fact that the negative plates of the nozzle were attracting all of the positive ions.

A new configuration, Fig. 15-b, was then constructed to produce the same effect and avoid the problem of the large negative plates of the

nozzle. The configuration consisted of a positive wire mounted near the outlet of the nozzle on its centerline. Two negative electrodes, 0.15 inch in diameter, were mounted just above and below the nozzle outlet. The steel nozzle top and bottom plates were replaced by plexiglas ones.

This configuration, like the first, gave no indication of affecting the flow pattern. However, with this configuration, it was very difficult to obtain currents more than 40 microamperes without breakdown.

The next configuration tested, Fig. 15-c, consisted of a positive wire located directly above a negative wire. This configuration was placed between the nozzle outlet and channel inlet and when it was tested, as described in the experimental procedure, gave indications of flipping the flow from one plate to the other.

An attempt was then made to construct a configuration in which the flow could be flipped up as well as down, Fig. 15-d. This configuration worked, but considerable sparking between the positive wire and the negative electrode, that was at floating potential, occurred. It was then decided to test the characteristics of the flow flipping in only one direction before further attempts to flip it both ways would be made.

Current - Voltage Relationship

The voltage across the electrodes was plotted against the current flowing between the electrodes for each test run. This was done for each test, because the slightest change in geometry seemed to affect the current. It was noted that factors, such as distance between the electrodes, the amount of air flow over the wires, the cleanliness of the wires, and the geometry around the electrode all affected the current-voltage relationship. For example, Fig. 21 shows the current voltage relationship for a fine wire located above a heavier copper wire. Figure 30 shows the effect of air flow over the wires. This effect seems to be prominent at the lower currents.

As the current - voltage plot approaches a vertical line, the current begins to increase sharply for a small increase in the voltage. As the slope of the curve gets greater, the tendency for a spark to jump between the positive electrode and the negative electrode (breakdown) increases. Once this breakdown occurs, sparking has a tendency to repeat in the same position at lower voltages.

Current Required to Flip Flow

In the original test, Test 1, (Figs. 20-23) the flow was extremely easy to flip to the bottom plate at low Reynolds numbers, and became progressively more difficult, Fig. 22. In this test, in which the

electrodes were only 0.30 inch apart, the current was erratic at times and breakdown occurred intermittently at high voltages. For this reason the electrode spacing was increased for further tests.

In Test 2, (Figs. 24-28) the electrode spacing was increased to 0.75 inch and the tests were run with variable top air inlet spacing. In this test the current required to flip the flow was much less than in Test 1.

As the top air inlet was closed, (distance B moved from 0.3 to 0.275 inch) the amount of air entering through the top air inlet was reduced, and thus, the current required to flip the flow was increased.

Tests 2, 3, and 4 were run to find the optimum position of the nozzle and channel with respect to the electrodes, so that the flow could be flipped with the least power. Since the electrode spacing for Tests 2, 3, and 4 was the same, an increase or decrease in current gave a good indication as to the increase or decrease in power.

In Test 2, the nozzle and channel were both close to the electrodes. In Test 3, (Figs. 29-33) the nozzle was moved further from the electrodes and the channel inlet was left close to them. In Test 4, (Figs. 34-38) the nozzle was again close to the electrodes and the channel inlet was moved further away. Plots of the current required to flip the flow at various Reynolds numbers, Figs. 26, 31, and 36, indicated that less current was required when the nozzle and channel inlet were both close to the electrodes.

From the results of these first four tests, it was apparent that the flow could be flipped downward from the top plate, but could it be flipped in both directions? To examine this more closely, the two control nozzles, as described in the experimental apparatus section, were constructed. The test setup, with these nozzles installed, Fig. 11, was geometrically similar to an actual fluid jet amplifier, but was much larger in size.

A series of three test runs (Tests 5, 6, and 7 with Figs. 39-50) were made with this configuration. Two with the channel tilted slightly upward and one with the channel tilted slightly downward. The plot of the current required to flip the flow at various Reynolds numbers for all three of these tests, Figs. 41, 44, and 47, gave definite proof that the flow could be flipped both upward and downward. Figure 44, in which the flow is biased very strongly in the downward direction, shows that the flow can still be flipped upward.

The current required to flip the flow plotted against the Reynolds number indicates that the current increases exponentially with the Reynolds number. Plots of both the current and power, required to flip the flow upward and downward at various Reynolds numbers, are shown on semilogarithmic coordinate paper in Figs. 42, 45, and 48. Thus, the

equation for both the current and power required to flip the flow, in terms of the Reynolds number, would be of the forms

$$I = a(e)^{m.Re} \tag{8}$$

$$P = b(e)^{n.Re} \tag{9}$$

where a and b are the y intercepts of the current and power curves, respectively. m and n are the slopes of the curves in the form

$$m = \frac{\ln I_2 - \ln I_1}{Re_2 - Re_1} \tag{10}$$

$$n = \frac{\ln P_2 - \ln P_1}{Re_2 - Re_1} \tag{11}$$

For example, in Fig. 48, the equations for the power and current to flip the flow from the top plate to the bottom plate are:

$$I = 1.6(e)^{0.00335\ Re} \text{ microamp} \tag{12}$$

$$P = 0.019(e)^{0.00329\ Re} \text{ watts} \tag{13}$$

Velocity Profiles

The typical flow through a fluid jet amplifier is shown in Fig. 18.[12] There is a central core which has not yet been affected by entrainment and which consists of flow originally in the power stream. This flow has a relatively low kinetic energy and a low pressure. A vortex motion occurs in the separation bubble as the stream continually entrains fluid which is replaced by a backflow from the attachment point.

Between the separation bubble and the core is the inner mixing zone which consists of flow originally in the power stream and fluid entrained from the separation bubble.

Figure 18-c shows typical velocity profiles as the flow moves downstream. Initially, the velocity profile has a constant value across the core region where the flow has not yet felt the effects of entrainment in the zone of flow establishment. The established flow has essentially a Gaussian velocity distribution which becomes skewed after attachment to the boundary wall because of the effects of the boundary layer on one side and entrainment on the other.

It is the differential pressure across the stream which inclines the stream to the wall. If high pressure occurring downstream could proceed upstream through the boundary layer into the low-pressure region, the stream would leave the boundary wall in a manner similar to stall on an airplane wing. However, the local high pressure immediately downstream of the point of attachment, Fig. 18-d, but be exceeded before the equilibrium can be disturbed.

The velocity profiles in this experiment were measured at a point 5.75 inches downstream of the channel inlet. At this point the channel is one inch wide from divider to plate. All tests were run at a Reynolds number of 1325. They compare very well with those of a typical fluid jet amplifier shown in Fig. 18-c.

For the first four tests. the velocity profiles show that the flow was not very well attached to the top wall before flipping, but attached very well to the bottom wall after flipping.

In Tests 5 and 7, the flow was very well attached to both the top and bottom plates, and thus the currents to flip the flow either way were similar. In Test 5, the velocity profile is a little better attached to the bottom wall than it is in Test 7, and in Test 7 it is a little better attached to the top wall. Thus, more current was required to flip the flow down in Test 7 and a little more was required to flip it up in Test 5.

It should be noted that in Tests 5, 6, and 7 the channel was tilted slightly upward or downward. This was because of the fact that the point at which the flow could be flipped upward or downward at the same current could not be found. Therefore, the channel was tilted up two and four degrees and down two degrees. The results of these three tests indicate that there is a point at which the flow could be flipped either way with the same current.

Static Pressure Drop

The static pressure drops along the bottom plate, with flow attached to it, compare very favorably with those obtained by Olson[8] (Fig. 18-d). The only difference being that Olson's results show no static pressure increase near the channel outlet. The static pressure increase in these tests was caused by the continued development of the flow (the boundary layer continued to grow in height) and the divergence of the channel near its outlet.

In Test 2, the nozzle was close to the channel inlet and the flow attached very well to the bottom plate. The static pressure near the point of attachment is high which indicates that the flow attached to the plate at a sharp angle, Fig. 28.

In Tests 3 and 4, the nozzle is further from the channel and the flow does not attach as well to the bottom plate. The static pressure near the point of attachment is low and it is further downstream than in Test 1. This indicates that the flow struck the plate at a lesser angle than in Test 1 because of the increased distance between the nozzle outlet and channel inlet, Figs. 33 and 38.

The geometry and attachment of the flow to the bottom plate are similar in Tests 5 and 7 as is the static pressure drop along the bottom of the channel, Fig. 52.

SECTION IV

ANALYTICAL STUDY OF THE EFFECTS OF CORONA WIND ON THE JET

Analytical Solution

In order to analyze the air flow through the control jets, a one-dimensional approach will be taken. The geometry of the nozzle, Fig. 20, seems to indicate that this would be the best approach, since the electric field strength will vary in only one direction, the x direction, and since the velocity in the constant area section of the channel should be a constant.

Some electric field equations[9] that will be useful in the analysis, are as follows:

$$\bar{\nabla} \cdot \bar{E} = \frac{\rho_c}{\epsilon} \tag{14}$$

$$\bar{J} = \sigma_c \bar{E} = \rho_c \bar{V}_t \tag{15}$$

$$\bar{v}_i = K_o \bar{E} \tag{16}$$

$$\bar{F} = \rho_c \bar{E} \ . \tag{17}$$

The following assumptions were made:

(1) The flow is one-dimensional, incompressible, and steady.

(2) The electrical conductivity of a gas, such as air, is very small, approximately zero.

(3) Ions of only one sign exist a slight distance downstream of the corona wire.

(4) The mobility of the ions was approximately constant.

The total velocity of the ions, $\bar{v}_t$, is equal to the sum of the velocity of the air, $\bar{v}$, and the velocity of the ions in the air, $\bar{v}_i$.

$$\bar{v}_t = \bar{v} + \bar{v}_i \ .$$

From Eq. (16)

$$\bar{v}_t = \bar{v} + K_o\bar{E} \ . \tag{18}$$

The current density becomes

$$\bar{J} = \rho_c(\bar{v} + K_o\bar{E}) \ .$$

Typical values of K_o (ref. 10) and E at room temperature are:

$$K_o = 0.216 \text{ in.}^2/\text{volt-sec}$$

$$\bar{E} = \frac{17{,}500 \text{ volts}}{0.75 \text{ in.}} = \frac{23{,}200 \text{ volts}}{\text{in.}} \ .$$

Therefore $K_o\bar{E}$ is on the order of 420 ft/sec, while $\bar{v}$ is approximately 5 ft/sec. Since $\bar{v}$ is very small compared to $K_o\bar{E}$, it can be neglected. Thus,

$$\bar{J} = \rho_c K_c \bar{E} \tag{19}$$

The Navier Stokes equation[11] in the x direction is:

$$\left(\frac{\partial u}{\partial t} + u \frac{\partial u}{\partial x} + v \frac{\partial u}{\partial y} + w \frac{\partial u}{\partial z} = F - \frac{\partial p}{\partial x} + \mu \frac{\partial^2 u}{\partial x^2} + \frac{\partial^2 u}{\partial y^2} + \frac{\partial^2 u}{\partial z^2} \right)$$

The continuity equation:

$$\frac{\partial u}{\partial x} + \frac{\partial v}{\partial y} + \frac{\partial w}{\partial z} = 0$$

must also be satisfied.

Since the flow in one dimensional, $\bar{v}$ and $\bar{w}$ are zero everywhere, and it follows from the continuity equation that $\partial u/\partial x = 0$. This also satisfied the equation of the conservation of mass in a constant area channel

$$\rho AV = C \ .$$

Since the flow is incompressible, ρA = constant, and therefore V is a constant.

The Navier Stokes equation reduces to

$$F - \frac{\partial p}{\partial x} + \mu\left(\frac{\partial^2 u}{\partial y^2} + \frac{\partial^2 u}{\partial z^2}\right) = 0 \quad .$$

The body force F is equal to $\rho_c \bar{E}$, and from Eq. (19)

$$\rho_c = \frac{\bar{J}}{K_o \bar{E}} \quad .$$

Thus,

$$\bar{F} = \frac{\bar{J}}{K_o} \quad .$$

In a constant cross-sectional, one-dimensional channel

$$\bar{J} = \frac{\bar{I}}{A} \quad .$$

Therefore,

$$\bar{F} = \frac{\bar{I}}{K_o A} \quad . \tag{20}$$

The Navier Stokes equation becomes

$$\frac{I}{K_o A} - \frac{\partial p}{\partial x} + \mu\left(\frac{\partial^2 u}{\partial y^2} + \frac{\partial^2 u}{\partial z^2}\right) = 0 \quad .$$

The viscous forces, for low velocities, are small compared to the body force, thus the equation can be further reduced to

$$\frac{I}{K_o A} = \frac{\partial p}{\partial x} \quad .$$

Integrating,

$$\Delta p = \frac{I}{K_o A}(x_2 - x_o) \quad , \tag{21}$$

where x_o is a reference distance located a very short distance from the region of intense corona discharge (positive wire).

This equation, known as Chattock's relation, predicts that the pressure will increase linearly with both the current and the distance from the positive corona wire.

Equation (21) could be written in the form

$$p = \frac{c}{K_o} I \quad , \tag{22}$$

where c is a geometric shape factor.

From Fig. 57, it is apparent that the total pressure does increase linearly with the current. The experimental value of c/K_o, as obtained from Fig. 57, and the theoretical value of c/K_o are as follows:

$$c/K_o \text{ exp.} = 7.4 \text{ lb}_{f/in.^2 amp} \quad ,$$

$$c/K_o \text{ theo.} = 19.0 \text{ lb}_{f/in.^2 amp} \quad .$$

The actual air flow through the control nozzle is similar to the pumping of air through a pipe, Fig. 51. As the positive ions collide with the neutral molecules in the air, a mass motion away from the positive wire occurs. This creates a low-pressure region in the vicinity of the wire, and air is "sucked" into the converging nozzle. As the area of the nozzle decreases, the velocity of the air increases until it reaches the constant area section of the nozzle.

Figure 56 shows that the suction developed by the corona wind, at a point just before the positive wire, increases linearly with current.

Figures 52 and 53 show the total and static pressure variation along the control nozzle for various currents. From these figures, the velocity variation along the channel was calculated and plotted, Fig. 54. This figure indicates that the original assumption of a constant velocity in the constant area section of the nozzle was not correct. The flow continues to accelerate after it reaches the constant area section of the nozzle until it reaches a point near the negative plate, where it then decelerates. It appears that the velocity is not uniform over the entire cross section.

Since both the static and the total pressure vary linearly with current, it would seem that the velocity would vary with the square root of the current. Figure 55 shows that the control nozzle outlet velocity is a linear function of the square root of the current, given by the equation

$$V = 1.435 \sqrt{I} \quad 2.30 \text{ ft/sec} \quad . \tag{23}$$

Now that the control-nozzle outlet velocity is known as a function of the current, and the primary nozzle outlet velocity is known as a function of the Reynolds number (Eq. (27), sample calculations), the theoretical angle of deflection of the primary jet can be calculated.

From the conservation of momentum,

$$m\bar{V}_n + m_c\bar{V}_c = (m + m_c)\bar{V} \quad , \tag{24}$$

where

$$m = \rho_n A_n V_n = \rho_n q \quad ,$$

$$m_c = \rho_c A_c V_c \ ,$$

$$m\bar{V}_n = \rho_n q\bar{V}_n \ , \text{ and}$$

$$m_c\bar{V}_c = \rho_c A_c V_c \bar{V}_c \quad .$$

Since the two flows meet at right angles, the angle of primary jet deflection is equal to

$$\alpha = \tan^{-1} \frac{\rho_c A_c V_c \bar{V}_c}{\rho_n q \ V_n} \tag{25}$$

Figure 58 shows the theoretical angle of primary jet deflection for various primary jet velocities and control jet currents. Figure 59 shows the angle of primary jet deflection for various currents at a Reynolds number of 1325, which corresponds to a velocity of 23.3 ft/sec. The actual angle of deflection of the jet could be calculated for each test run, since the relative position of the nozzle outlet with respect to the control nozzle outlet and the channel inlet was known, and since the actual point of attachment could be determined from the plots of the static pressure along the bottom plate, similar to that shown in Fig. 18.

It is apparent from Fig. 59 that the actual angles of jet deflection were much greater than those calculated. This was as expected, since the Coanda effect causes the primary jet to attach to one wall or the other once the control jet has deflected the primary jet slightly upward or downward in the channel.

Perhaps a better method of correlating the results is to plot the ratio of the control jet mass flow, required to flip the flow, to the primary jet mass flow at various Reynolds numbers, Fig. 60.

$$\frac{Q_c}{Q} \quad \frac{\rho_c A_c V_c}{\rho_n \ q} \quad . \tag{26}$$

In a typical fluid jet amplifier Q_c/Q is seldom more than 0.25, but in these tests values as high as 1.0 were recorded. This is caused by the fact that this model has dimensions many times larger than those employed in fluid jet amplifiers, and its design made the jet much more stable than in fluid jet amplifiers.

SECTION V

CONCLUSIONS AND RECOMMENDATIONS

Conclusions

Although the experimental model used in these tests was much larger and not in exact proportion to a typical fluid jet amplifier, the model's characteristics, such as flipping mechanism, velocity profile, and static pressure drop, were very similar to those of a fluid jet amplifier. It is, therefore felt that any results, contained herein, could be easily incorporated into a wide variety of fluid jet control systems.

The actual results of this series of tests indicate that the mass motion of air, produced by corona wind, can definitely influence the attachment of flow to a flat plate. The influence of this mass motion is great enough to cause the air flow to flip from one plate to another, in either the upward or downward direction.

The only limitations on the mass motion of the air from the corona wire were caused by the power requirements to achieve the flow and the potential that could be applied before breakdown.

The current required to trigger this attachment, for a given geometry and Reynolds number, was constant and repeatable to within a few microamp.

The control of the air flow at Reynolds numbers above 2,500 was not achieved in this series of tests. However, the results of tests shown in Fig. 60, show that very high values of the ratio of control jet flow to primary jet flow were required to cause the flow to switch from one plate to another. In an actual fluid amplifier, this ratio is much less. Thus, it would seem that flows with higher Reynolds numbers could be controlled in such a device.

Recommendations

This series of test indicates that corona wind would make a very adaptable control source for many types of fluid amplifiers. To confirm this, it would be advisable to construct an actual model fluid amplifier, in which a corona wind mechanism is incorporated. Air, as used in this test, or other suitable gases or insulating liquids could be used as the carrier material.[15]

A great deal of difficulty was encountered in these tests because of breakdown between the electrodes before a suitable current could be obtained. Because of this fact, it would appear to be logical to undertake a careful study to select the best electrode configuration prior

to the construction of a model fluid amplifier. The design of the amplifier would have to be centered around this configuration. An important fact, that would play a major role in this design, is that the geometry around the current producing electrode has some effect upon its performance.

SECTION VI

Illustrations

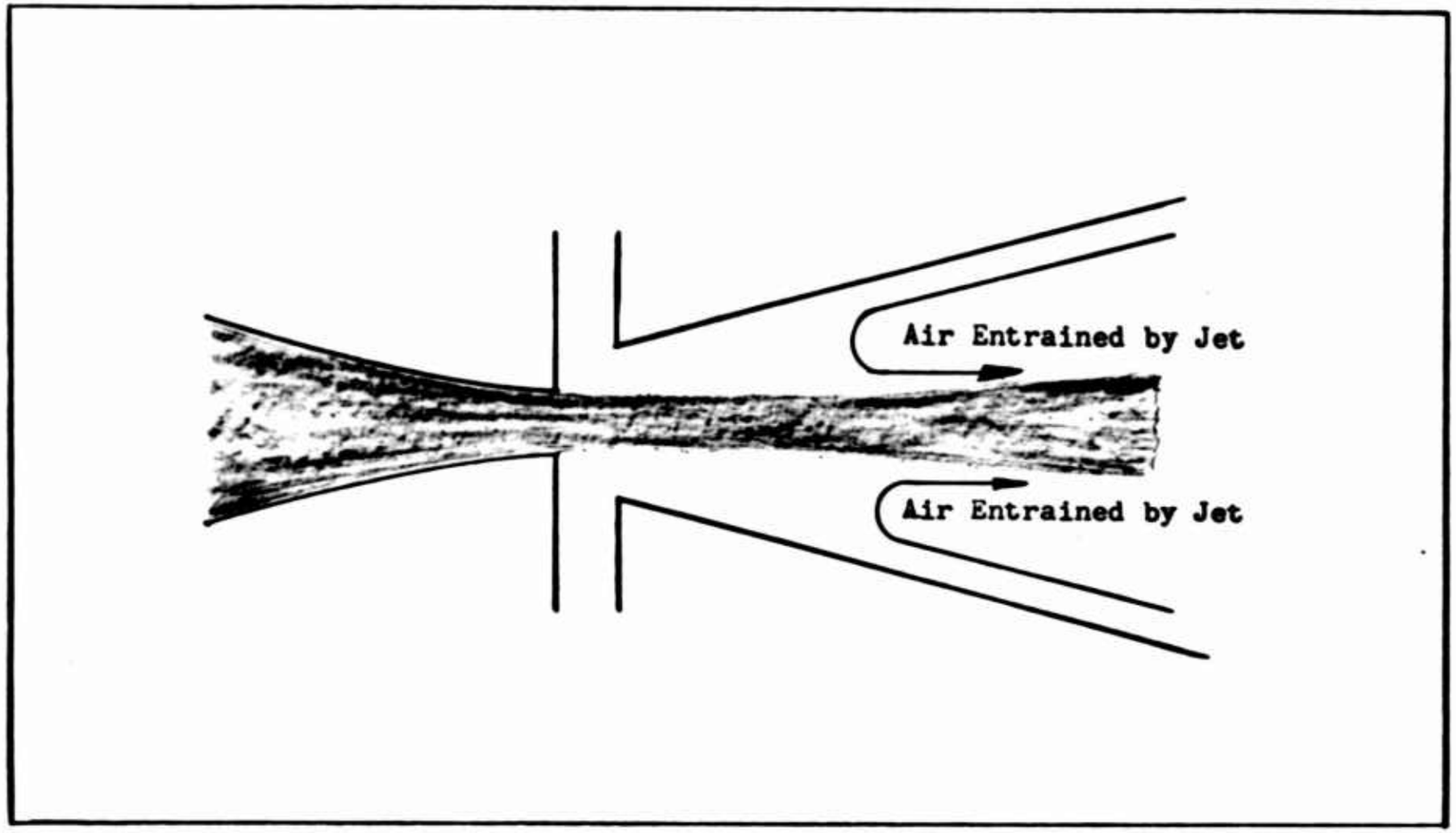

Figure 1 - Typical Fluid Jet Amplifier in an Unstable Position

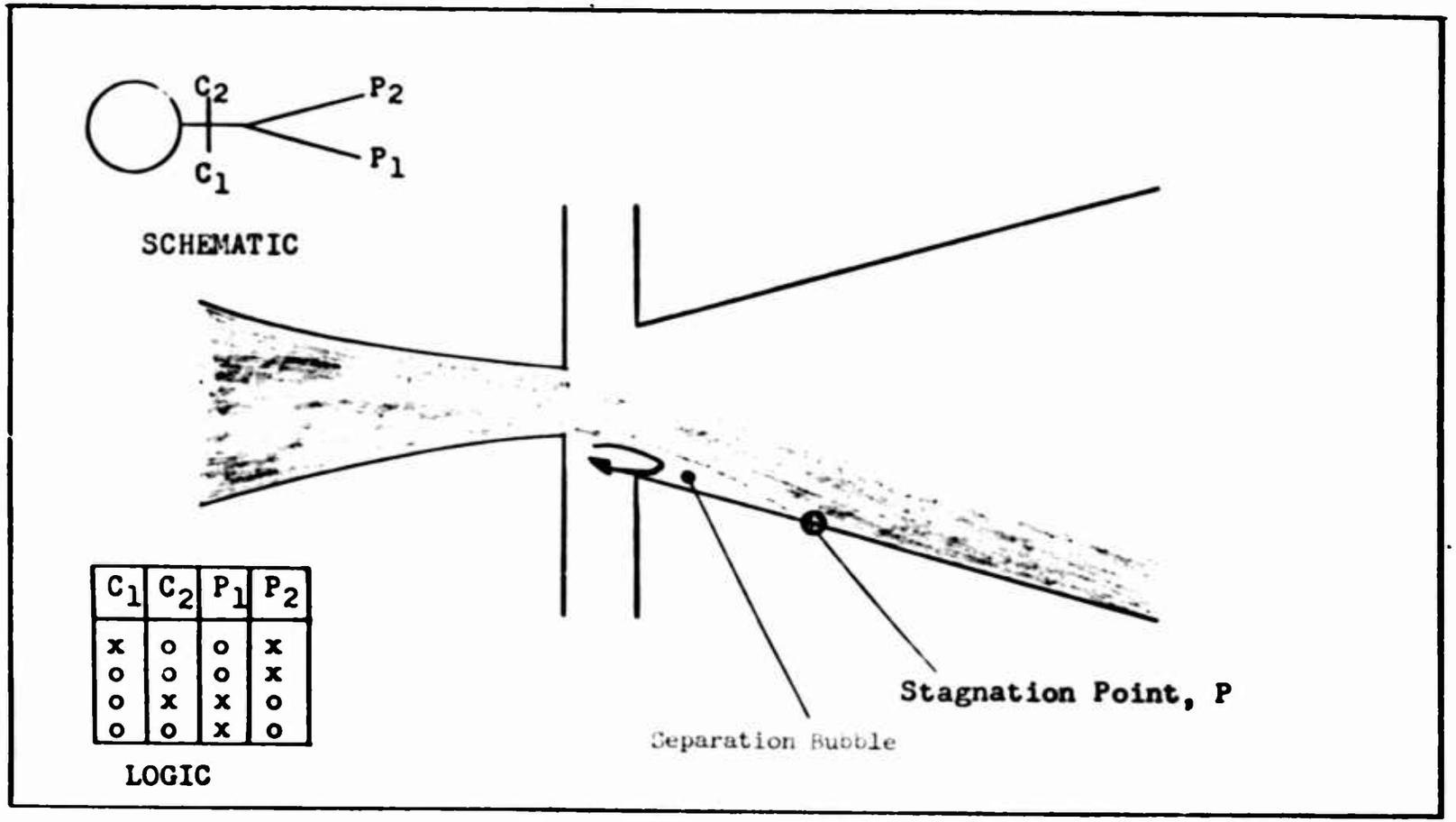

C_1	C_2	P_1	P_2
x	o	o	x
o	o	o	x
o	x	x	o
o	o	x	o

Figure 2 - Fluid Jet Amplifier with Flow Attached to Bottom Wall, with Schematic and Logic of System

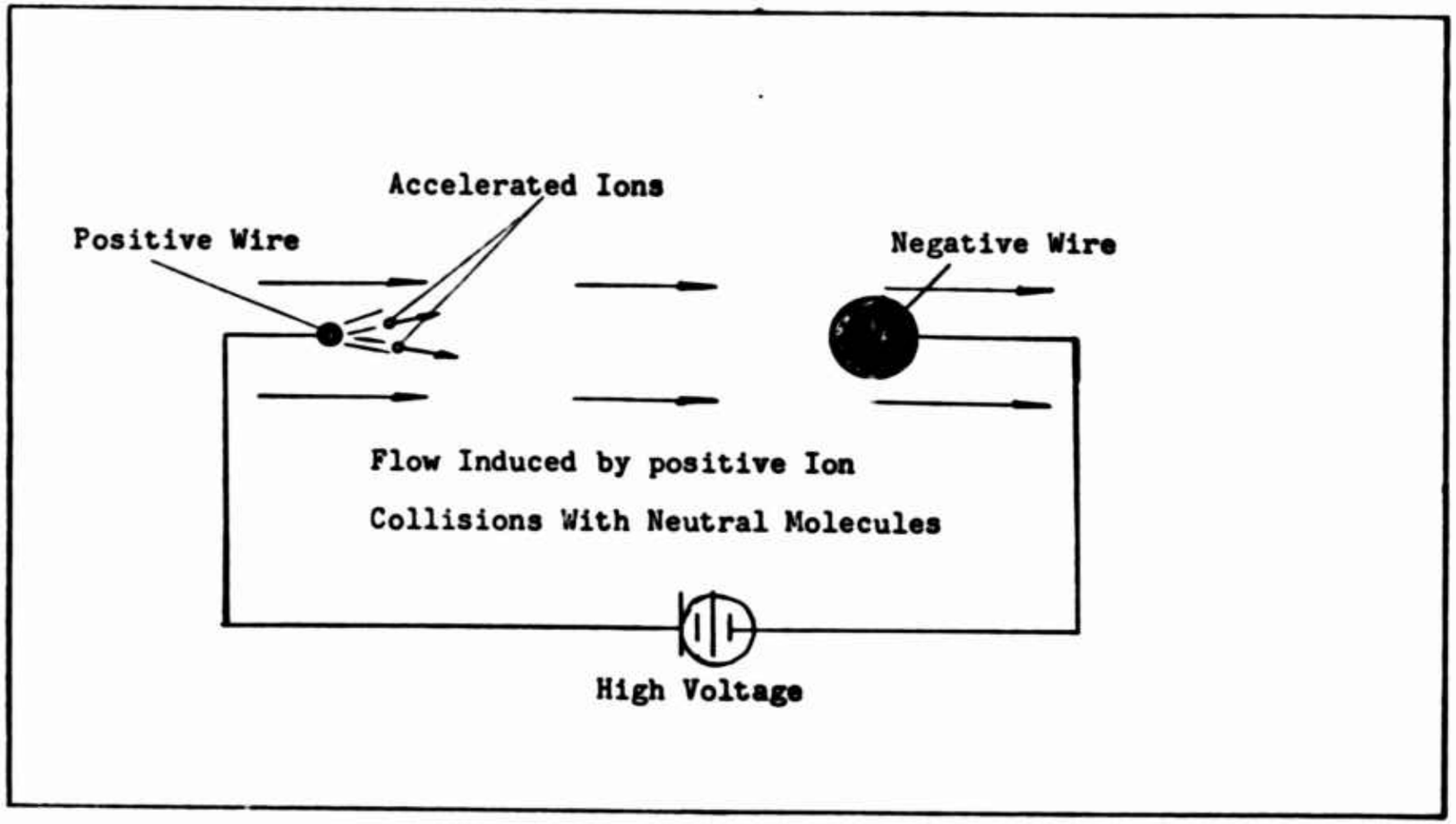

Figure 3 - Corona Wind from a Charged Wire

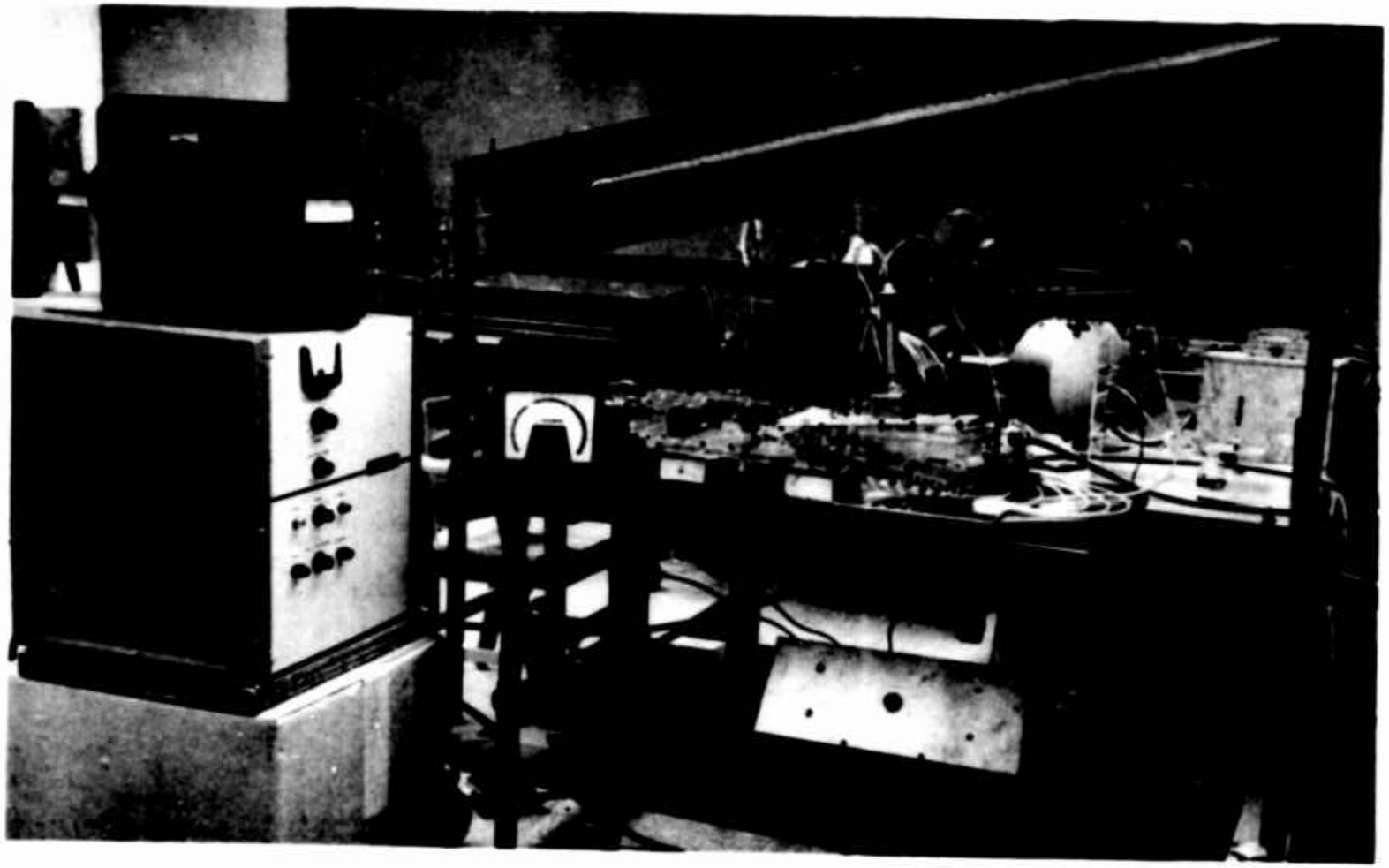

Figure 4 - Over-all View of Test Setup. Sorensen High Voltage Power Supply, Lower Left; Singler Electrostatic Voltmeter, Upper Left

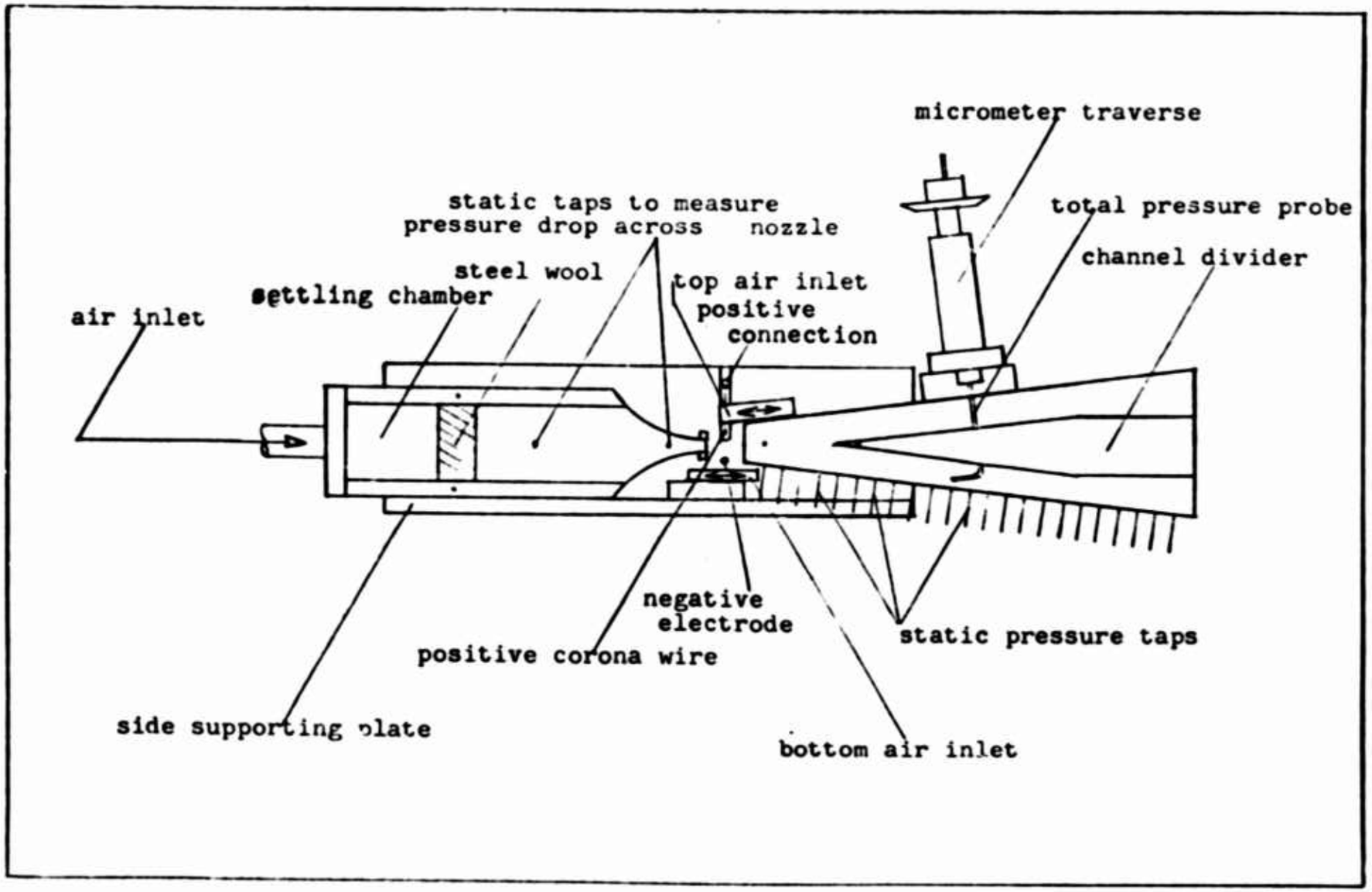

Figure 5 - Diagram of Original Test Setup

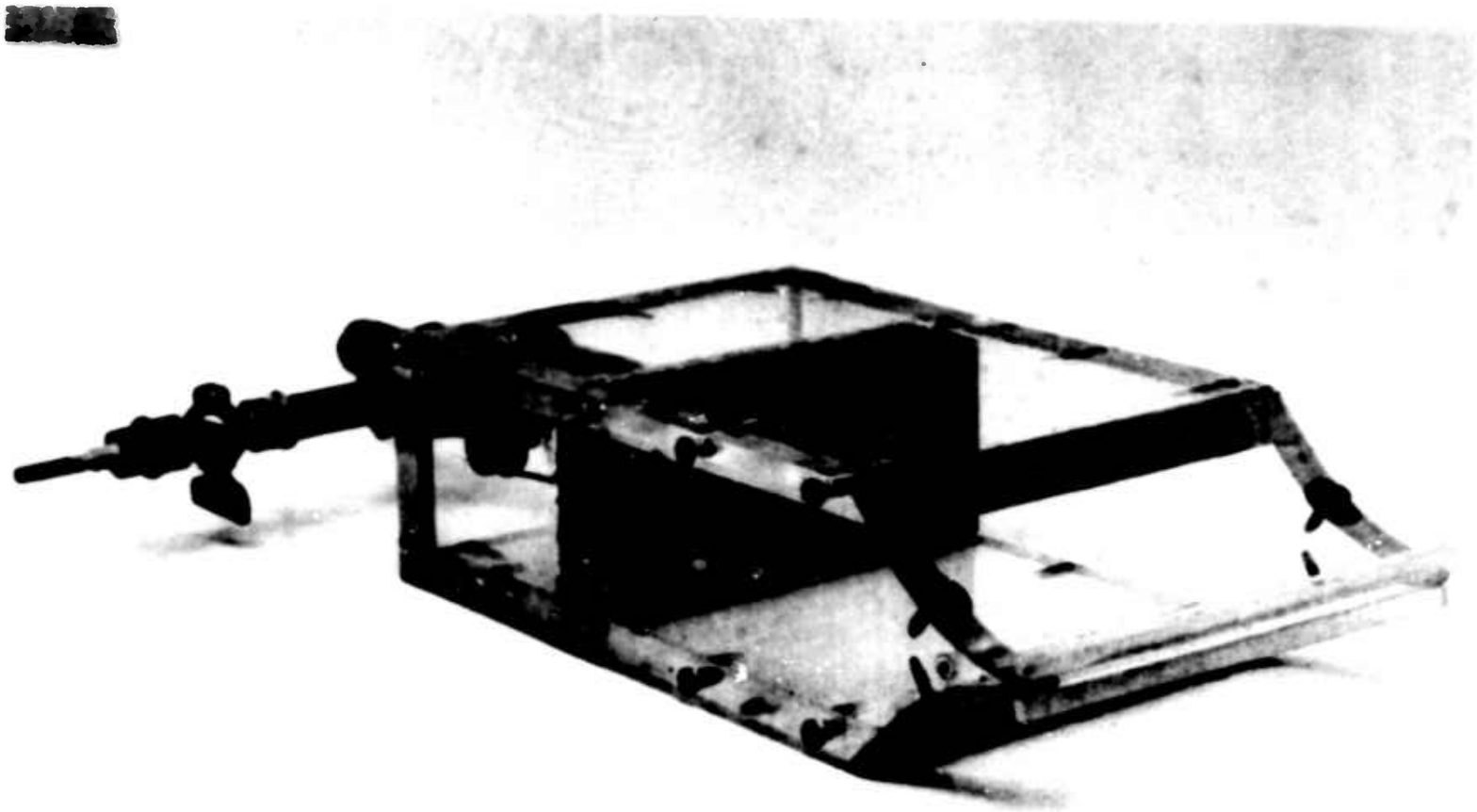

Figure 6 - Close-up View of Settling Chamber, Settling Screen and Nozzle Outlet

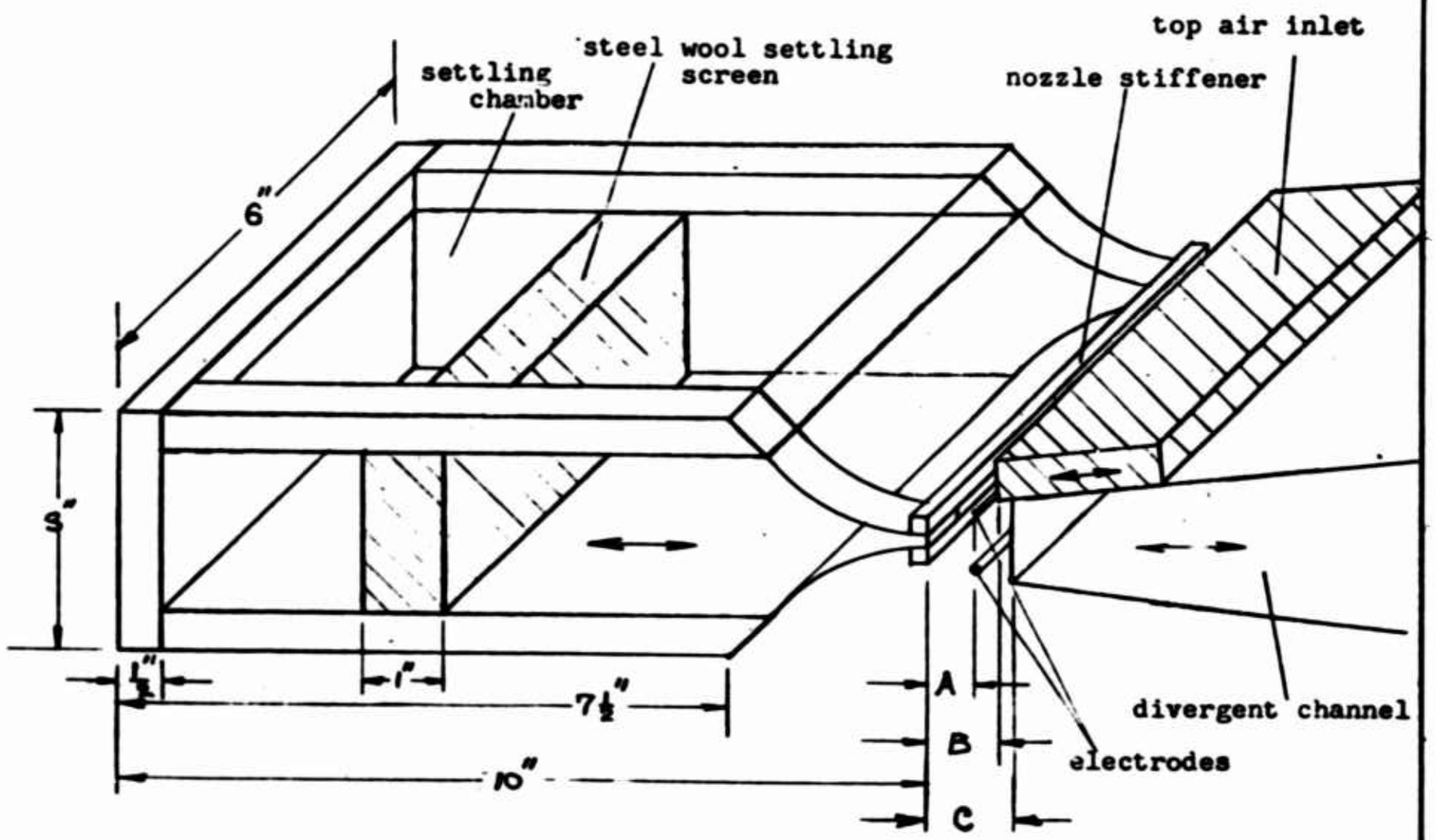

Figure 7 - Diagrammatic Sketch of Nozzle Showing its Relative Position with Respect to the Channel Inlet and Electrodes

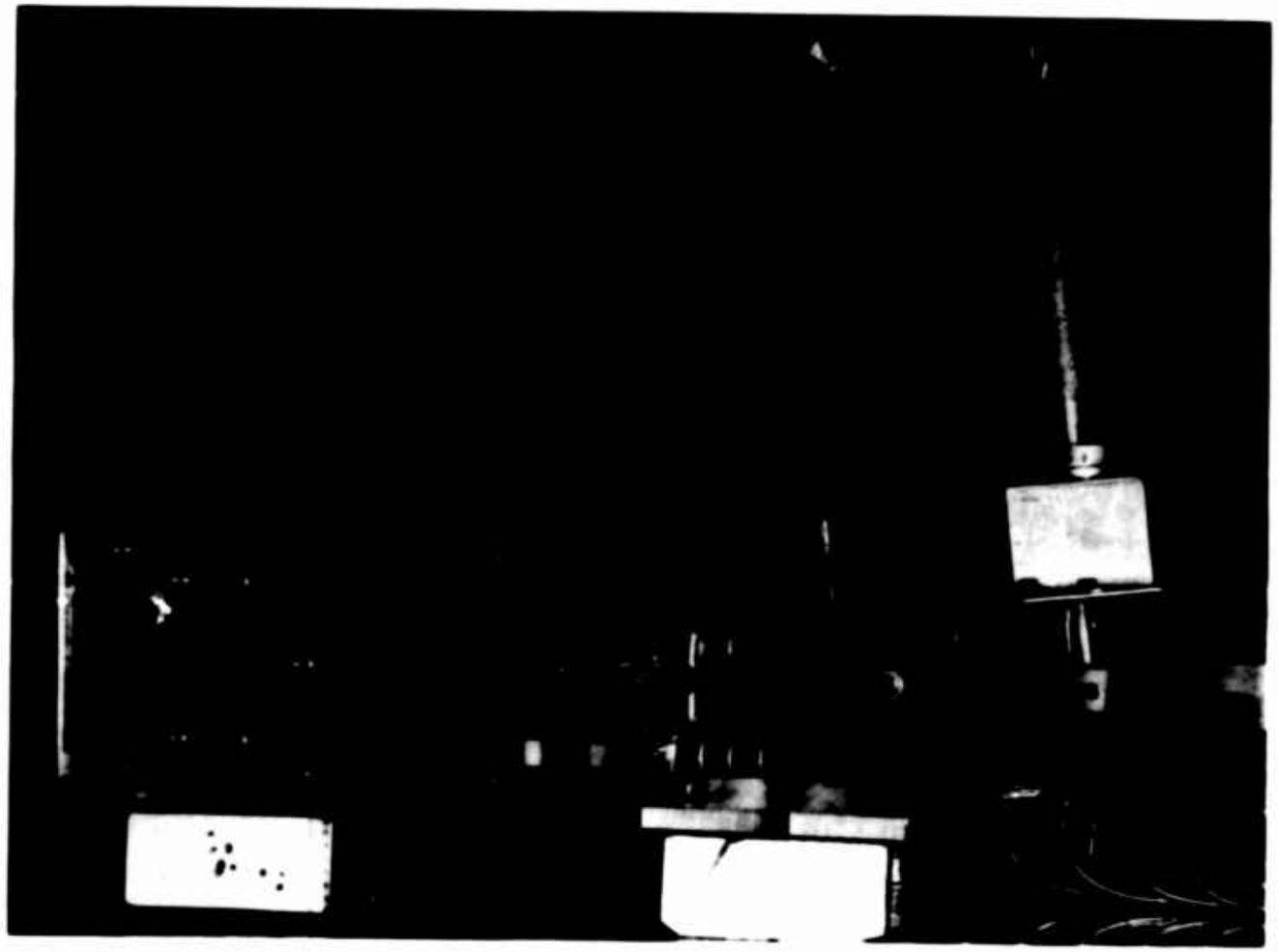

Figure 8 - Front View of Test Setup Showing Relative Position of Nozzle with Respect to the Channel Top and Bottom Plate, Micrometer Traverse, and Glass Total Pressure Probe

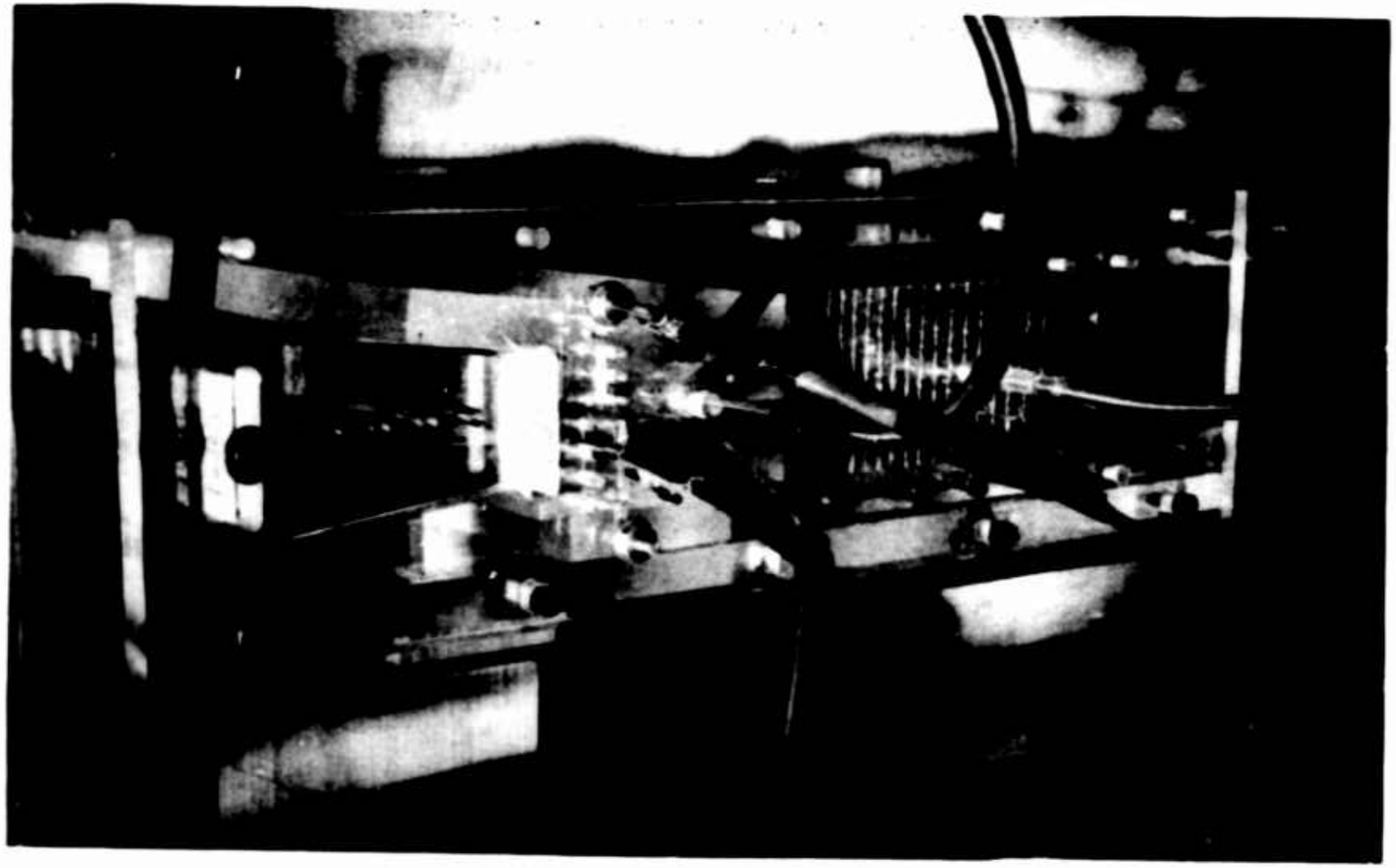

Figure 9 - Close-up View of High Voltage Positive and Negative Connections and Pressure Taps for Measuring Pressure Drop Across Nozzle

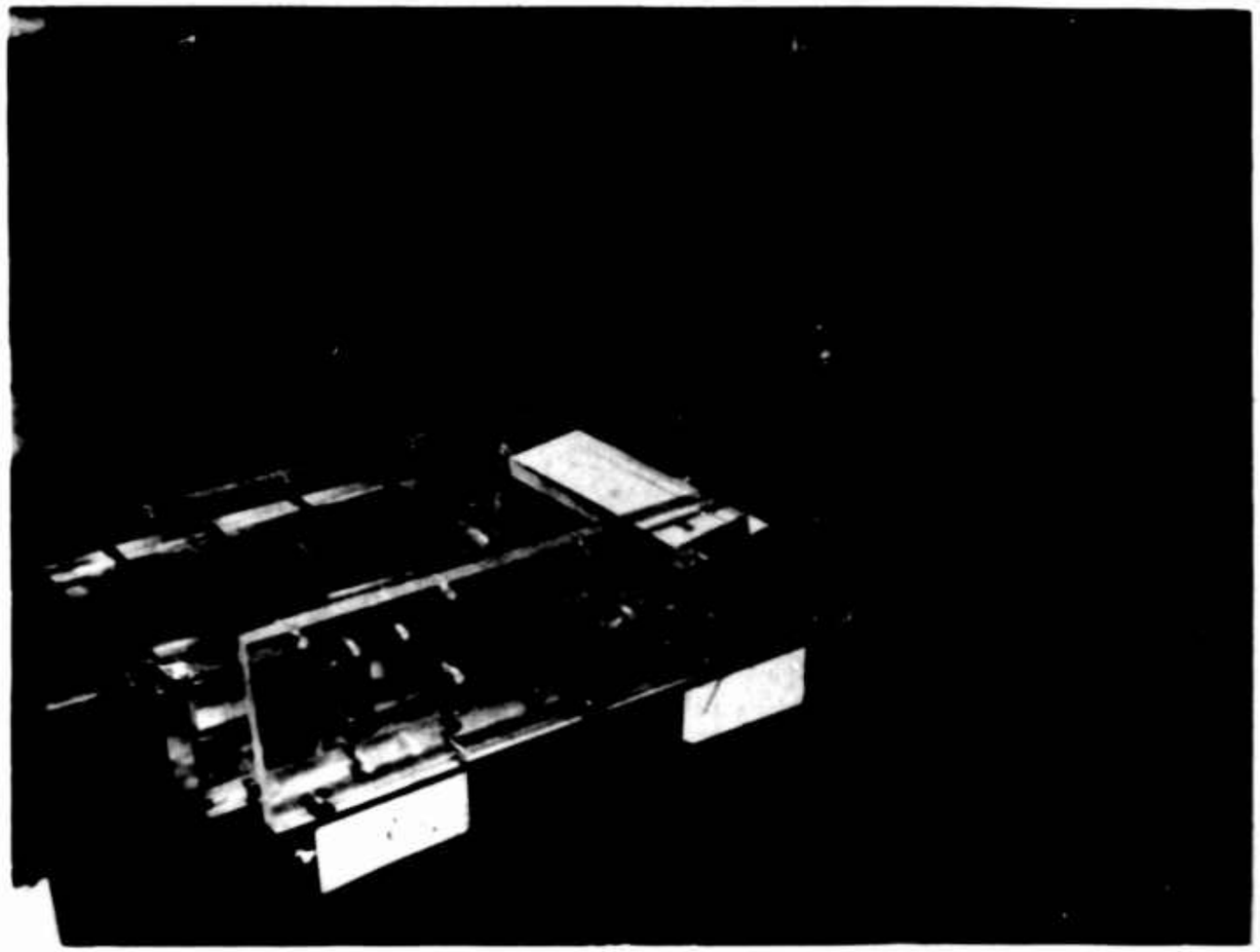

Figure 10 - Top View of Channel Showing Top Air Inlet, Center and Micrometer Traverse, Upper Right

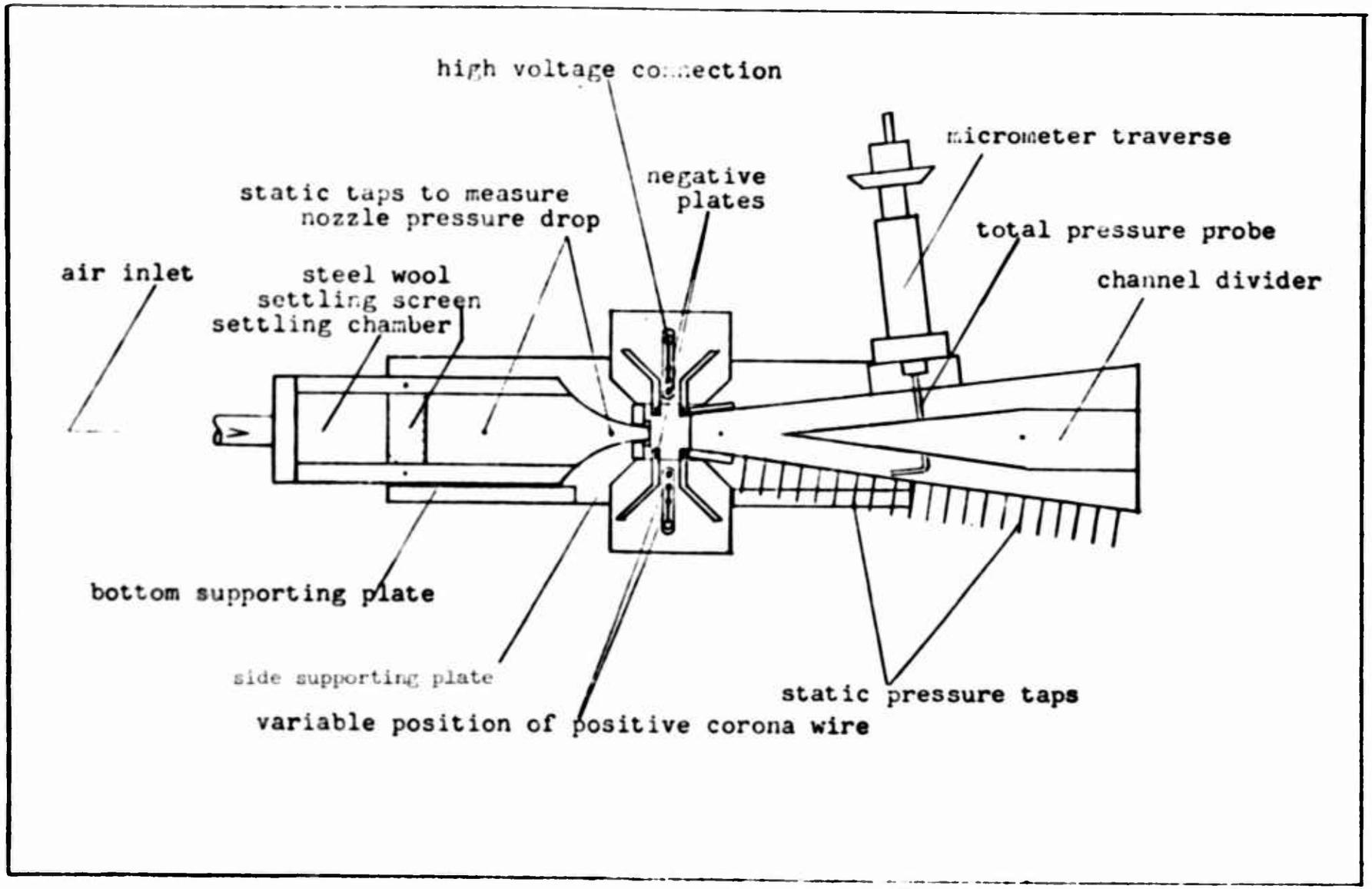

Figure 11 - Diagram of Test Setup with Control Nozzles

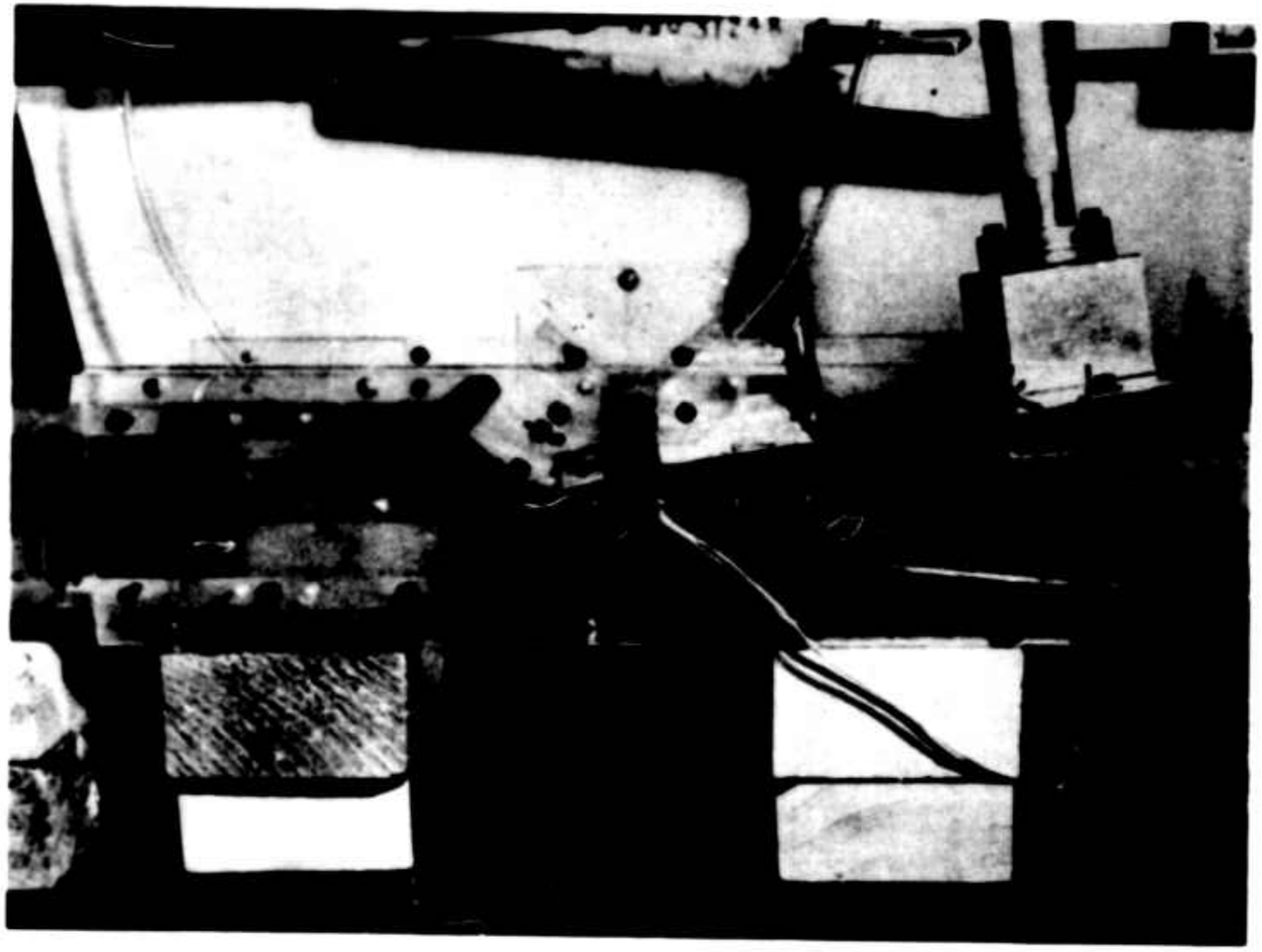

Figure 12 - Test Setup with Top and Bottom Control Nozzles Installed

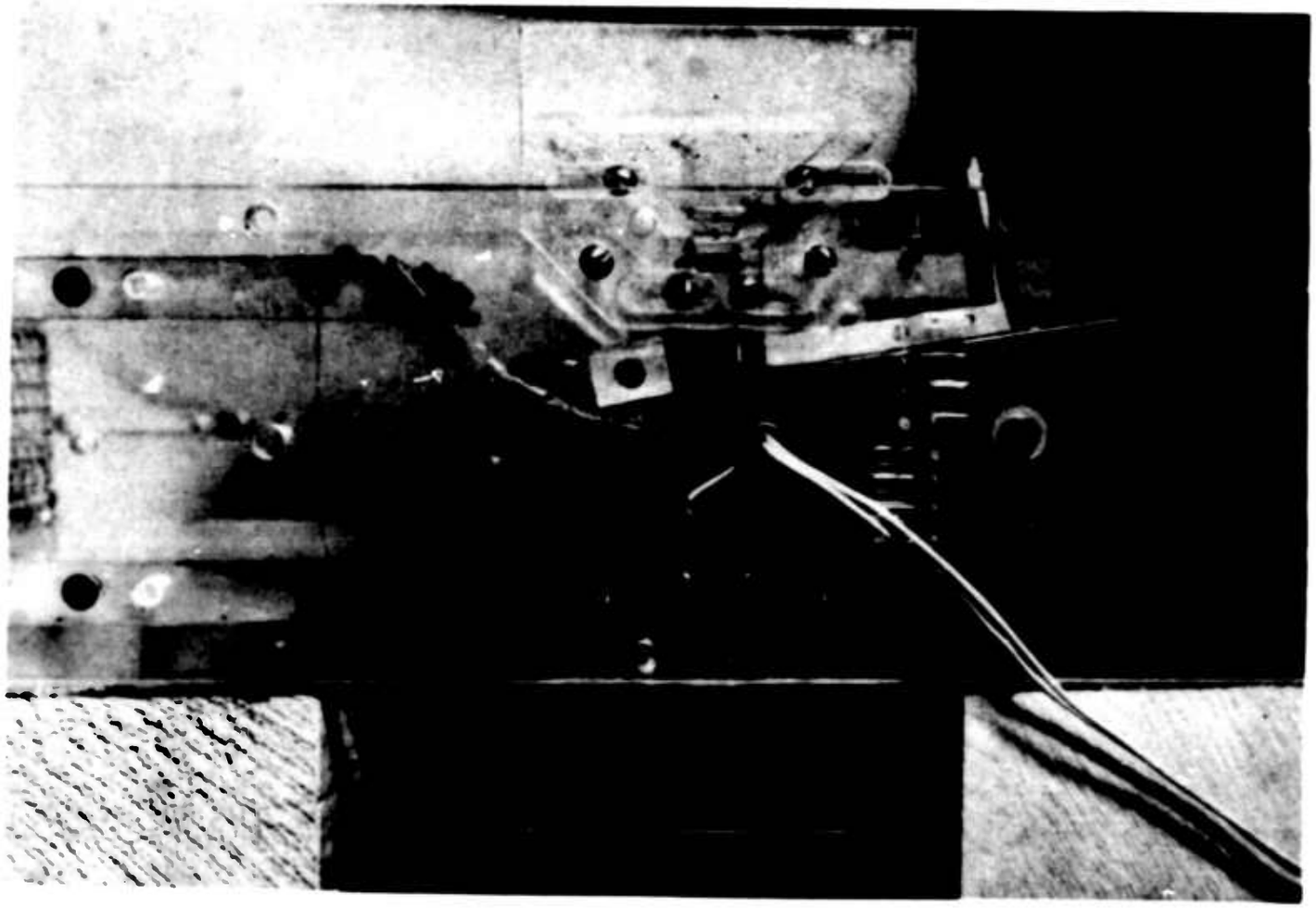

Figure 13 - Close-up View of Nozzle Outlet, Channel Inlet and Control Nozzles

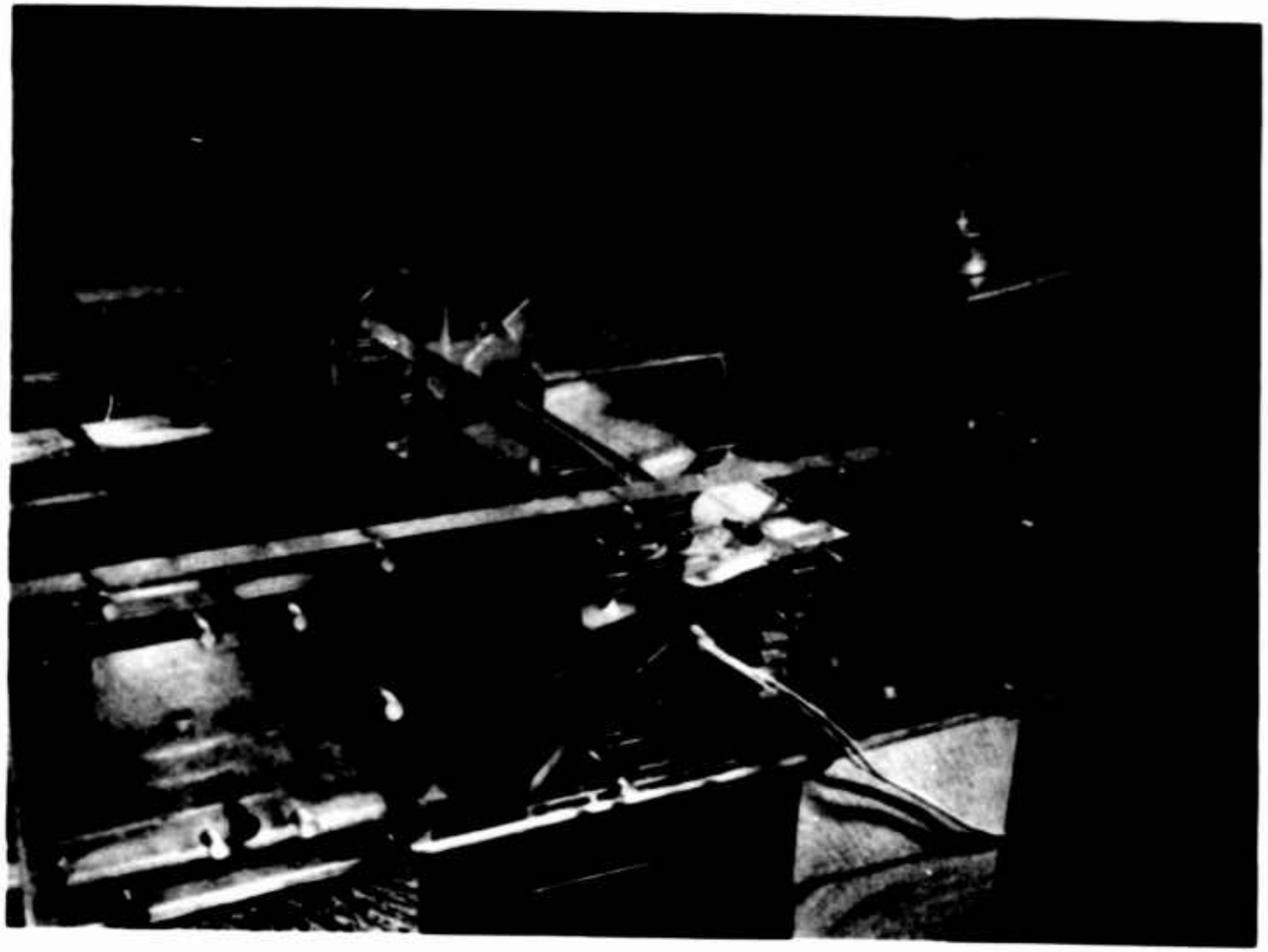

Figure 14 - Top View of Test Setup with Control Nozzles

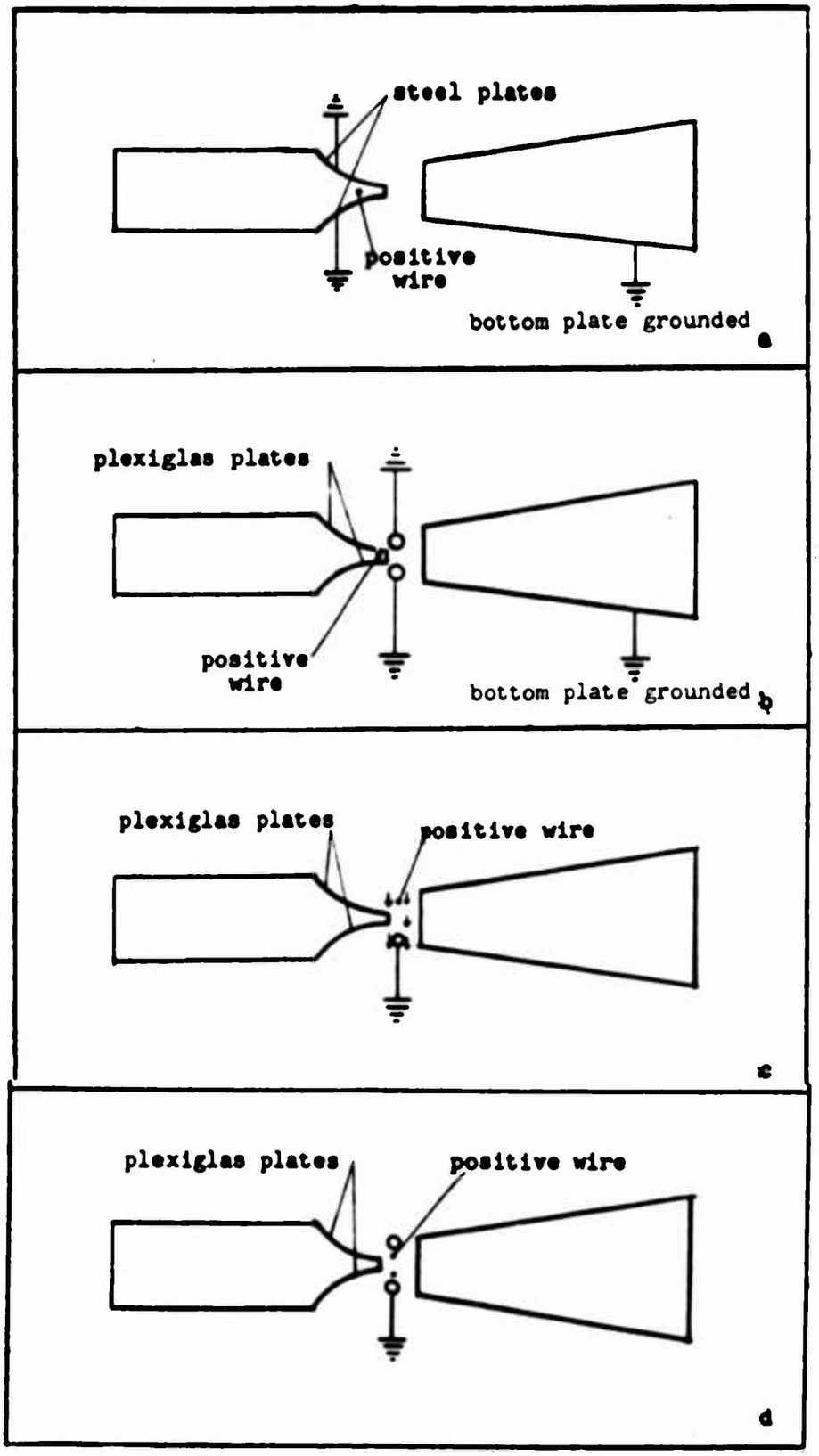

Figure 15 - Electrode Configurations Tested

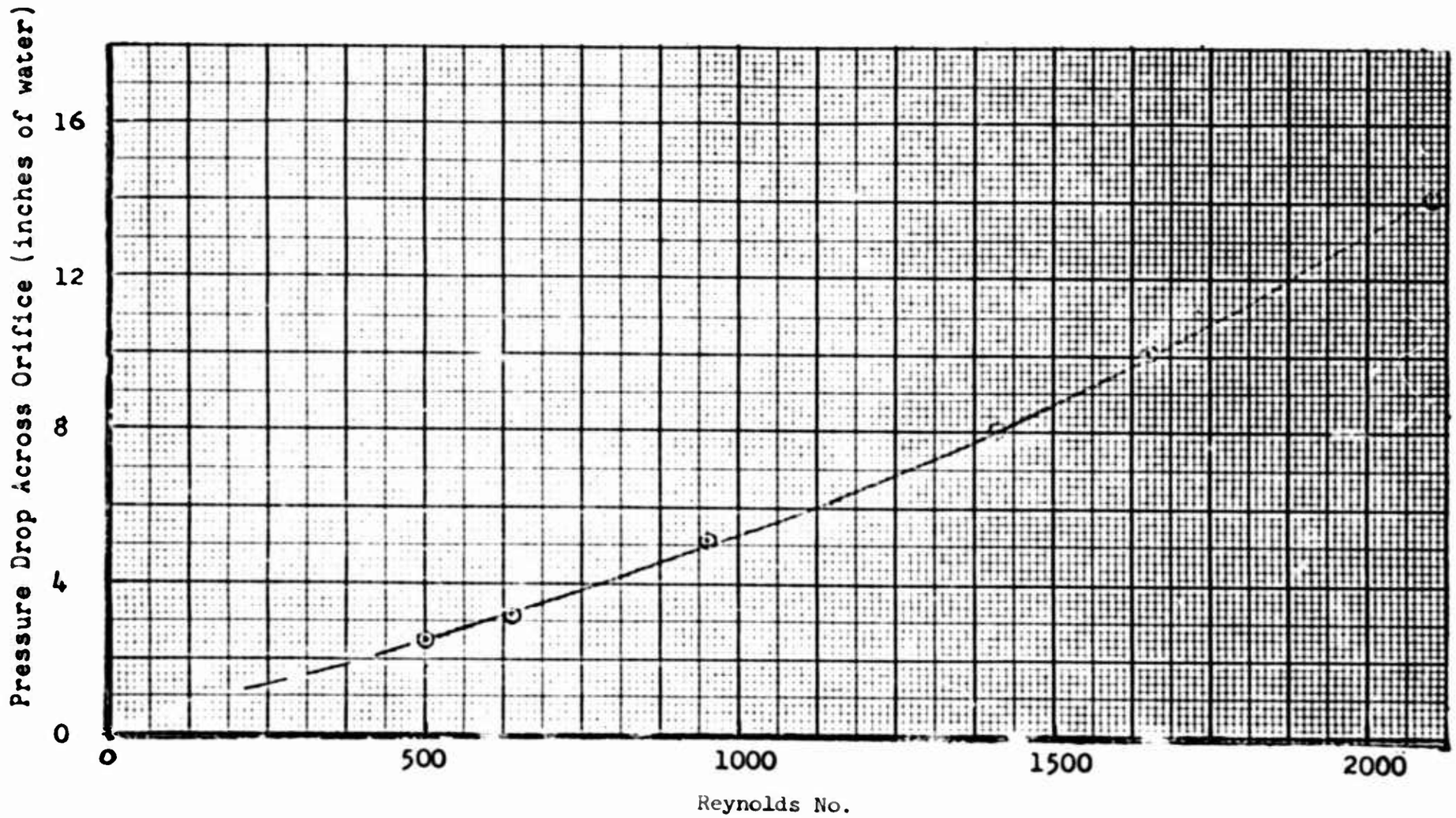

Figure 16 - Reynolds Number for Various Pressure Drops Across a Standard ASME Orifice

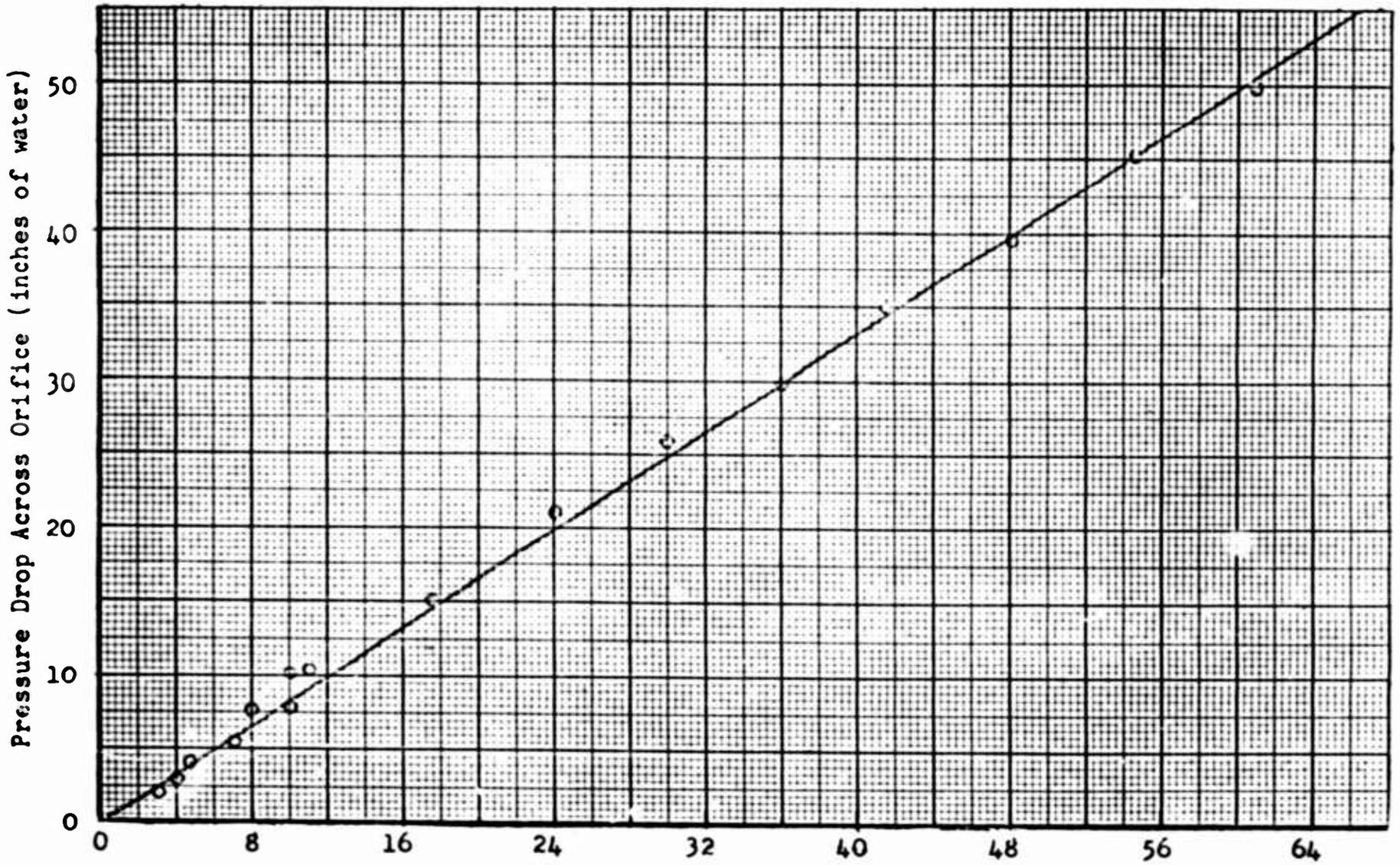

Figure 17 - Pressure Drop Across Nozzle (inches of water x 10^3)

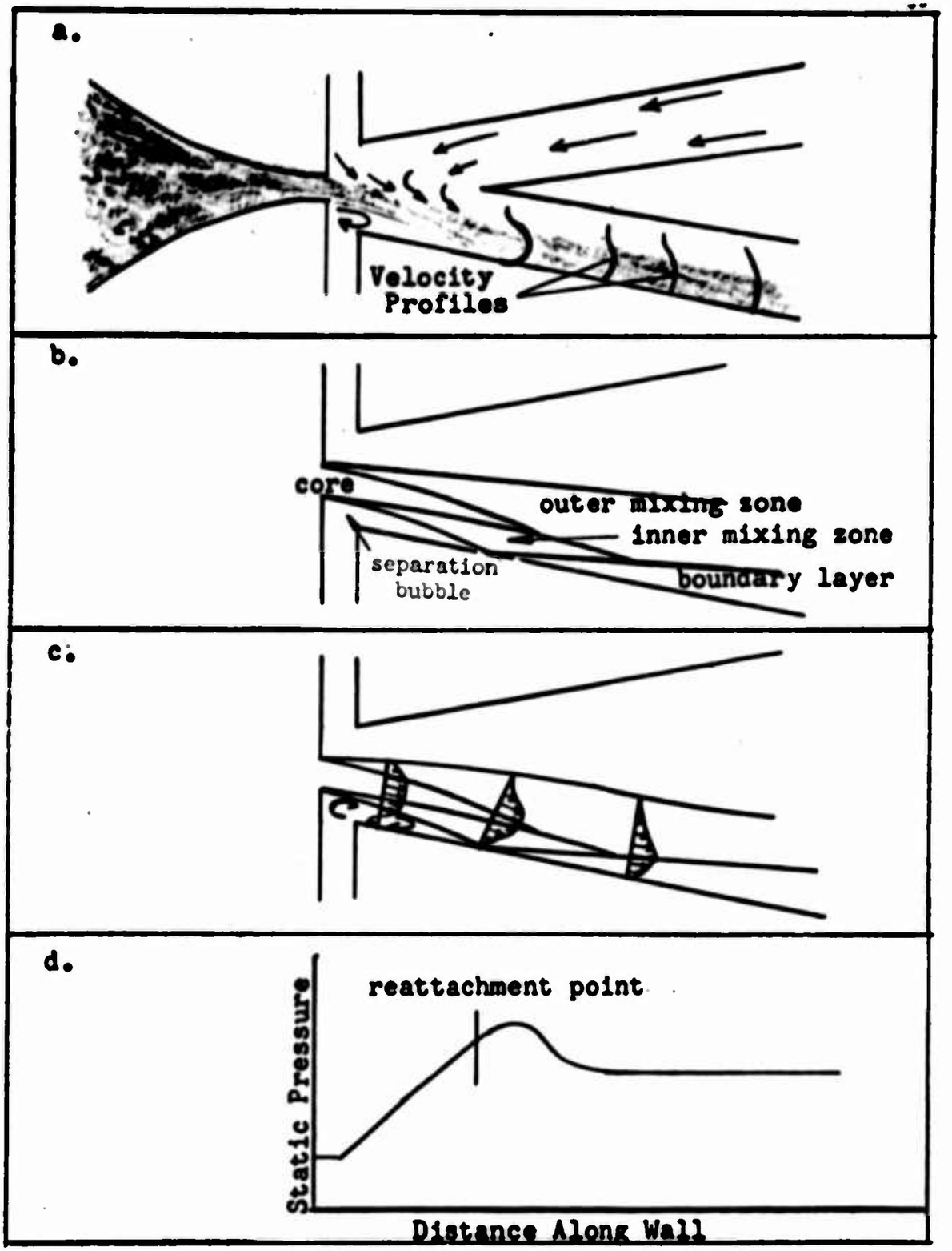

Figure 18 - Schematic of Channel Flow and Diffusion of Attached Jet

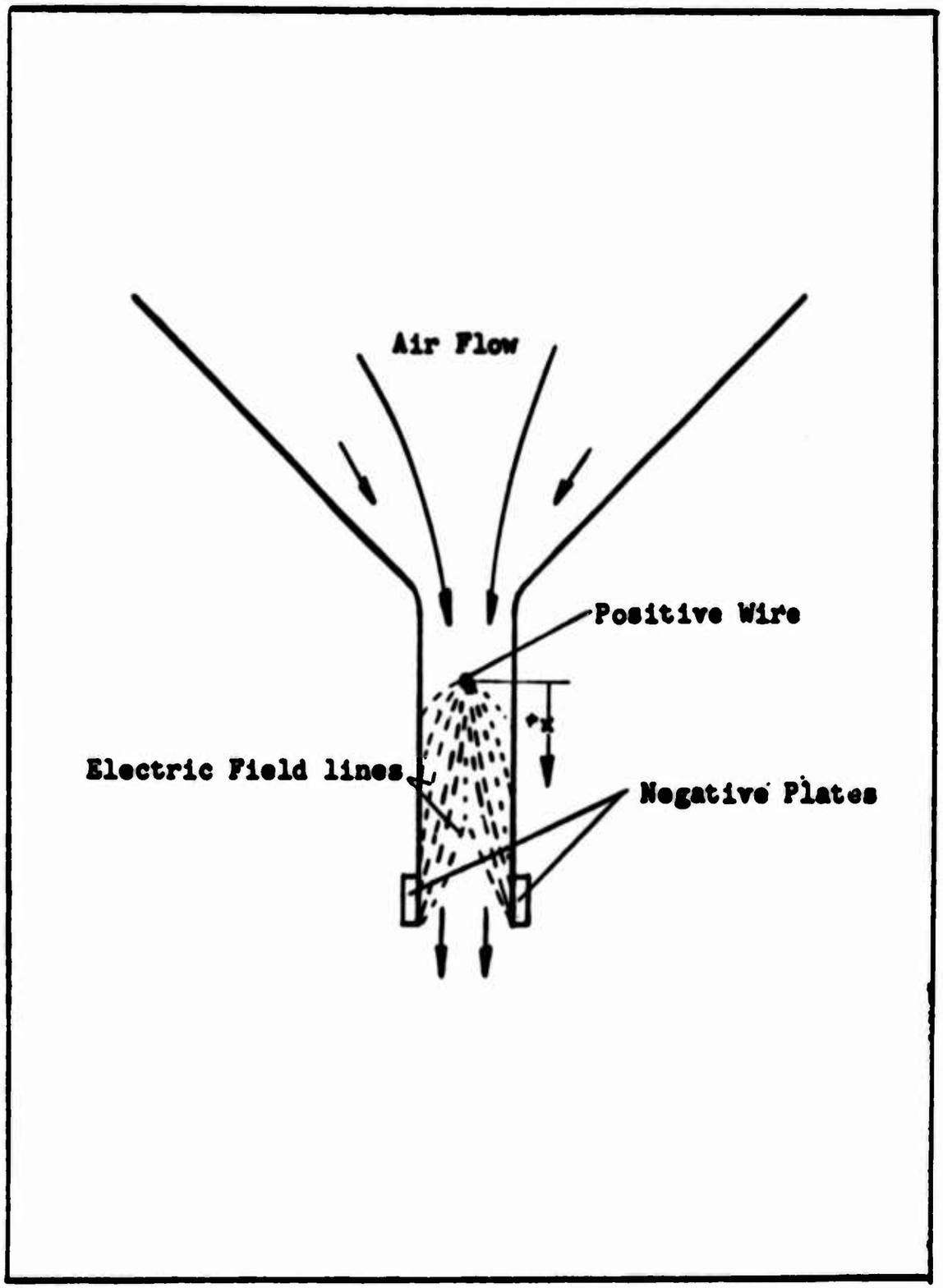

Figure 19 - Schematic of Flow in Control Nozzle

Figure 20 - Description of Test 1

Positive Electrode	0.004-inch steel wire
Negative Electrode	0.08-inch copper wire
Distance between Electrodes	0.30 inch
Distance from Nozzle Outlet to Electrodes - A	0.45 inch
Distance from Nozzle Outlet to Top Air Inlet - B	0.40 inch
Distance from Nozzle Outlet to Channel Inlet - C	0.60 inch
Channel Angle	0 degrees
Current	0 - 500 microamps
Voltage	0 - 11,000 volts
Reynolds Number	0 - 2800
Electrode Geometry	c - Fig. 15

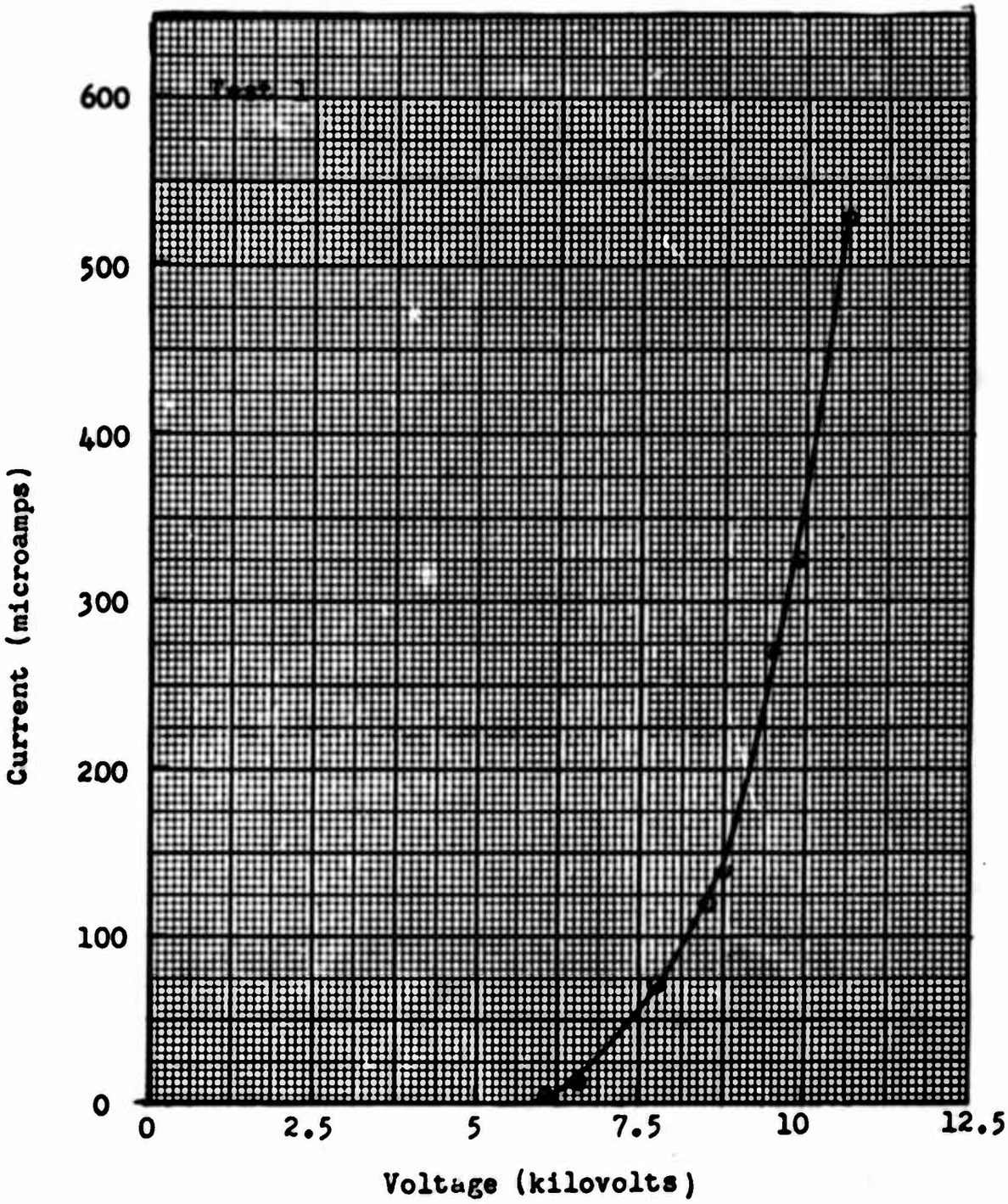

Figure 21 - Current-Voltage Relationship for a 0.004-Inch Wire 0.30 Inch Above a 0.08-Inch Copper Wire

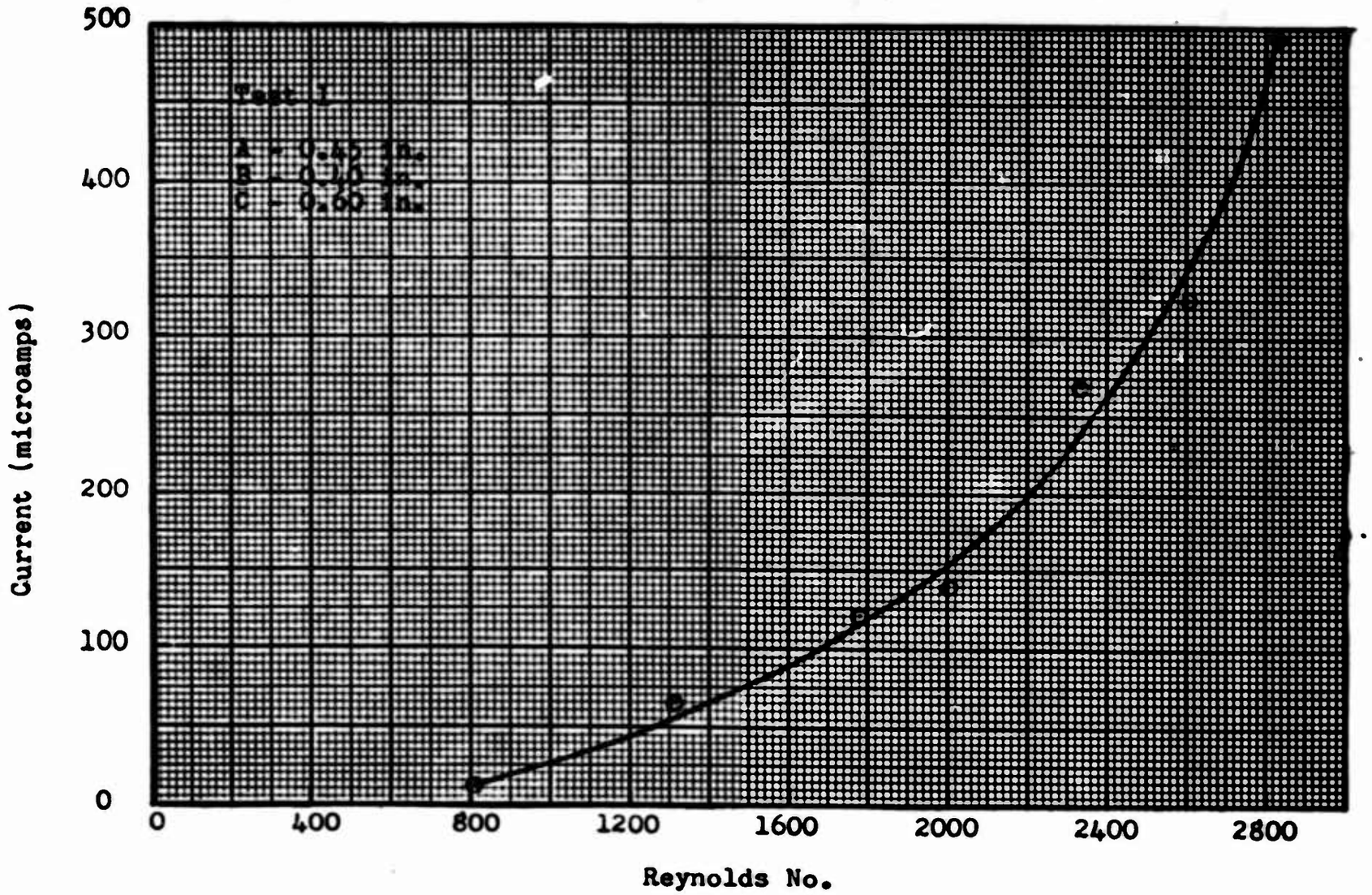

Figure 22. Current Required to Flip Flow from Top Plate to Bottom Plate at Various Reynolds Numbers

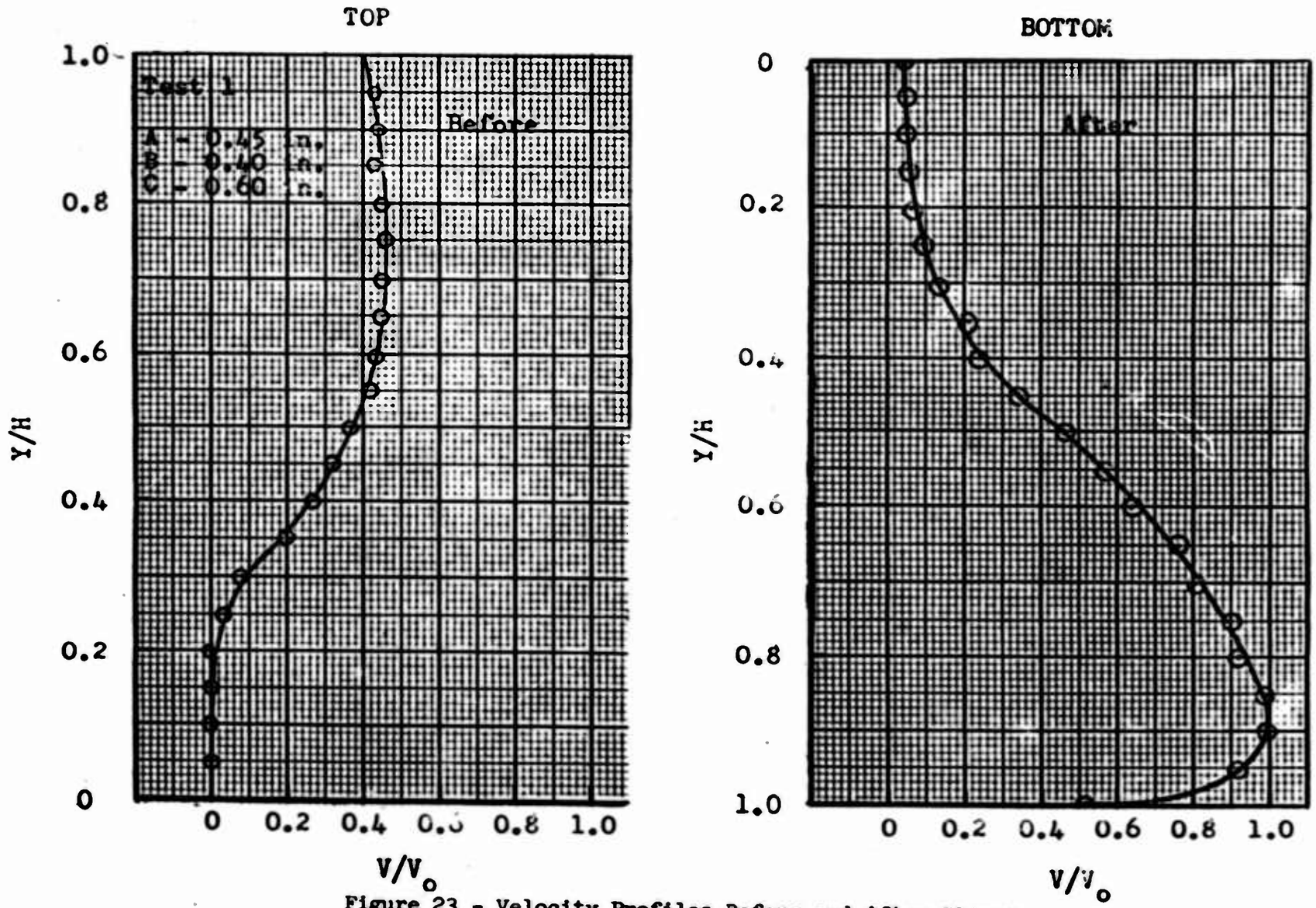

Figure 23 - Velocity Profiles Before and After Flipping

Figure 24 - Description of Test 2

Positive Electrode	0.004-inch steel wire
Negative Electrode	0.08-inch copper wire
Distance between Electrodes	0.75 inch
Distance from Nozzle Outlet to Electrodes - A	0.45 inch
Distance from Nozzle Outlet to Top Air Inlet - B	0.250, 0.275, 0.300 inch
Distance from Nozzle Outlet to Channel Inlet - C	0.60 inch
Channel Angle	0 degrees
Current	0 - 30 microamps
Voltage	0 - 22,000 volts
Reynolds Number	700 - 2200
Electrode Geometry	c - Fig. 15

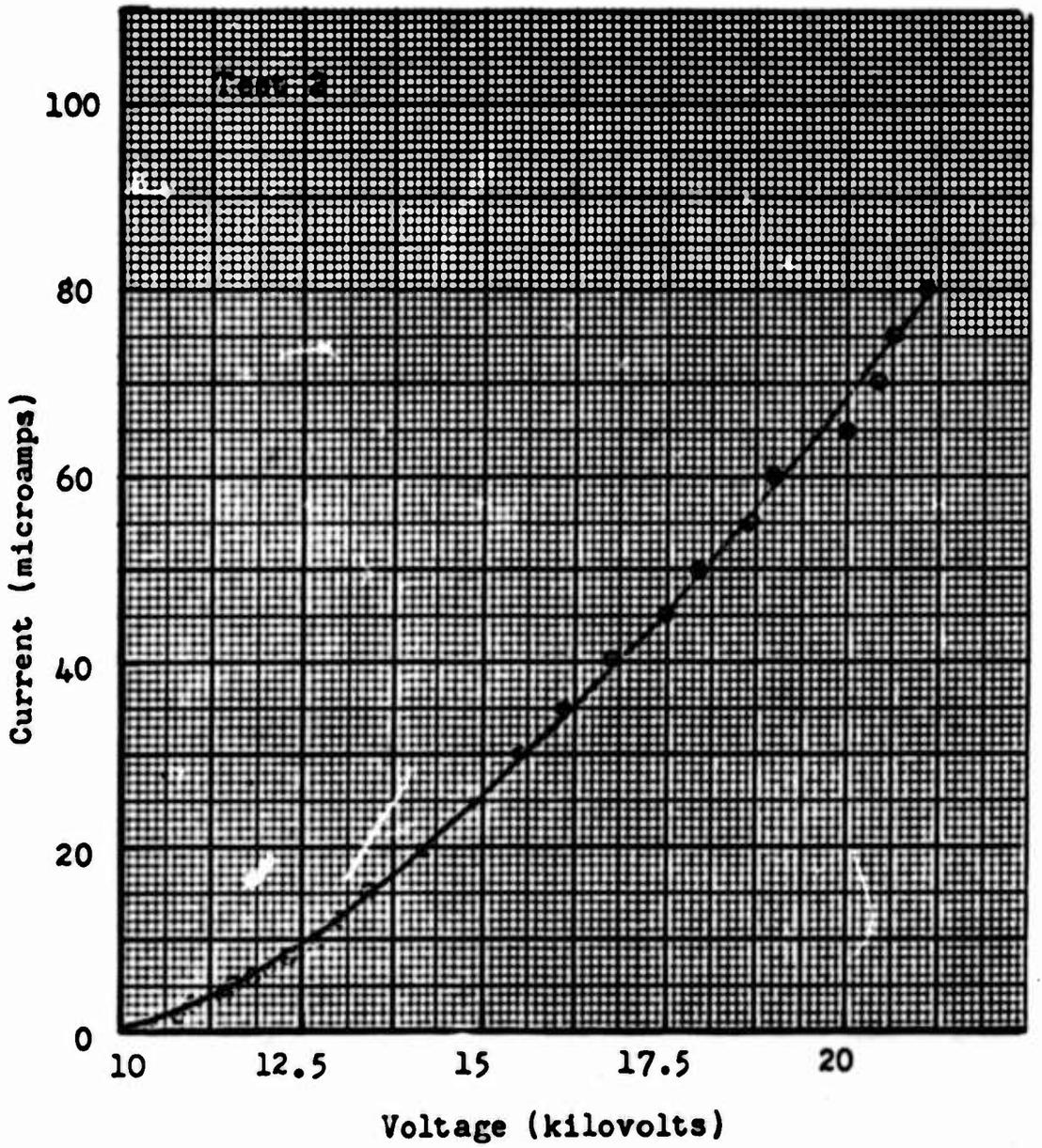

Figure 25 - Current-Voltage Relationship. 0.004-Inch Wire 0.75-Inch above 0.08-Inch Copper Wire

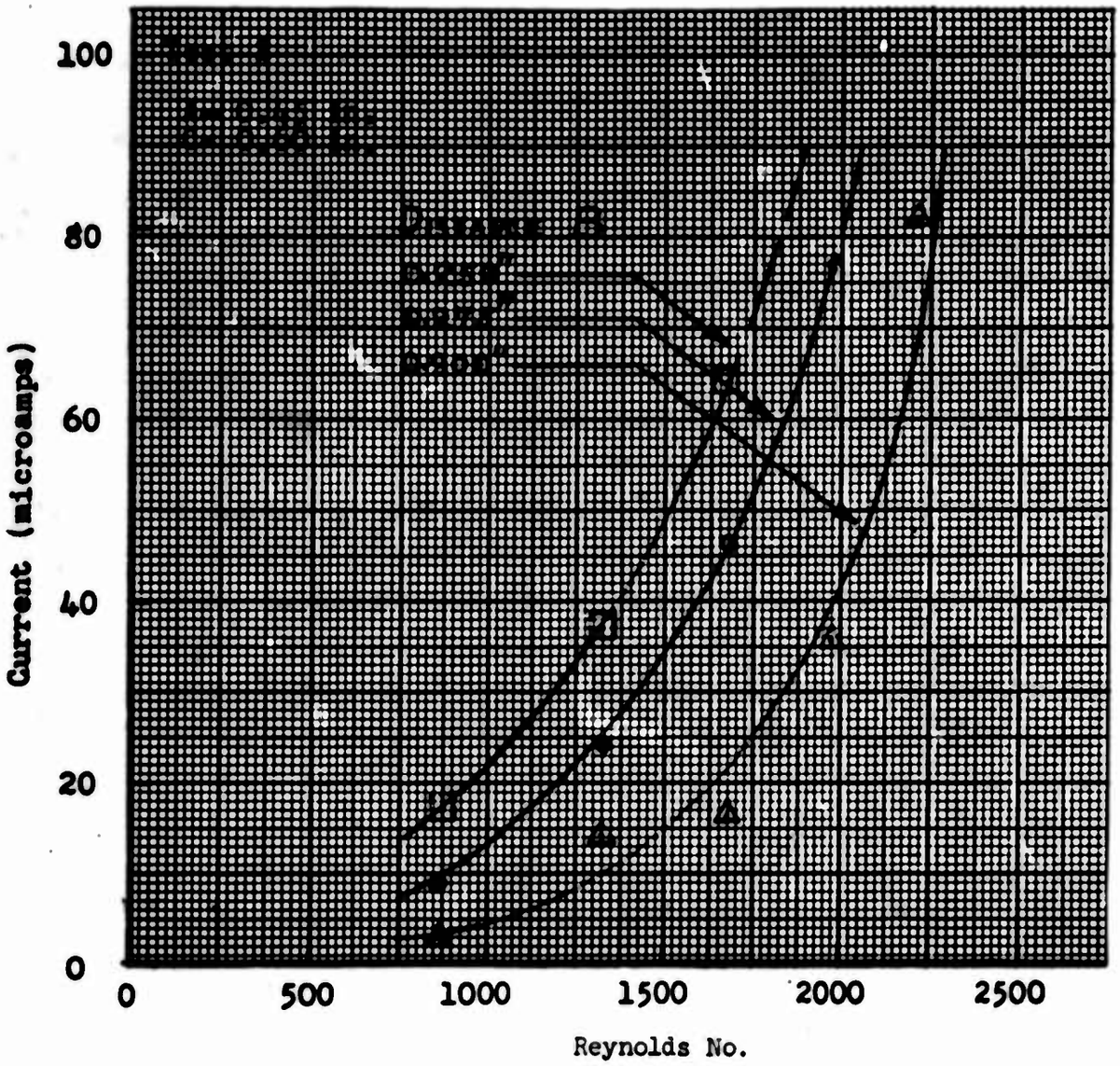

Figure 26 - Current Required to Flip Flow from Top Plate to Bottom Plate with Various Reynolds Numbers

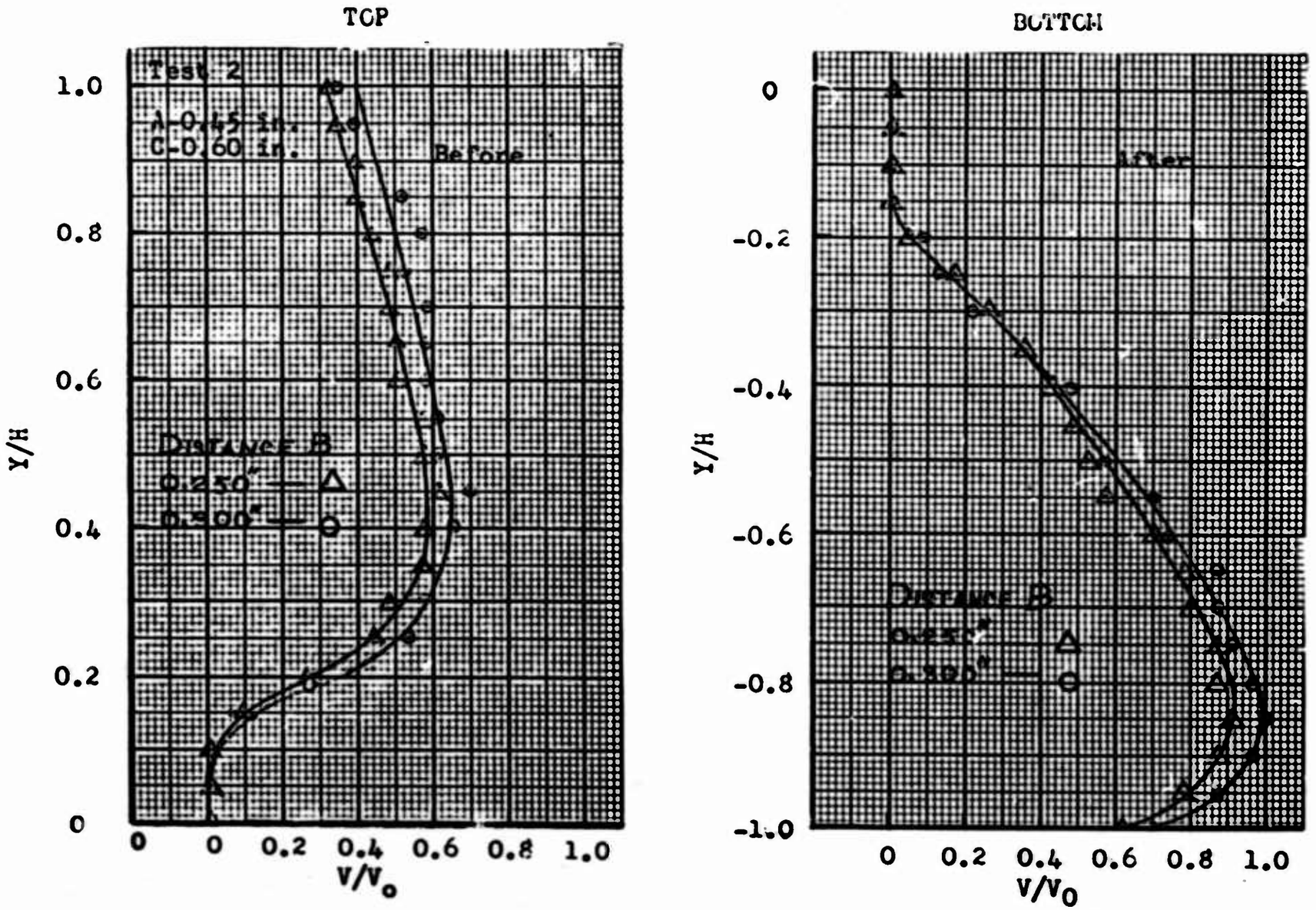

Figure 27 - Velocity Profile Before and After Flipping

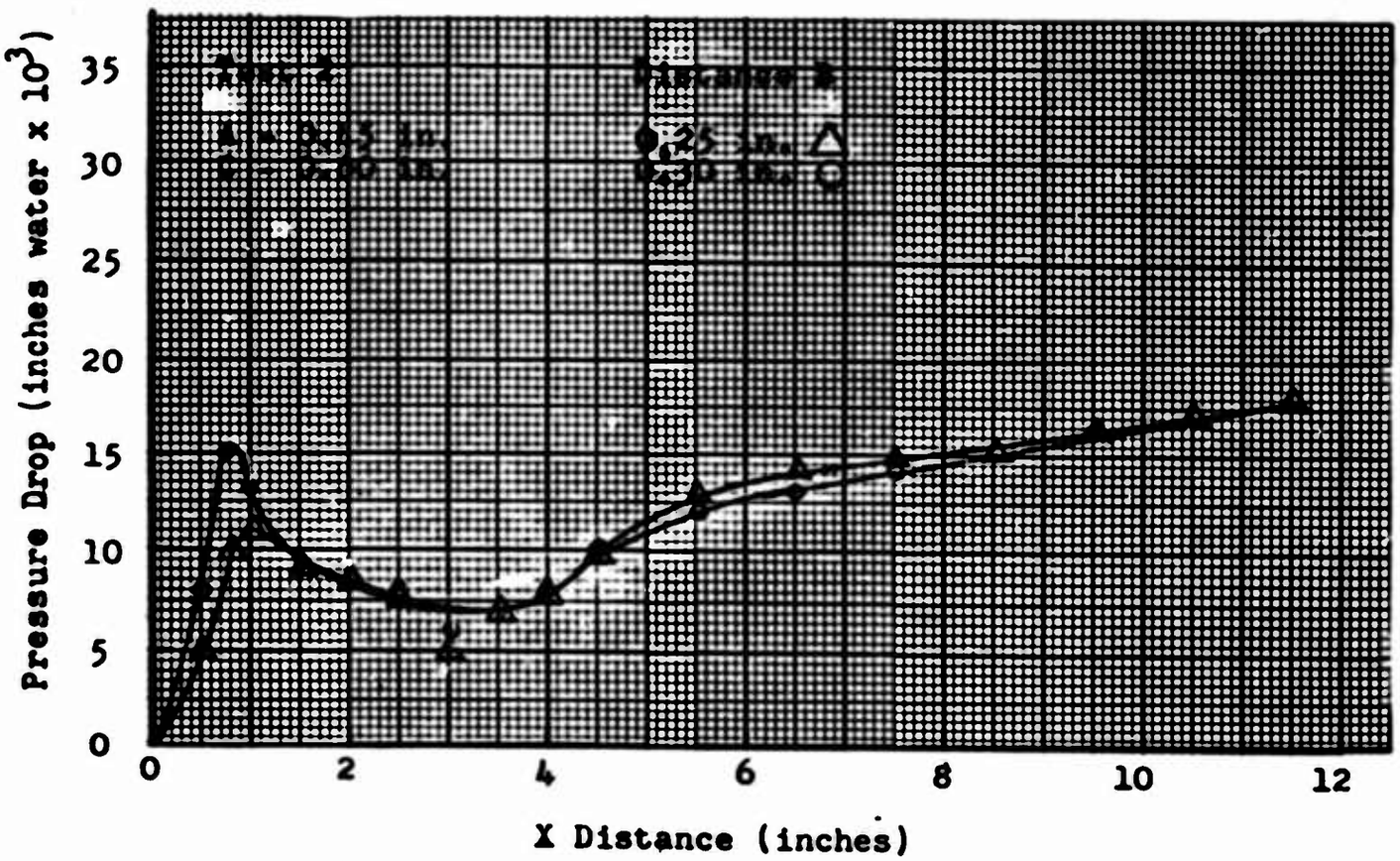

Figure 28 - Static Pressure Drop Along Bottom Plate with Flow Attached to It

Figure 29 - Description of Test 3

Positive Electrode	0.004-inch steel wire
Negative Electrode	0.08-inch copper wire
Distance between Electrodes	0.75 inch
Distance from Nozzle Outlet to Electrodes - A	1.00 inch
Distance from Nozzle Outlet to Top Air Inlet - B	0.050, 0.75, 0.100 inch
Distance from Nozzle Outlet to Channel Inlet - C	1.15 inches
Channel Angle	0 degrees
Current	0 - 80 microamps
Voltage	0 - 20,000 volts
Reynolds Number	700 - 2200
Electrode Geometry	c - Fig. 15

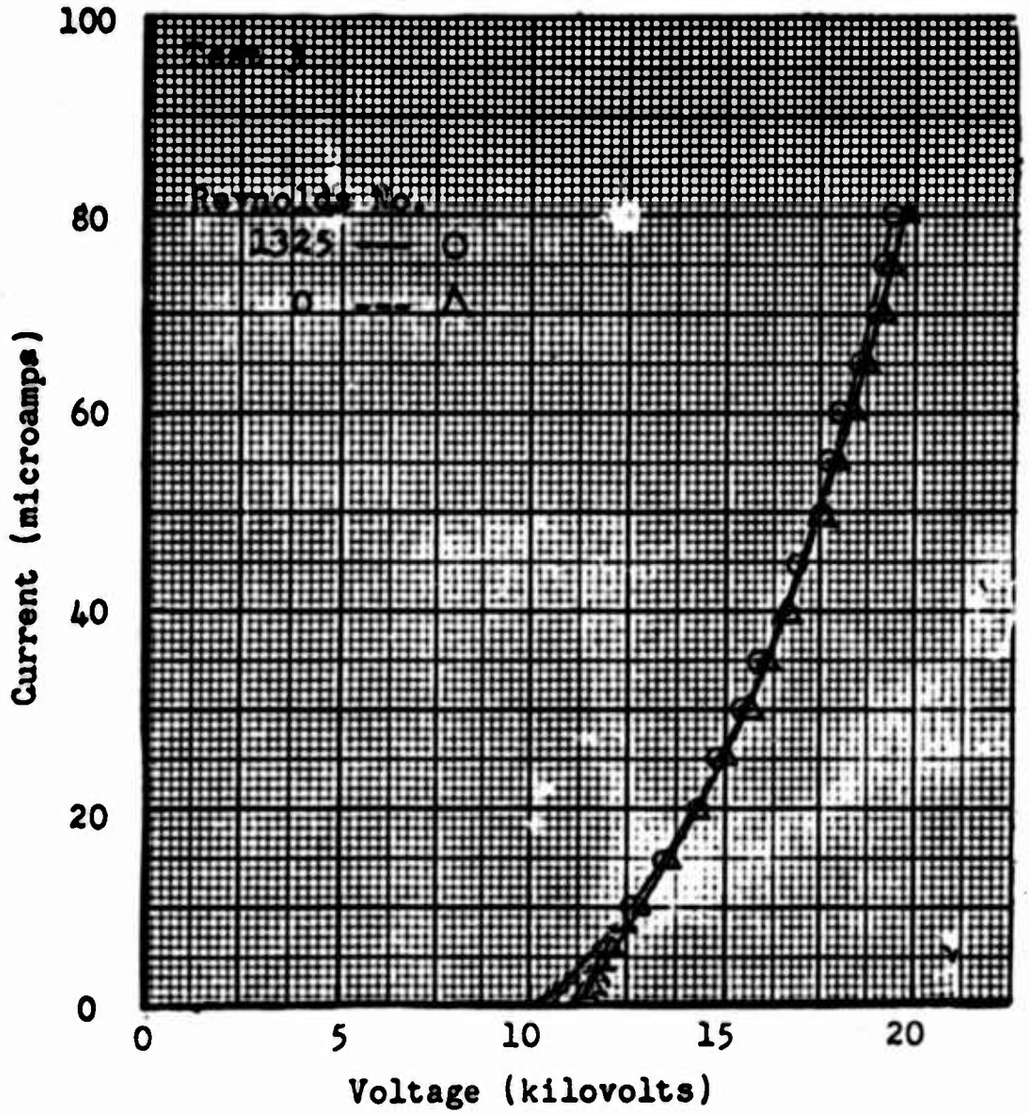

Figure 30 - Current-Voltage Relationship. 0.004-Inch Wire 0.75-Inch above 0.08-Inch Copper Wire

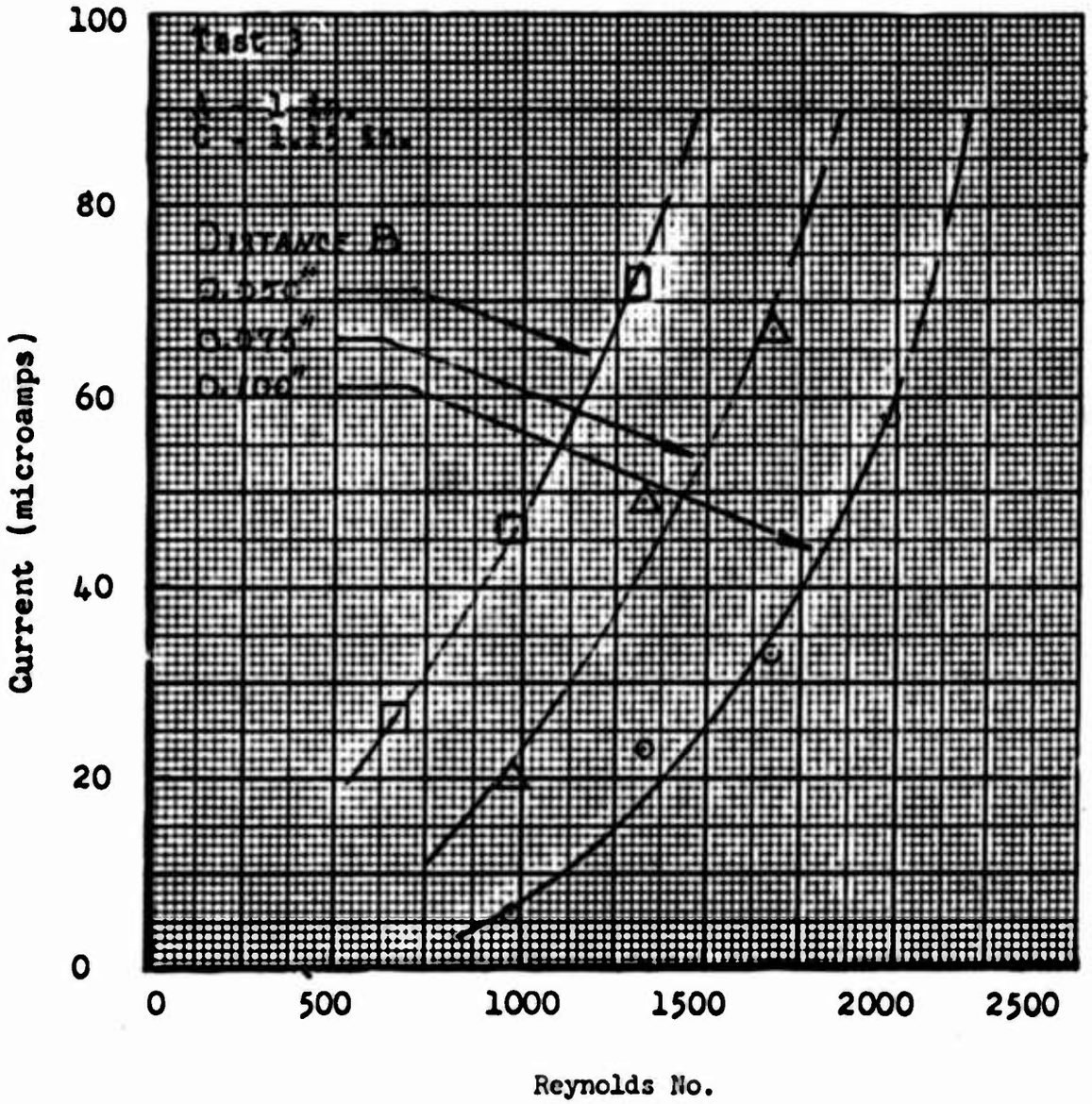

Figure 31 - Current Required to Flip Flow from Top Plate to Bottom Plate at Various Reynolds Numbers

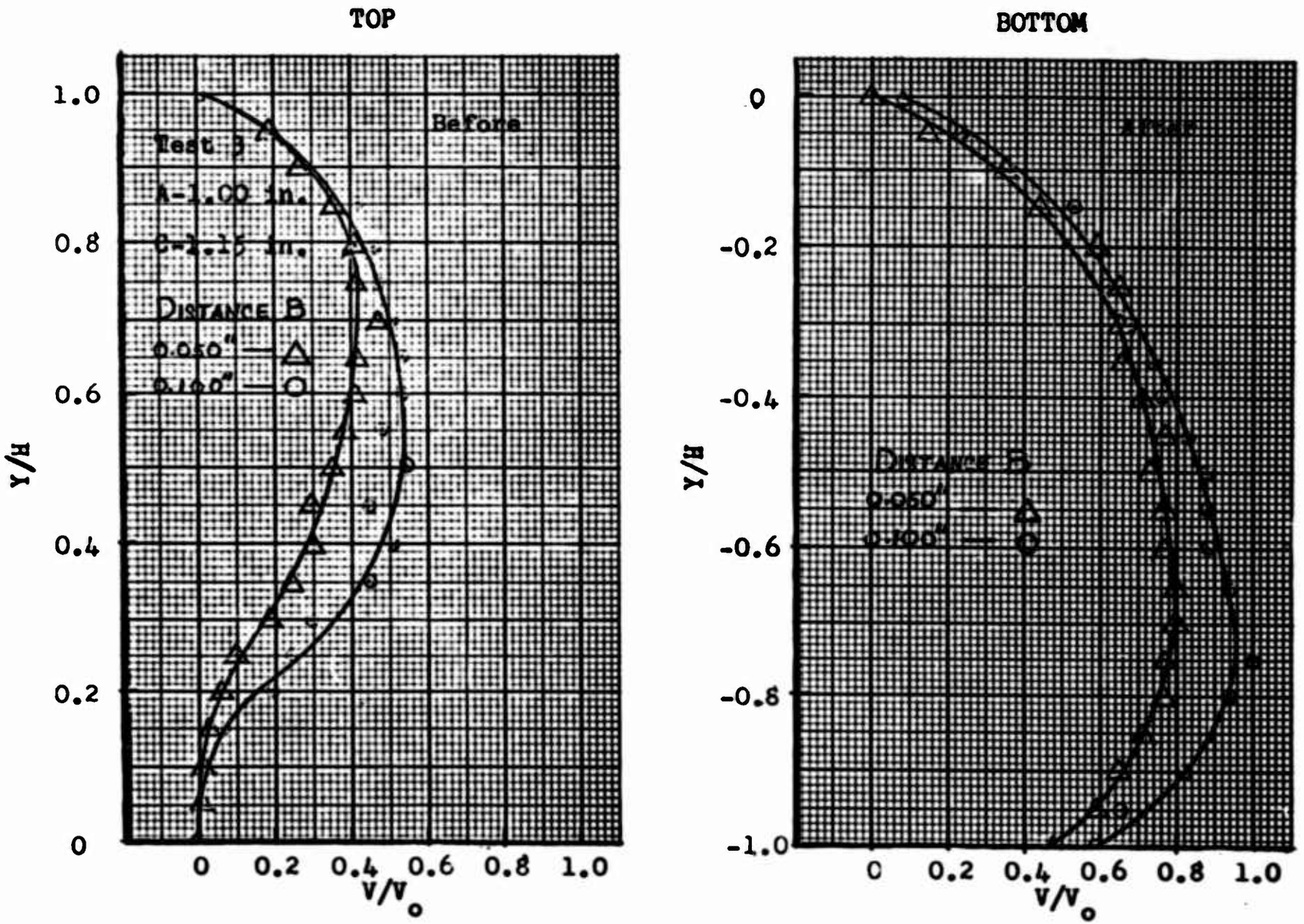

Figure 32 - Velocity Profile before and after Flipping

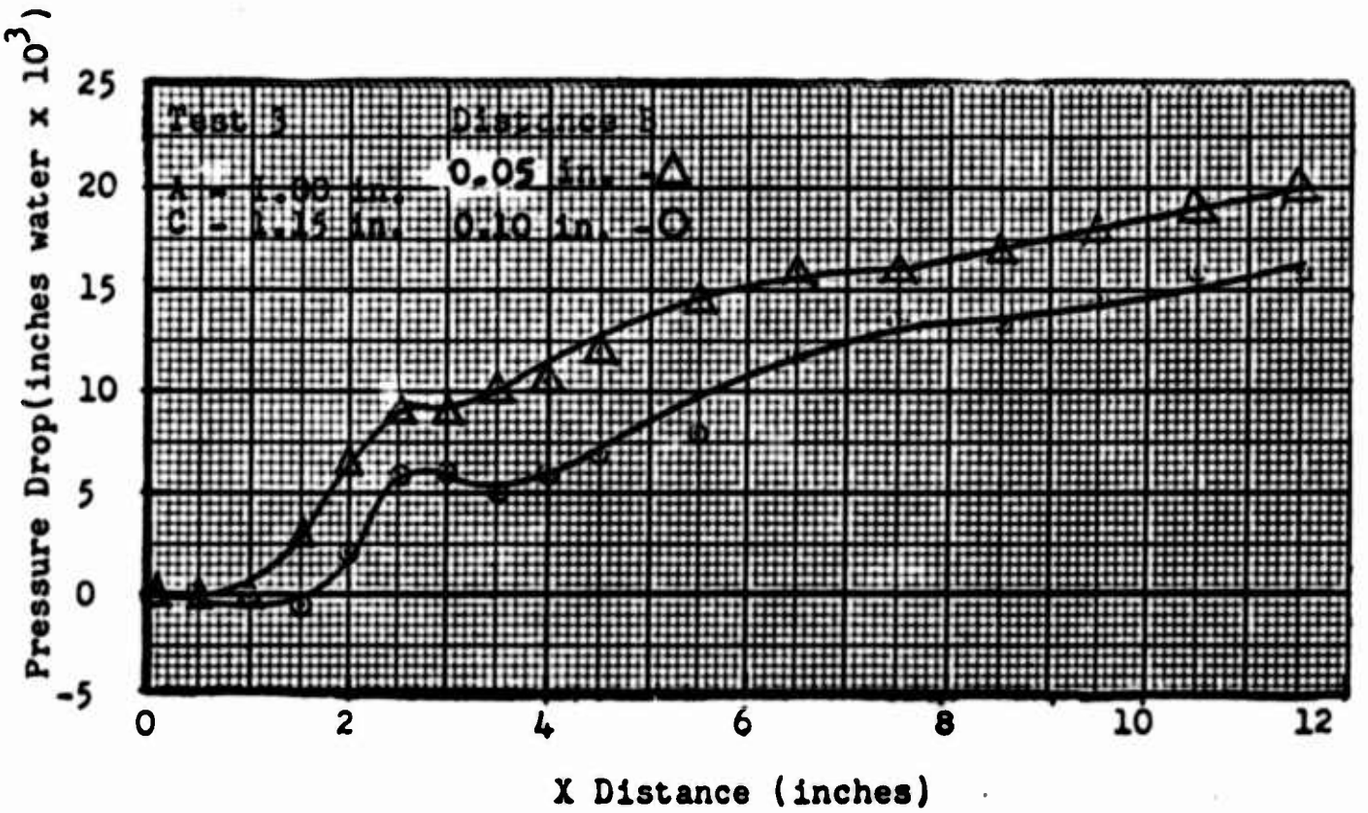

Figure 33 - Static Pressure Drop Along Bottom Plate with Flow Attached to It

Figure 34 - Description of Test 4

Positive Electrode	0.004-inch steel wire
Negative Electrode	0.08-inch copper wire
Distance between Electrodes	0.75 inch
Distance from Nozzle Outlet to Electrodes - A	0.45 inch
Distance from Nozzle Outlet to Top Air Inlet - B	0.225, 0.250, 0.275 inch
Distance from Nozzle Outlet to Channel Inlet - C	1.60 inches
Channel Angle	0 degrees
Current	0 - 120 microamps
Voltage	0 - 22,500 volts
Reynolds Number	700 - 2200
Electrode Geometry	c - Fig. 15

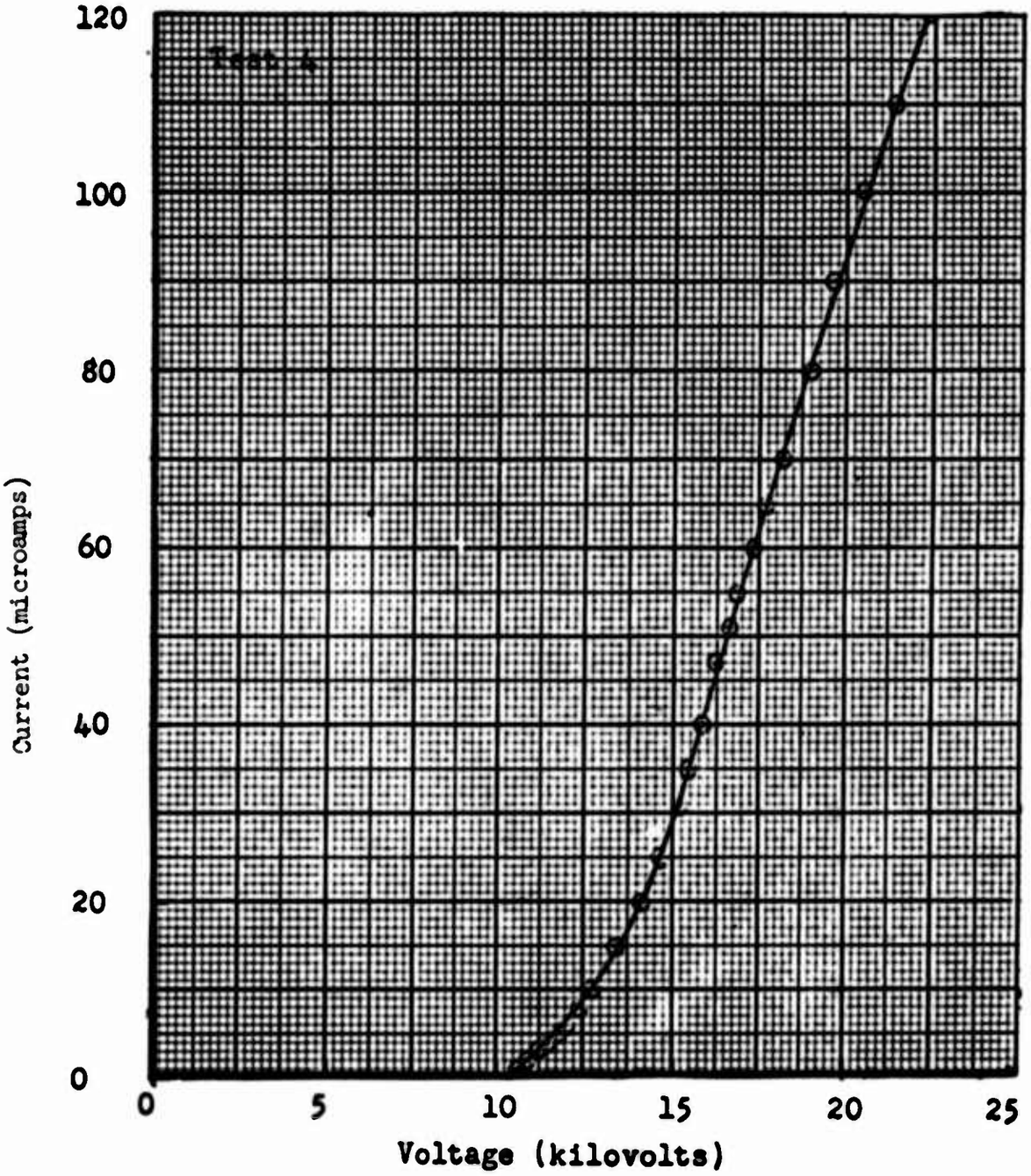

Figure 35 - Current-Voltage Relationship. 0.004-Inch Wire 0.75-Inch above 0.08-Inch Copper Wire

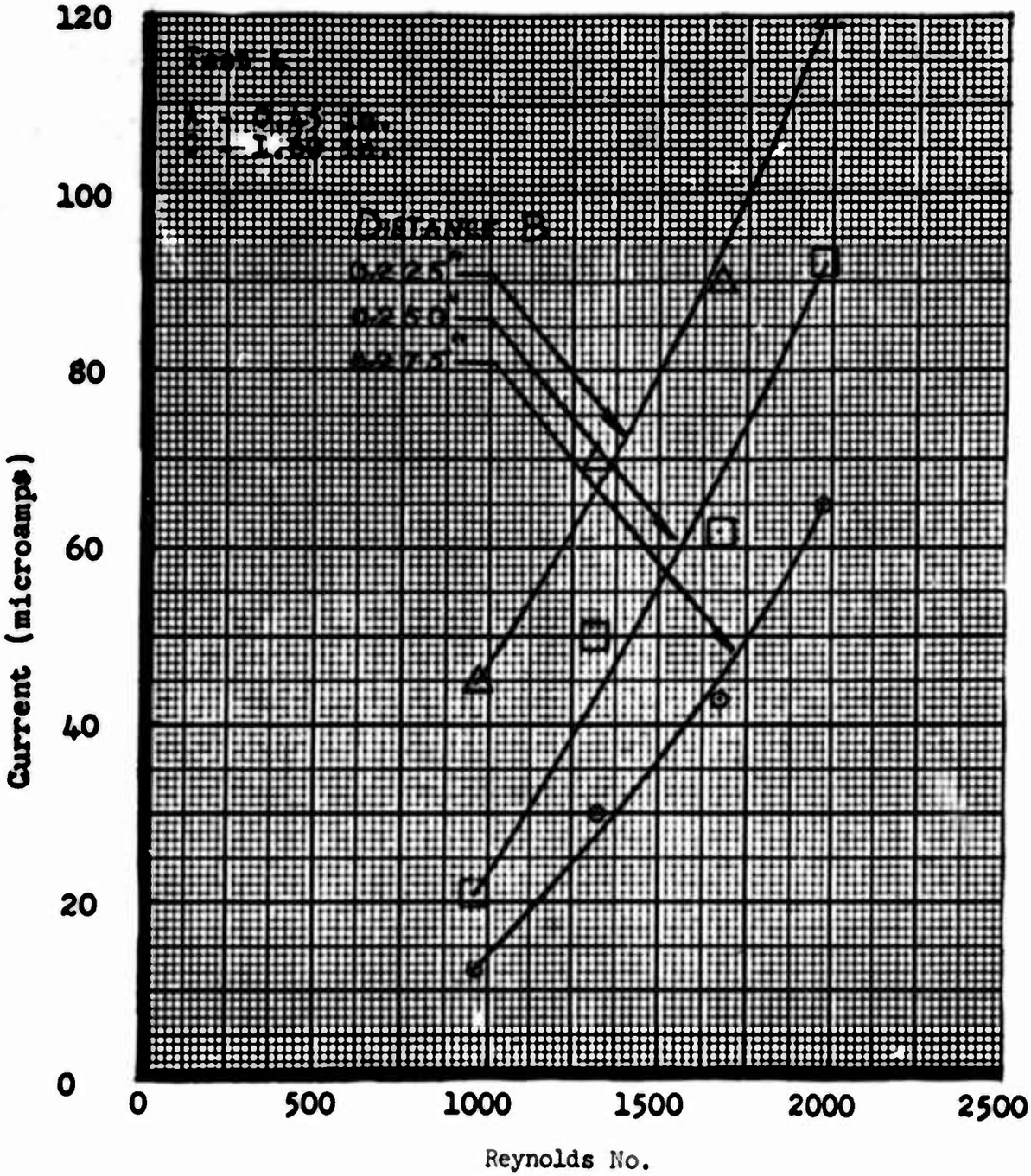

Figure 36 - Current Required to Flip Flow from Top Plate to Bottom Plate at Various Reynolds Numbers

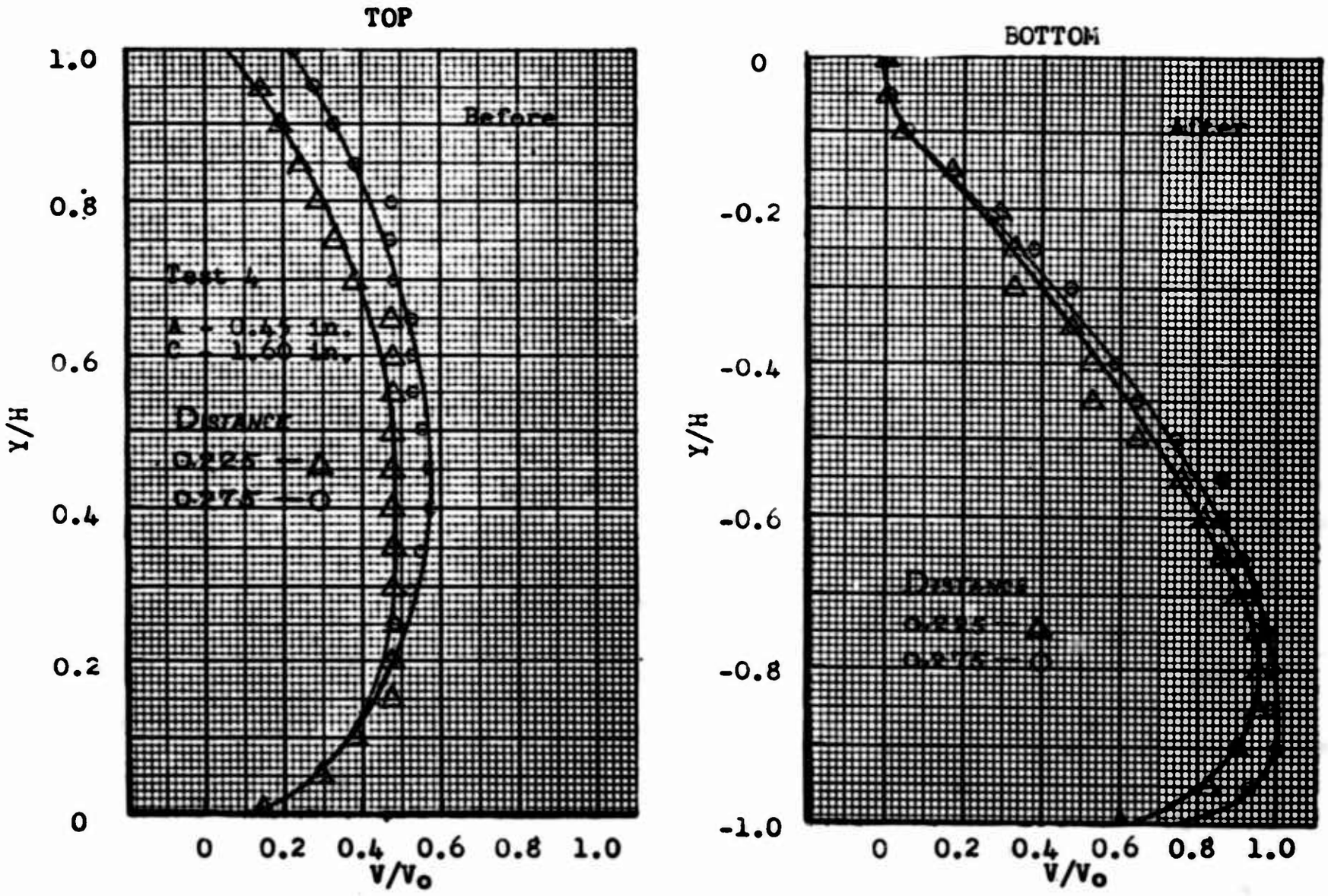

Figure 37 - Velocity Profile before and after Flipping

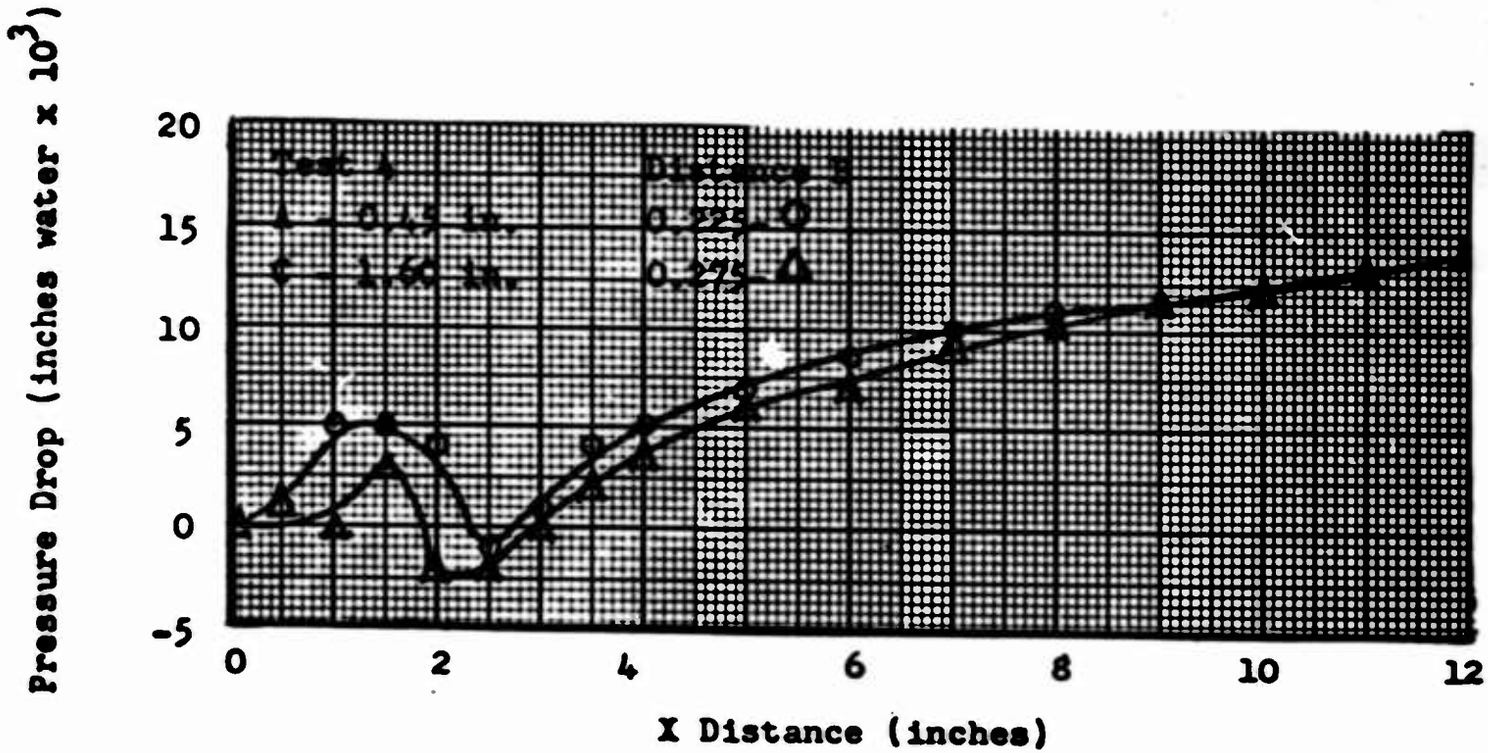

Figure 38 - Static Pressure Drop Along Bottom Plate with Flow Attached to It

Figure 39 - Description of Tests 5, 6, and 7

Positive Electrode	0.004-inch steel wire
Negative Electrode	5.44 x 0.15 x 0.08-inch flat brass plate
Distance between Electrodes	0.75 inch (maximum)
Width of Control Nozzle	0.32 inch
Horizontal Distance from Nozzle Outlet to Center of Control Nozzle	0.26 inch
Horizontal Distance from Nozzle Outlet to Channel Inlet	0.57 inch
Channel Angle	Up 2,4 degrees, down 2 degrees
Current	0 - 100 microamps
Voltage	0 - 22,000 volts
Reynolds Number	600 - 2,000
Electrode Geometry	Fig. 19

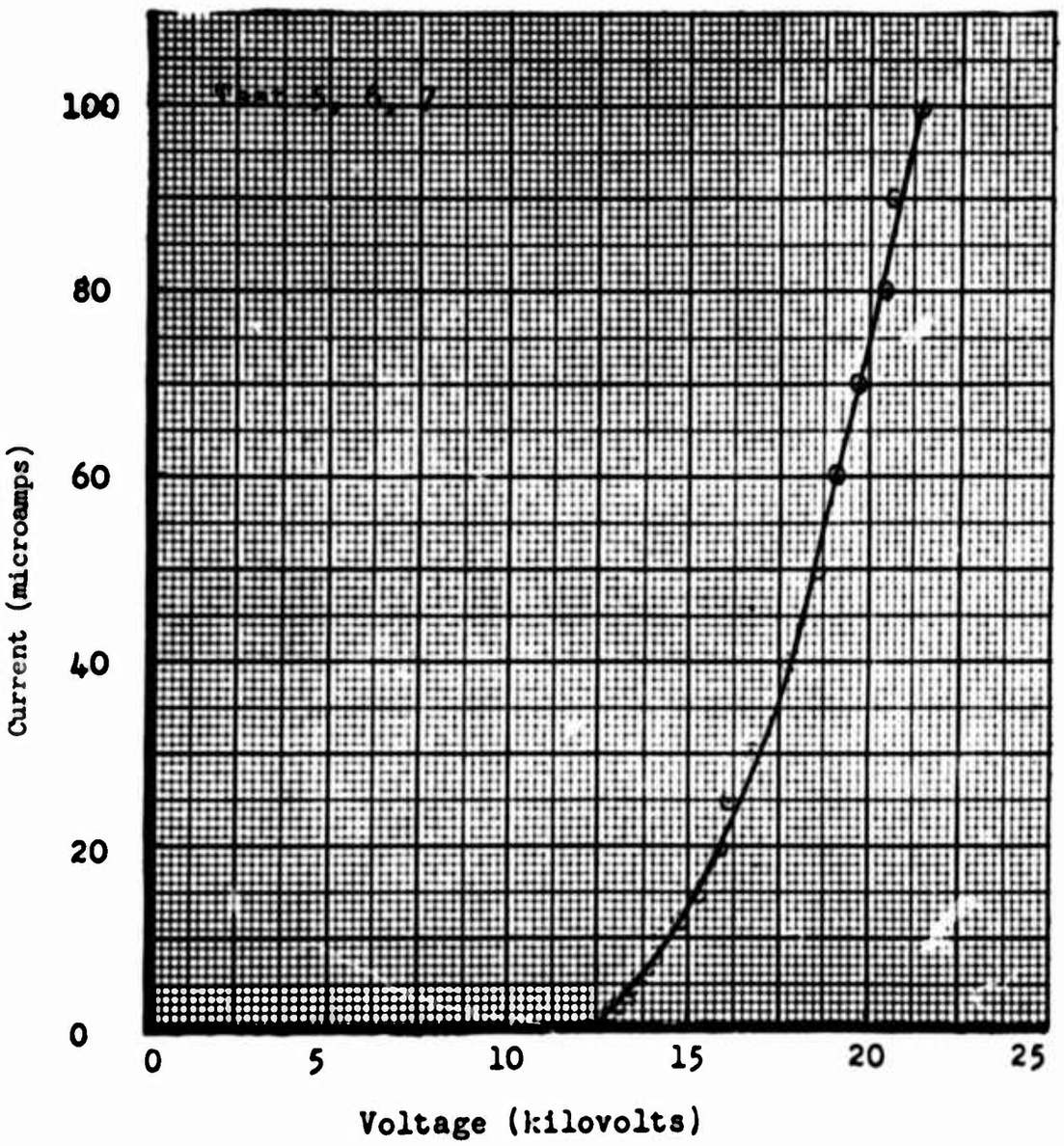

Figure 40 - Current-Voltage Relationship for Control Nozzle. 0.004-Inch Wire 0.75-Inch above Nozzle Outlet. Nozzle Height 0.32 Inch

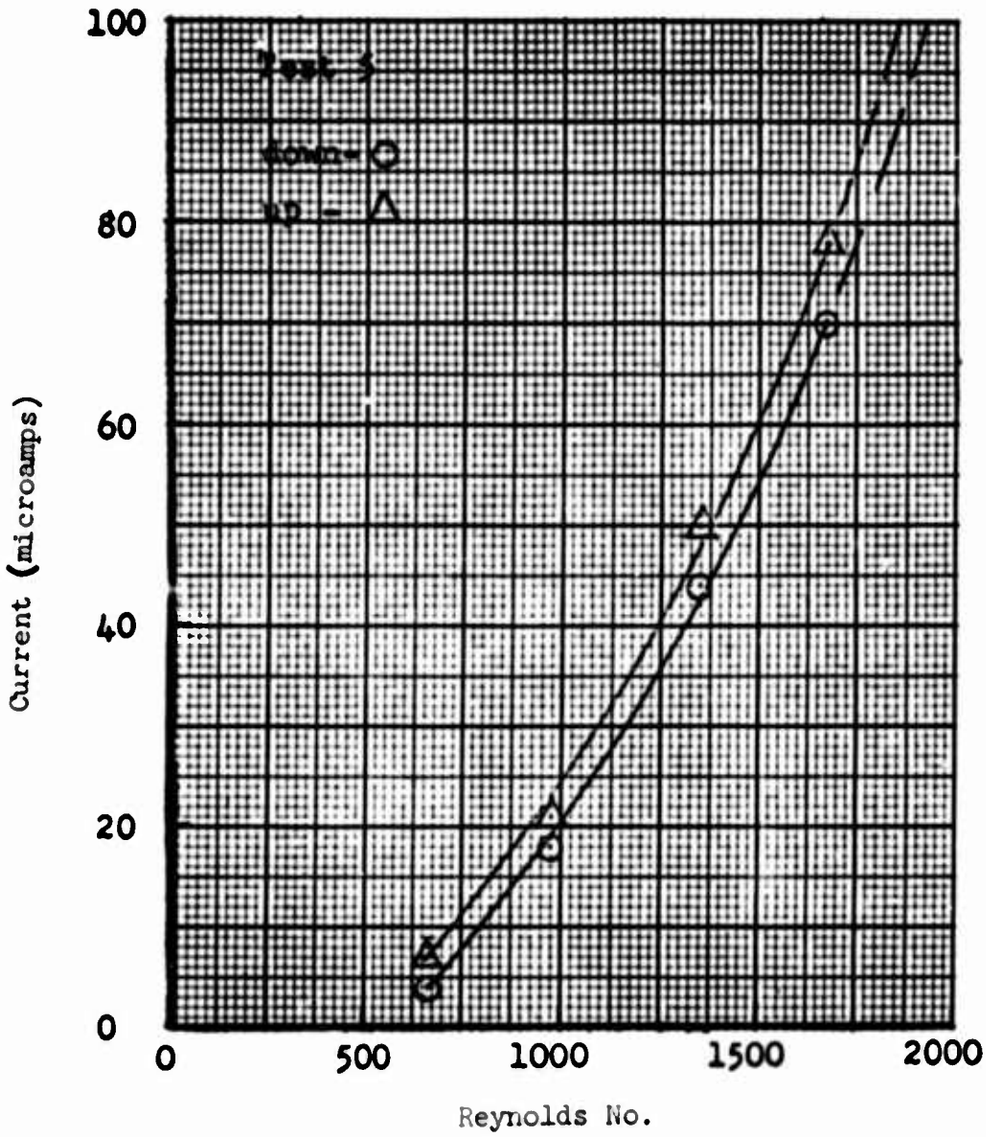

Figure 41 - Current Required to Flip Flow up to Top Plate and Down to Bottom Plate at Various Reynolds Numbers. Channel Tilted up Two Degrees

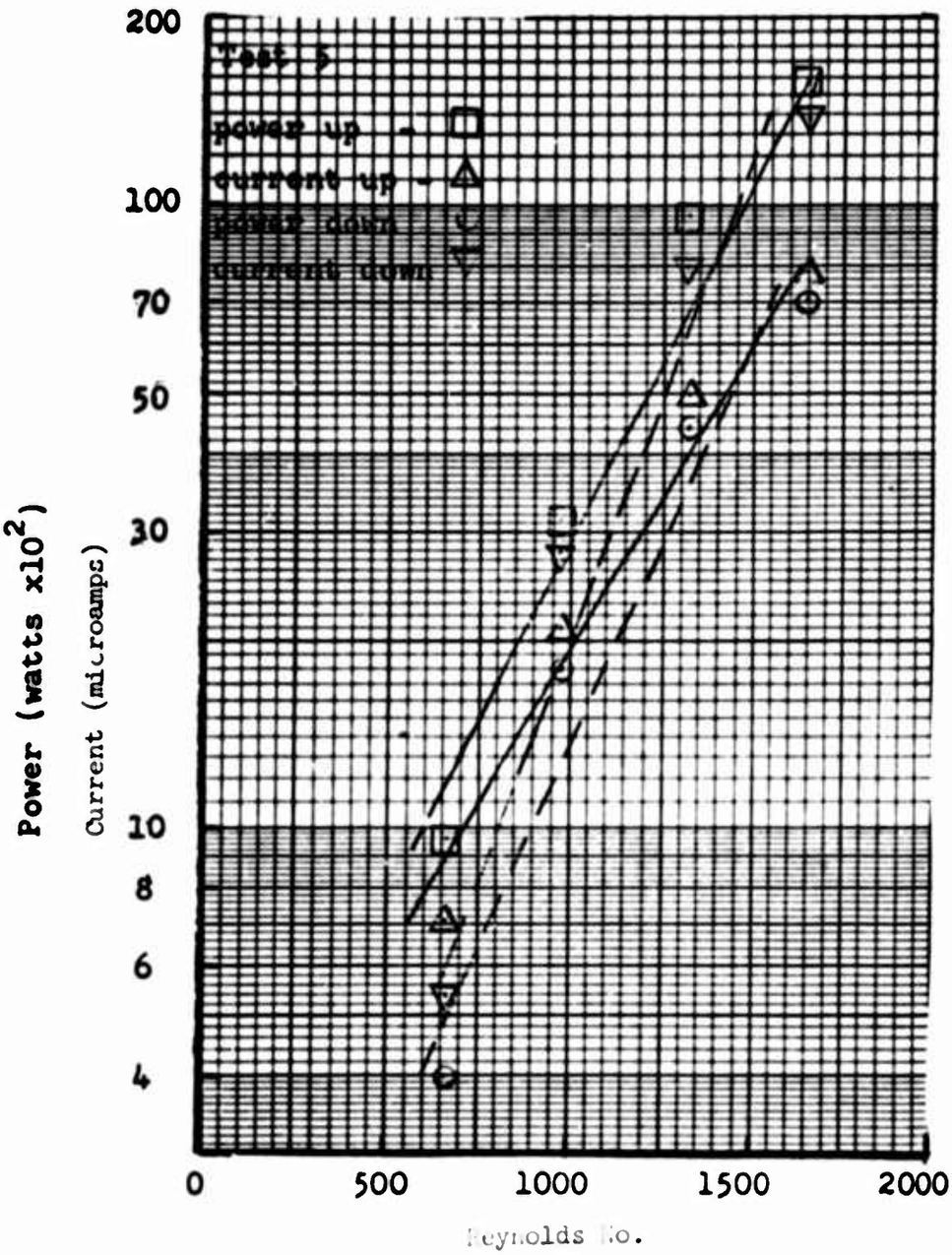

Figure 42 - Power and Current Required to Flip Flow Both Ways at Various Reynolds Numbers. Channel Tilted up Two Degrees

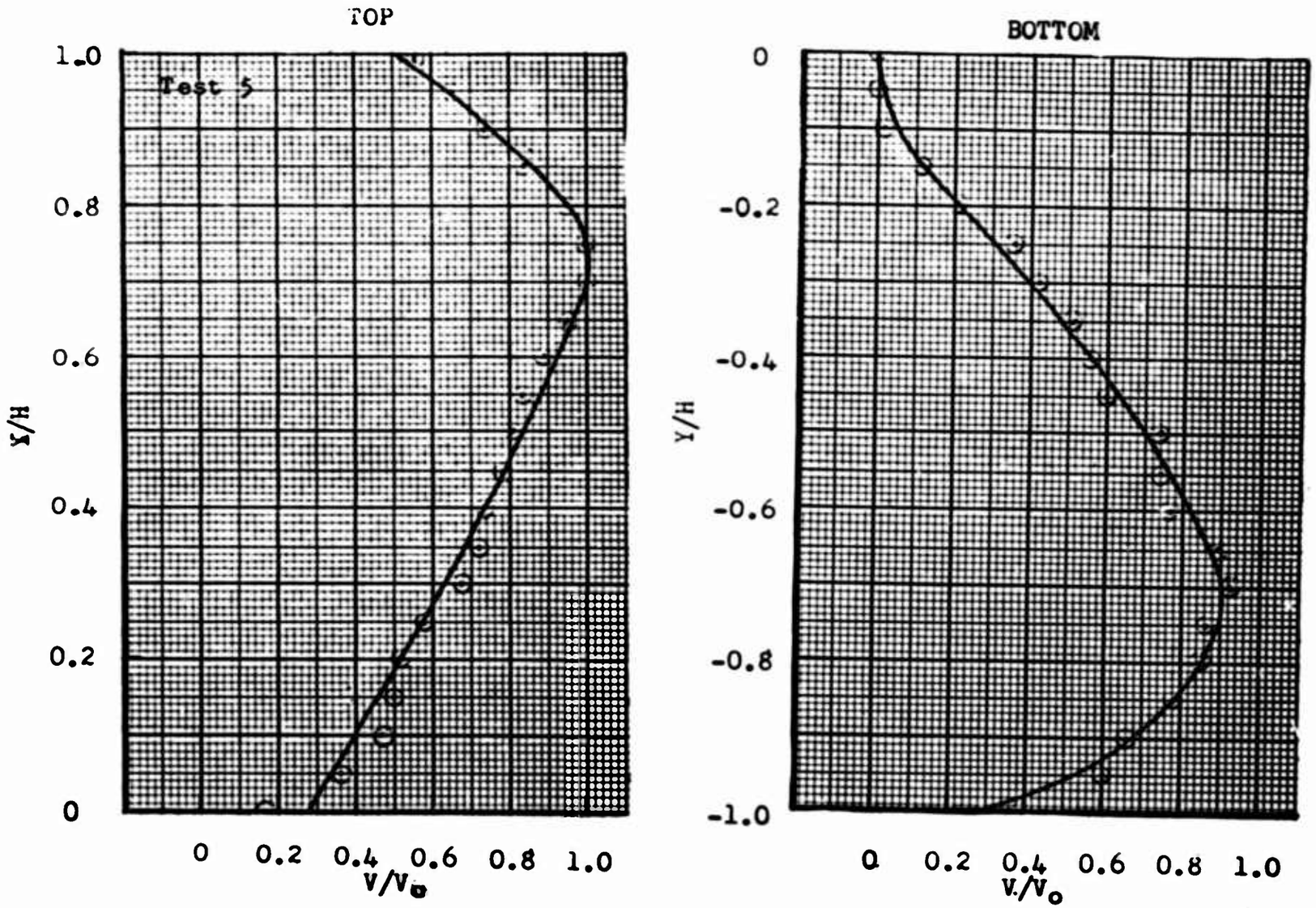

Figure 43 - Velocity Profiles before and after Flipping Both Ways.
Channel Tilted up Two Degrees

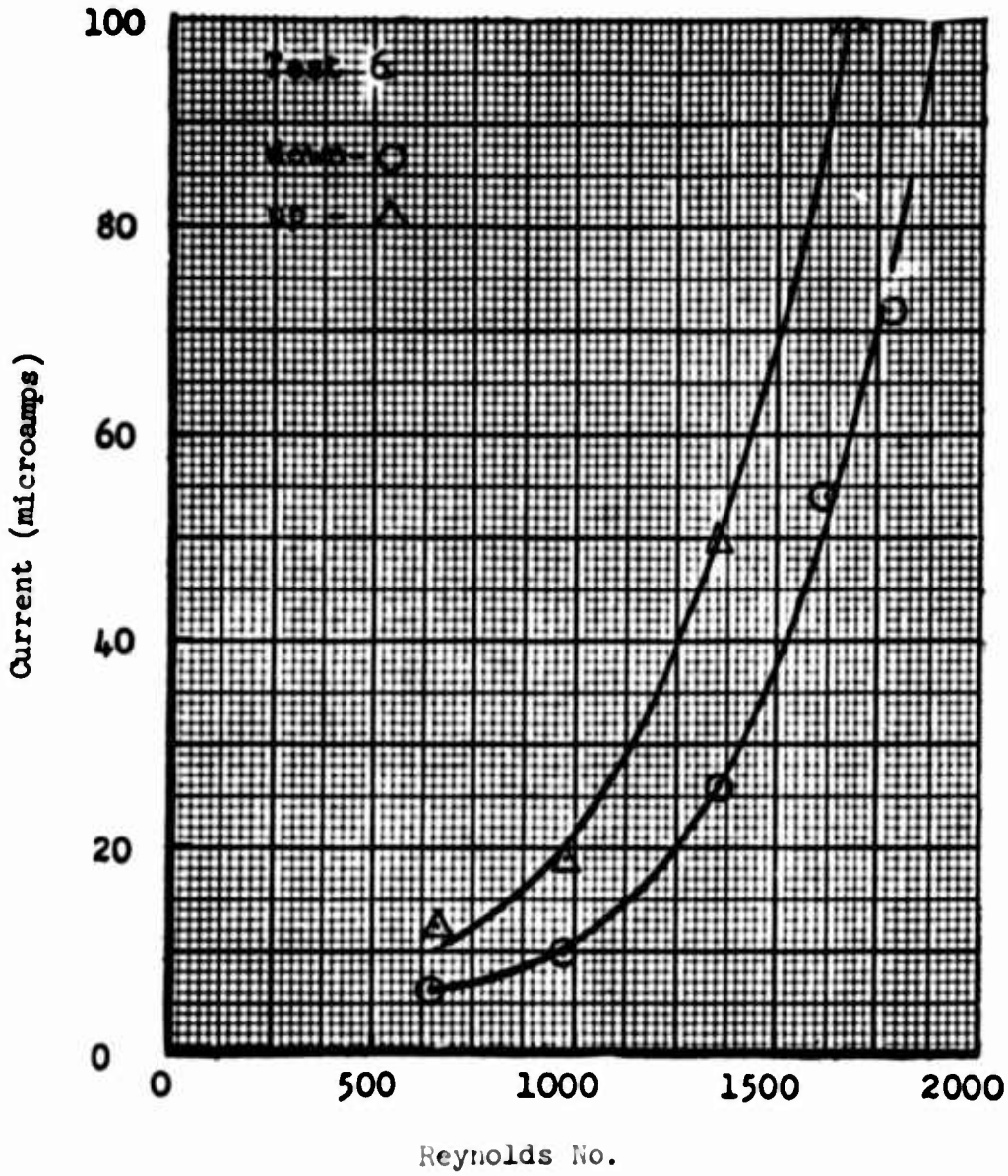

Figure 44 - Current Required to Flip Flow Both Ways at Various Reynolds Numbers. Channel Tilted up Four Degrees

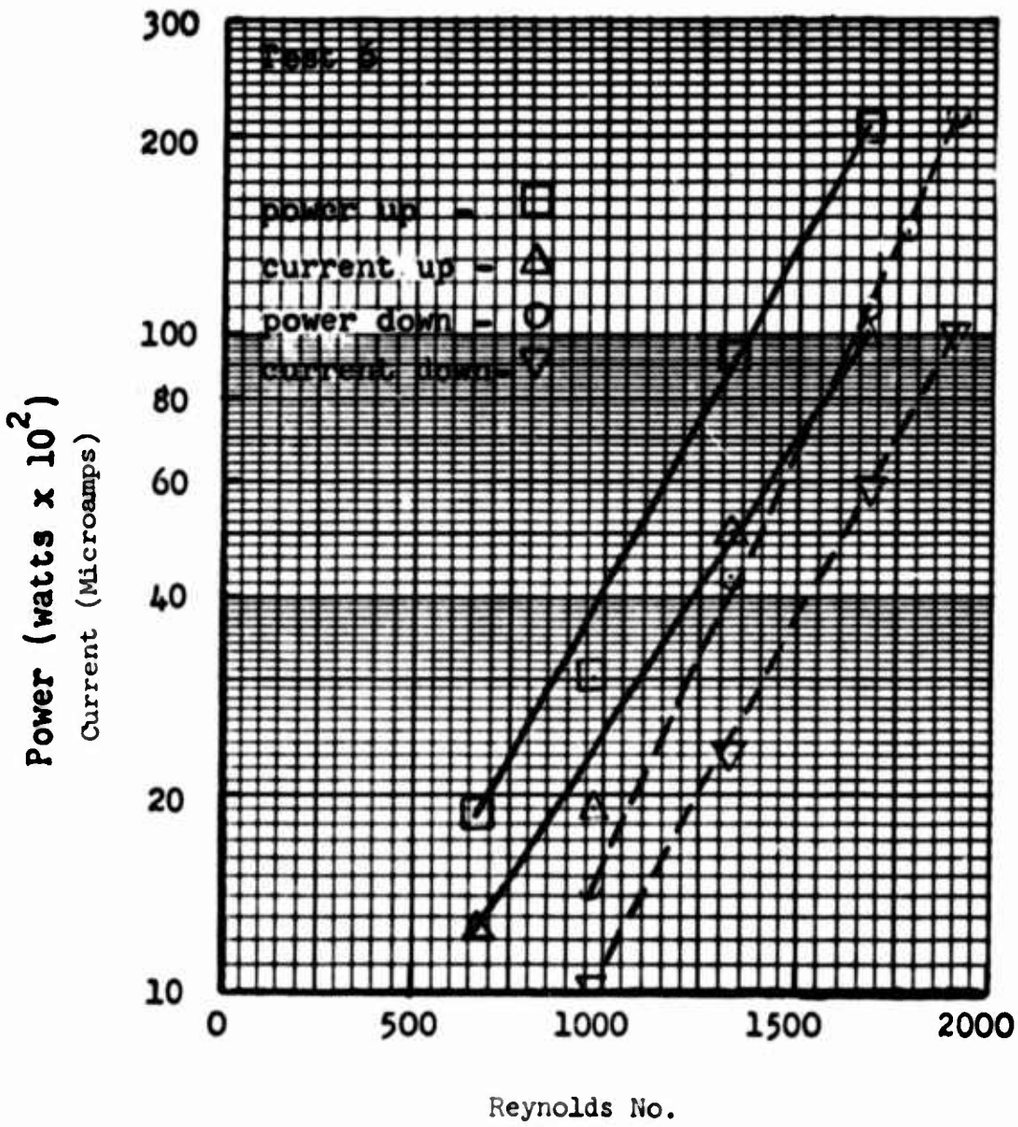

Figure 45 - Power and Current to Flip Flow Both Ways at Various Reynolds Numbers. Channel Tilted up Four Degrees

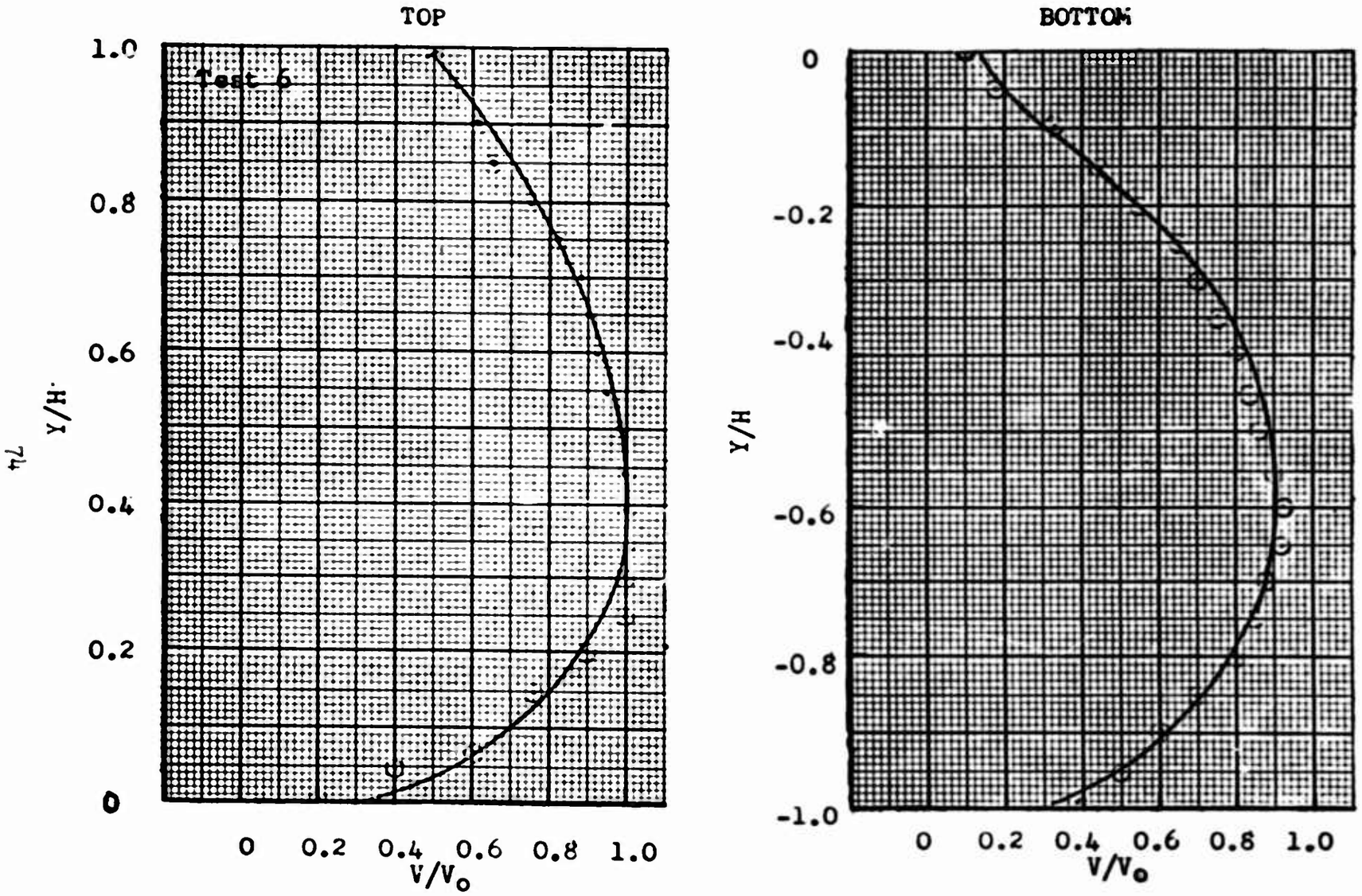

Figure 46 - Velocity Profiles before and after Flipping Both Ways.
Channel Tilted up Four Degrees

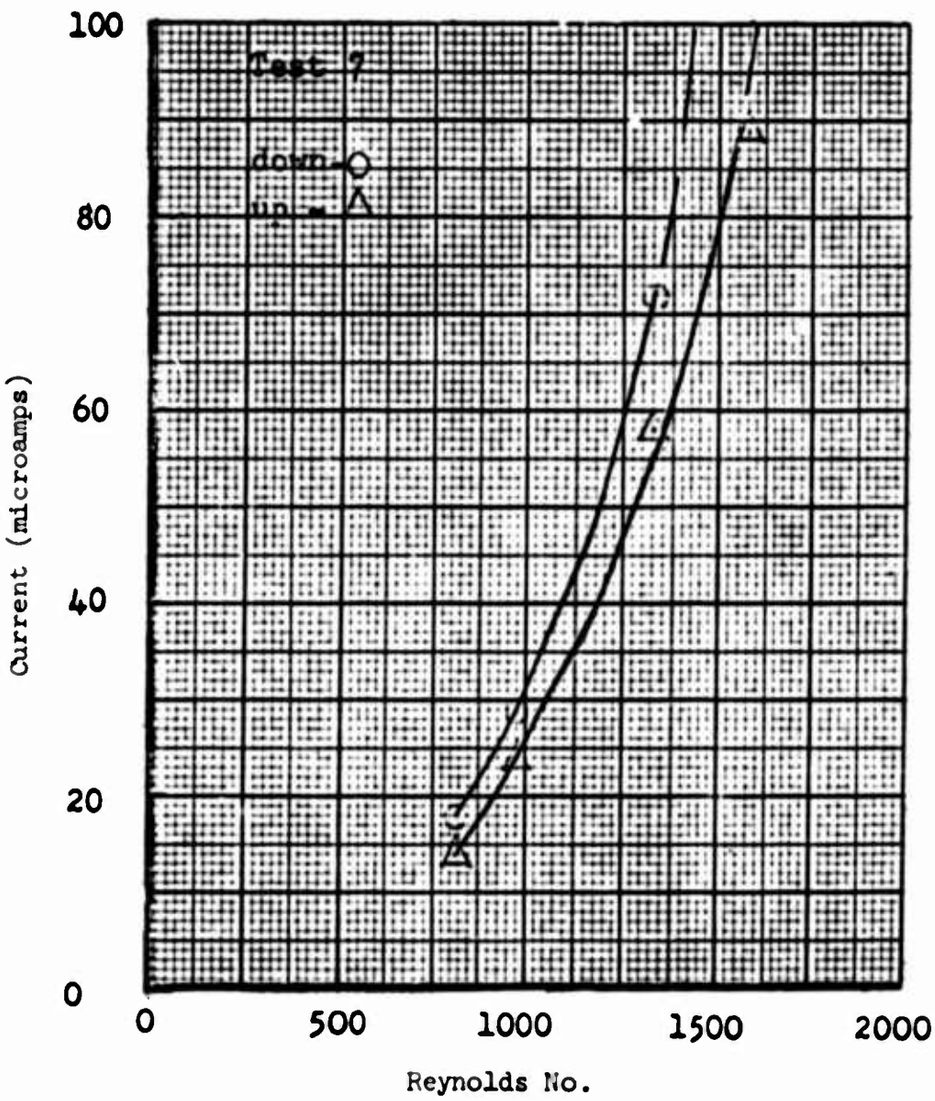

Figure 47 - Current Required to Flip Flow Both Ways at Various Reynolds Numbers. Channel Tilted Down Two Degrees

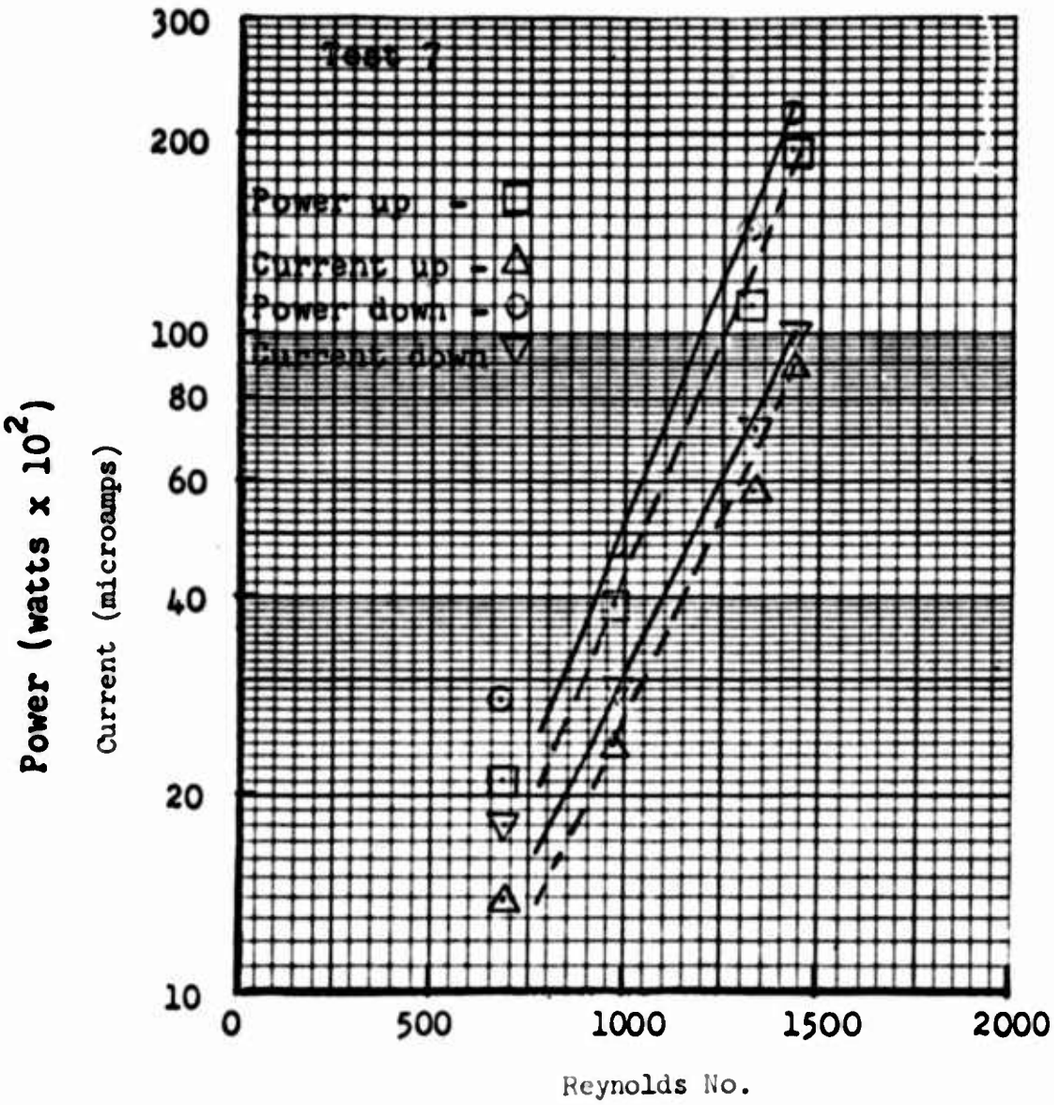

Figure 48 - Power and Current to Flip Flow Both Ways at Various Reynolds Numbers. Channel Tilted Down Two Degrees

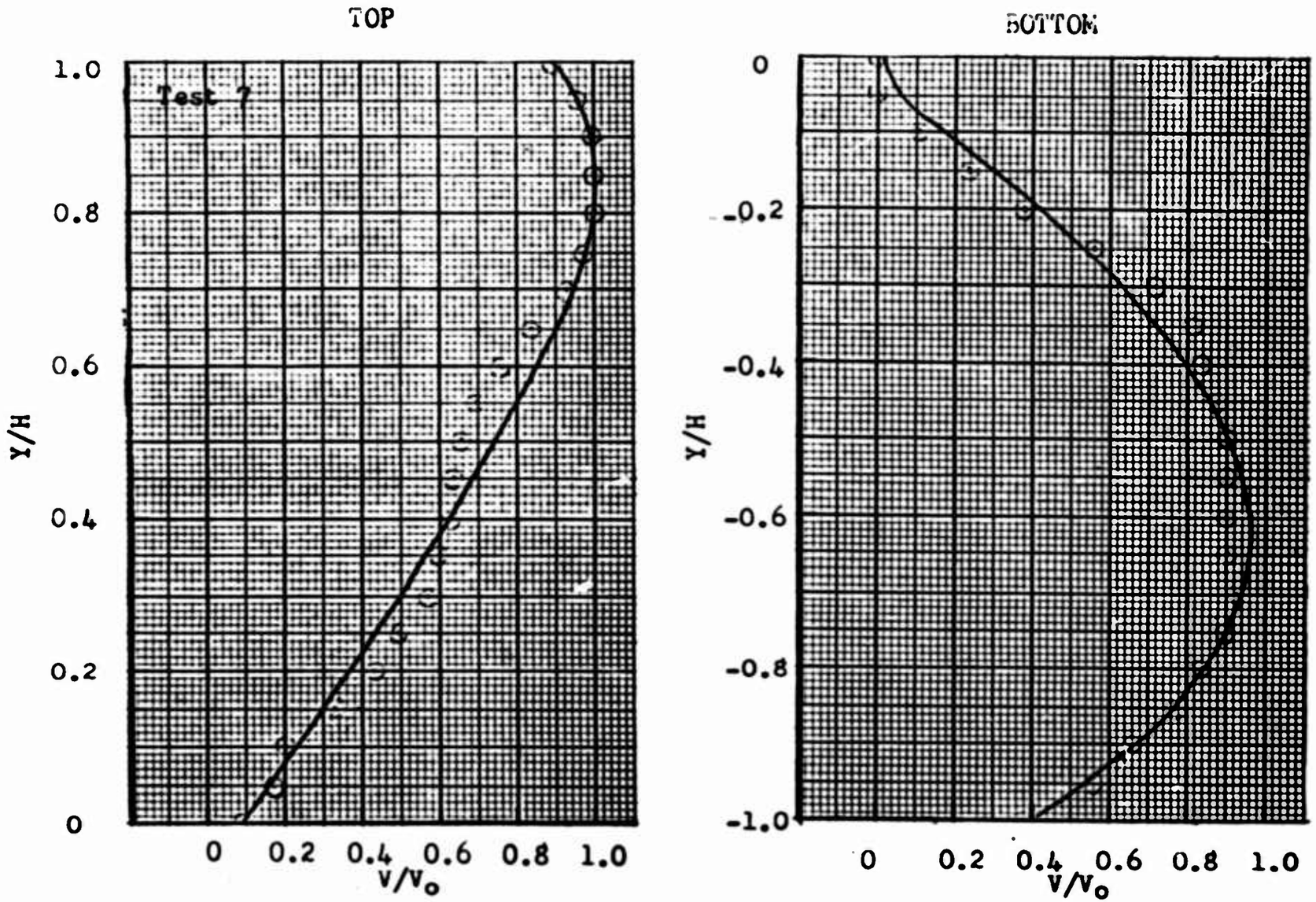

Figure 49 - Velocity Profiles before and after Flipping Both Ways. Channel Tilted Down Two Degrees

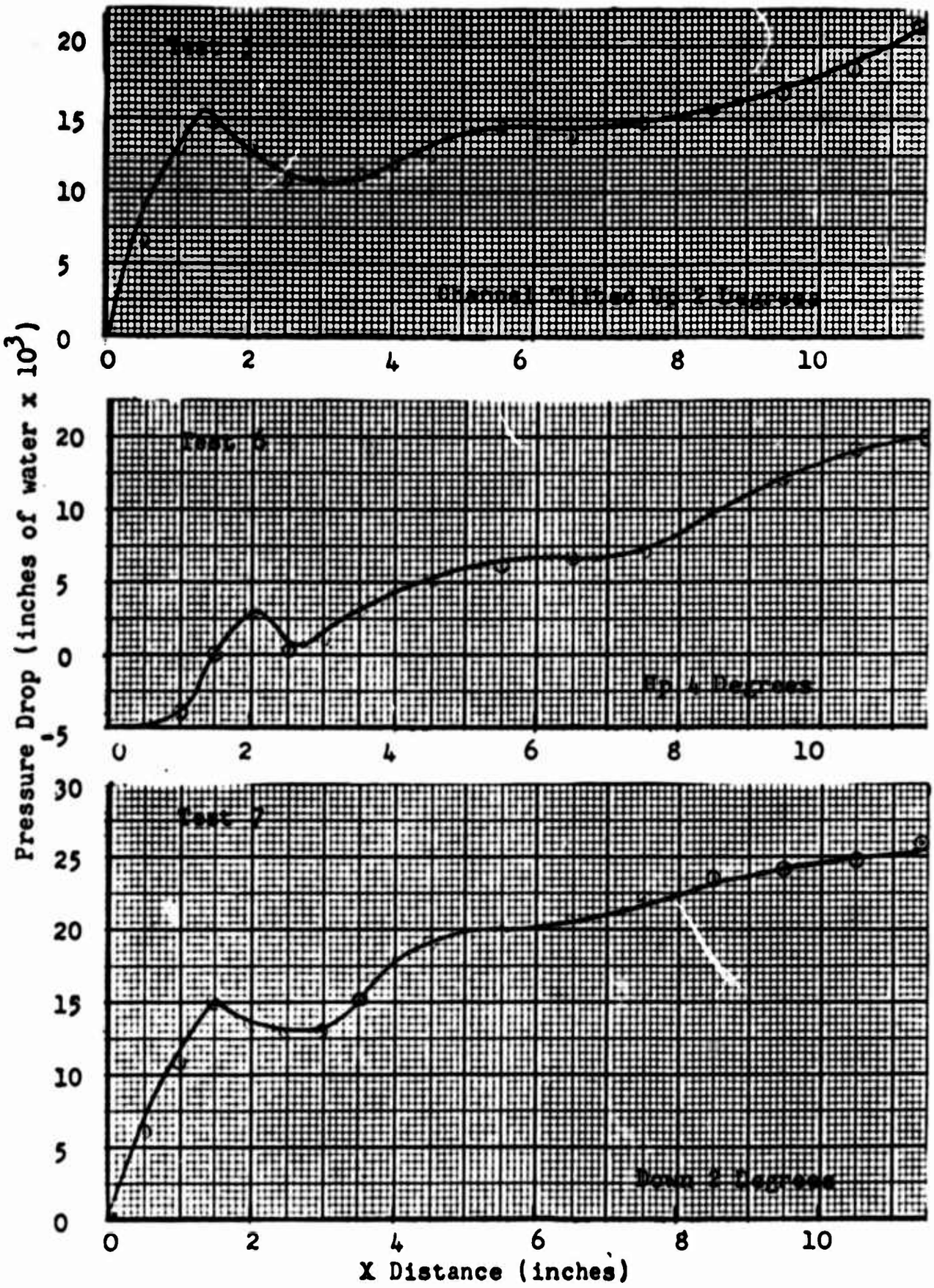

Figure 50 - Static Pressure Drop Along Bottom Plate, with Flow Attached to It

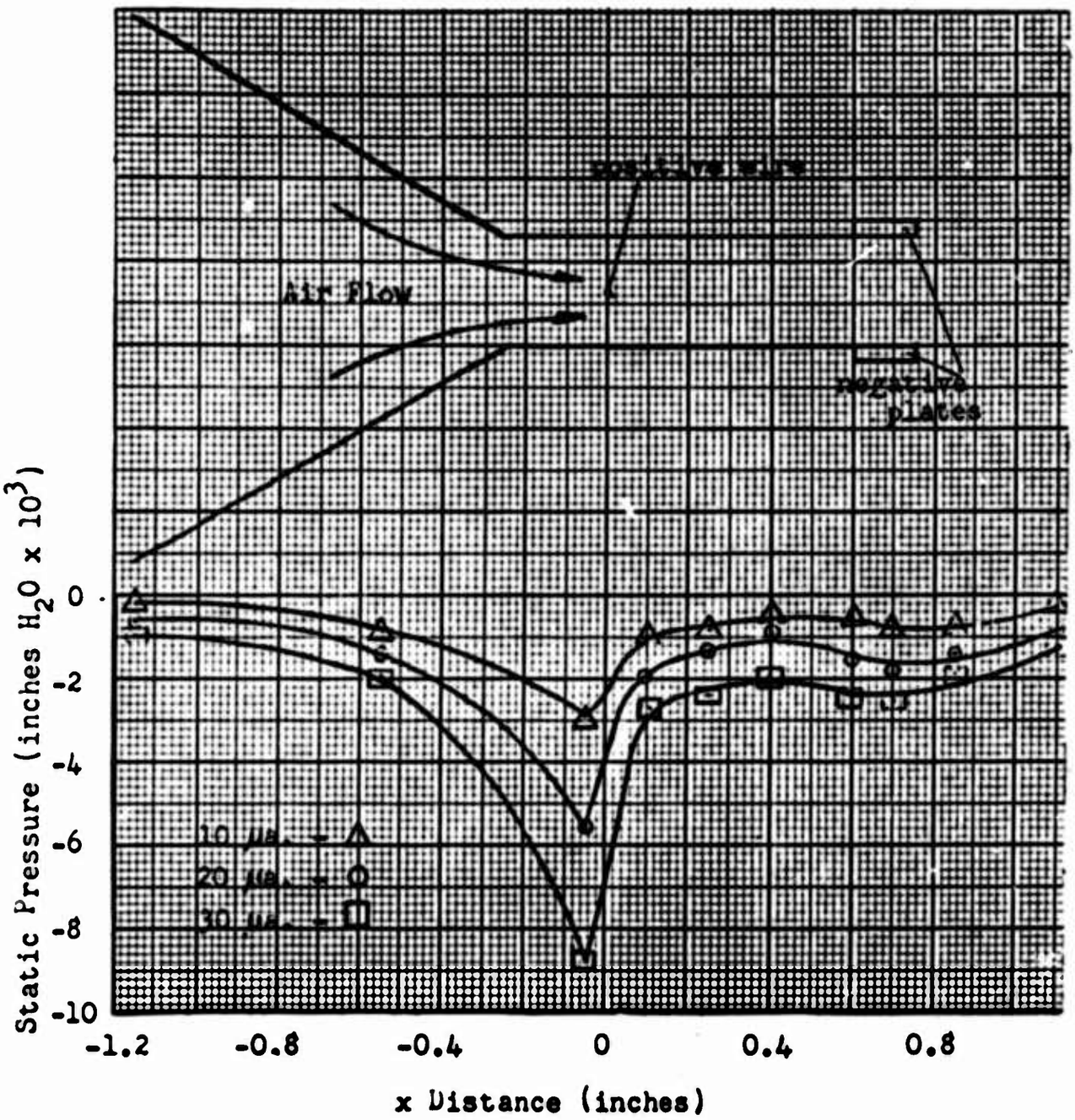

Figure 51 - Static Pressure Along Control Nozzle for Various Currents

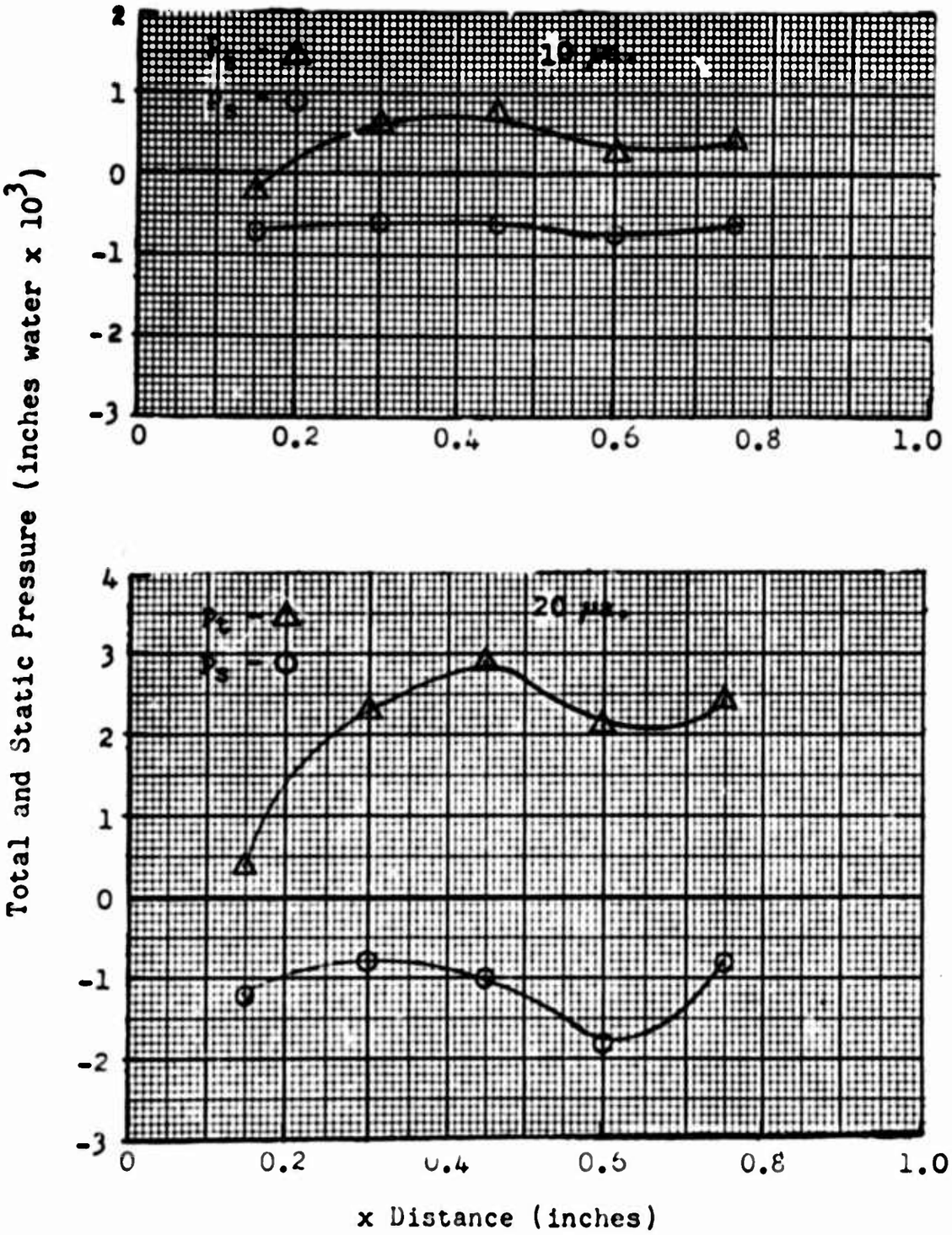

Figure 52 - Total and Static Pressure Variation along Control Nozzle for Various Currents

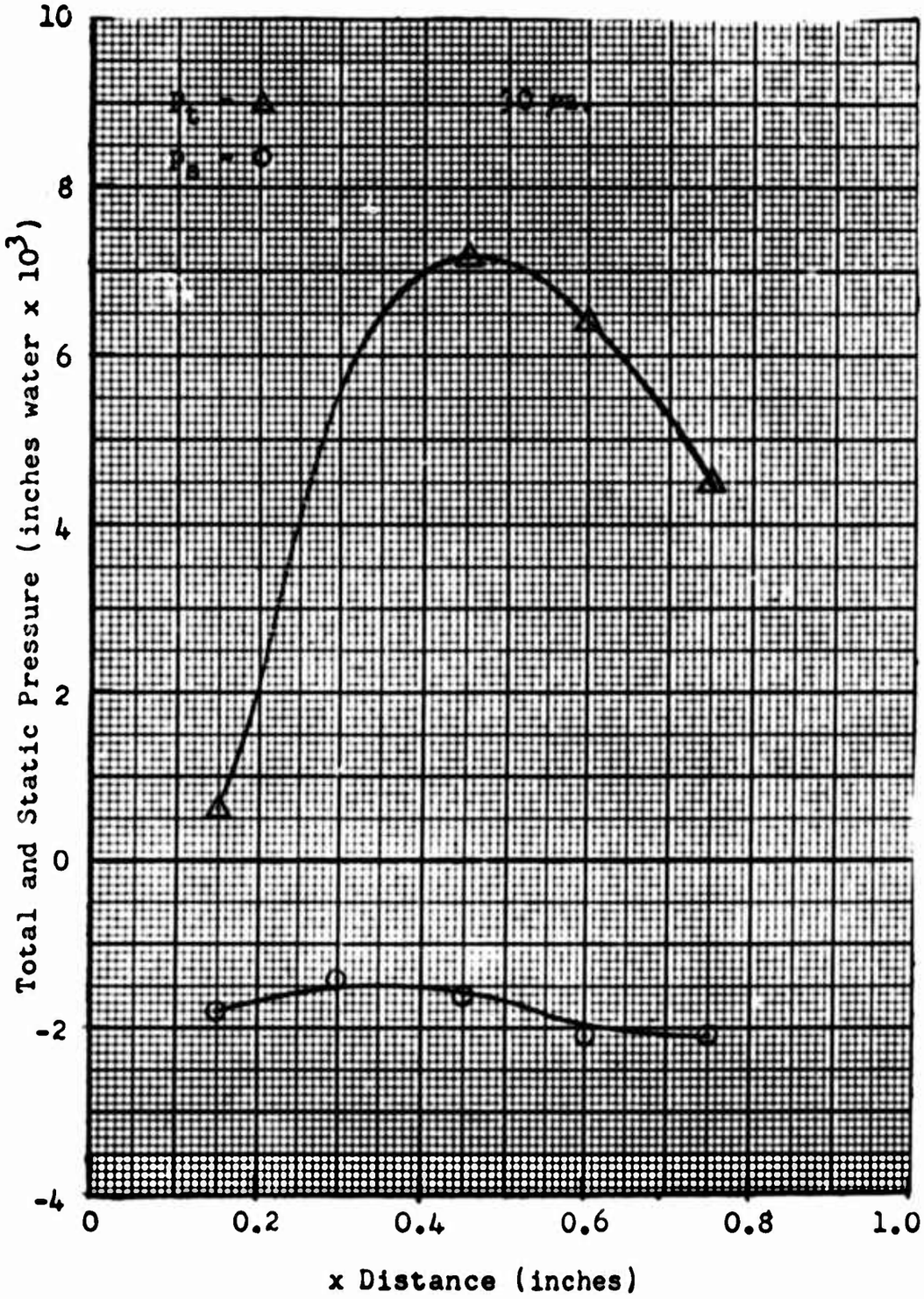

Figure 53 - Total and Static Pressure Variation Along Control Nozzle for 30 Microamps

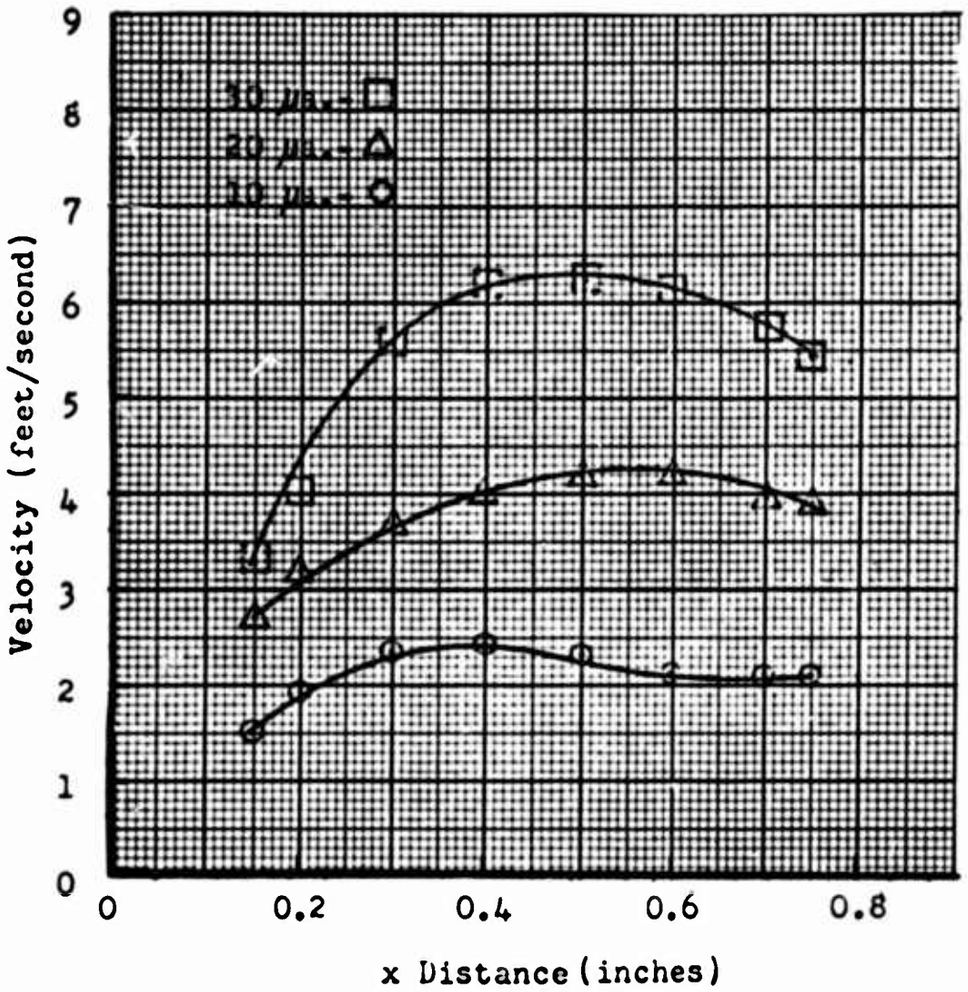

Figure 54 - Velocity Along Control Nozzle, at Various Currents

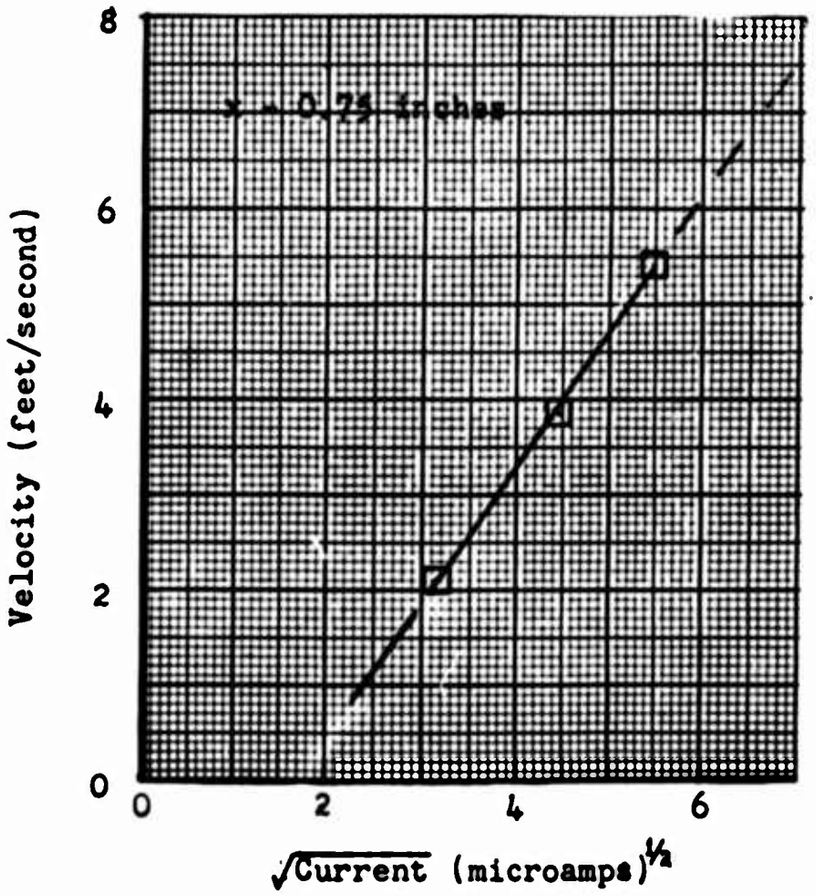

Figure 55 - Control Nozzle Exit Velocity at Various Currents

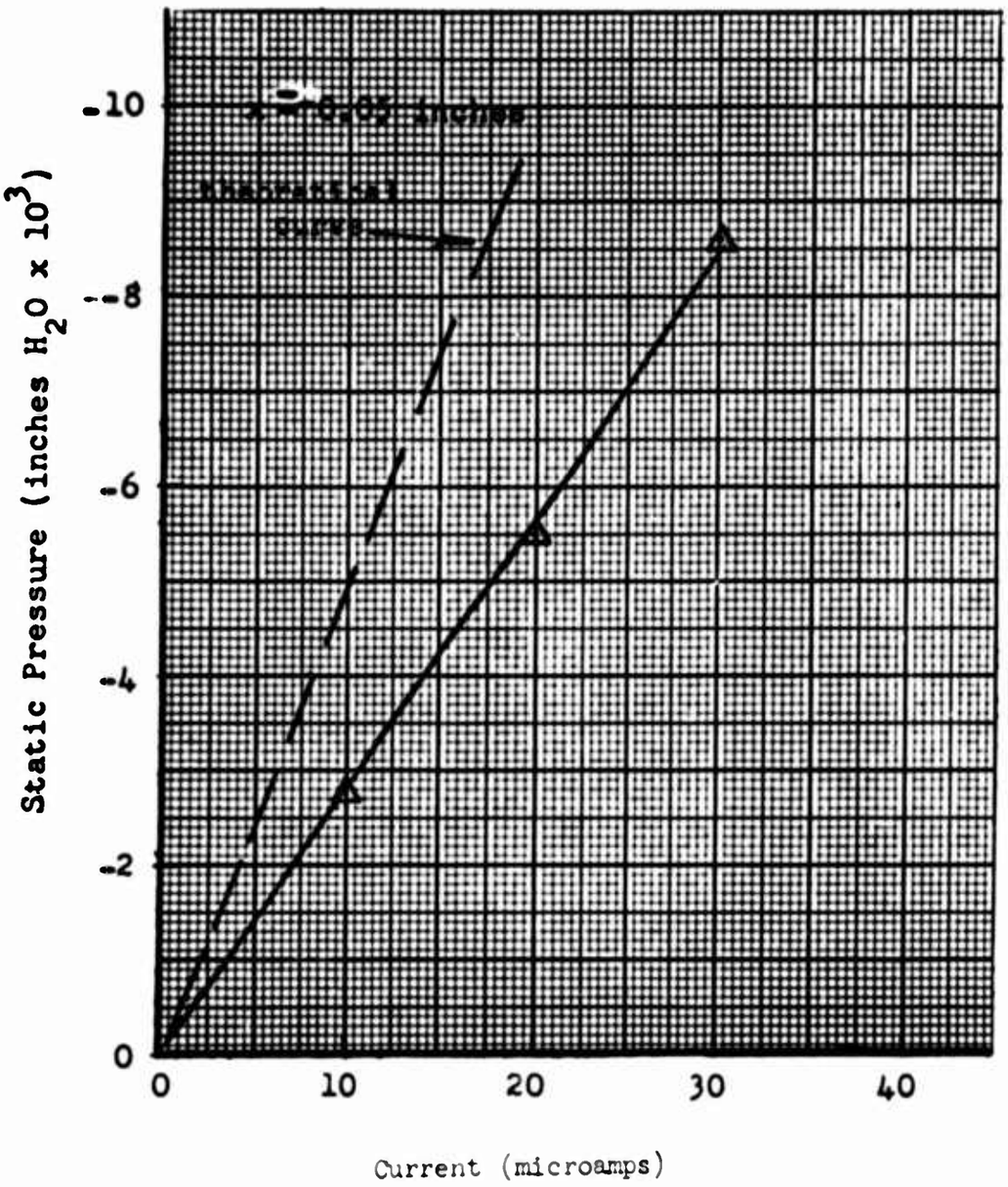

Figure 56 - Suction Developed by Corona Wind at a Point Just before Positive Wire

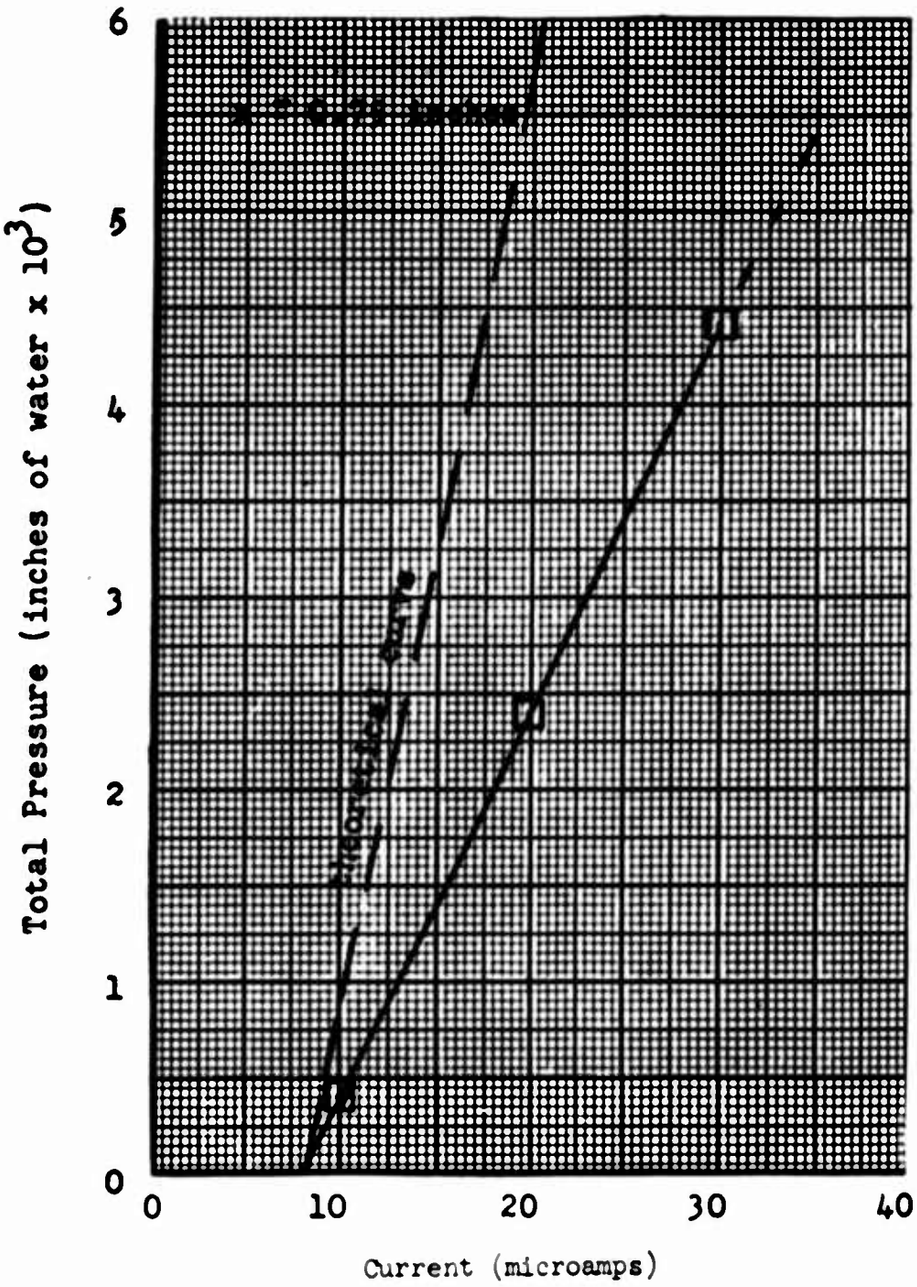

Figure 57 - Total Pressure Increase at Control Nozzle Exit at Various Currents

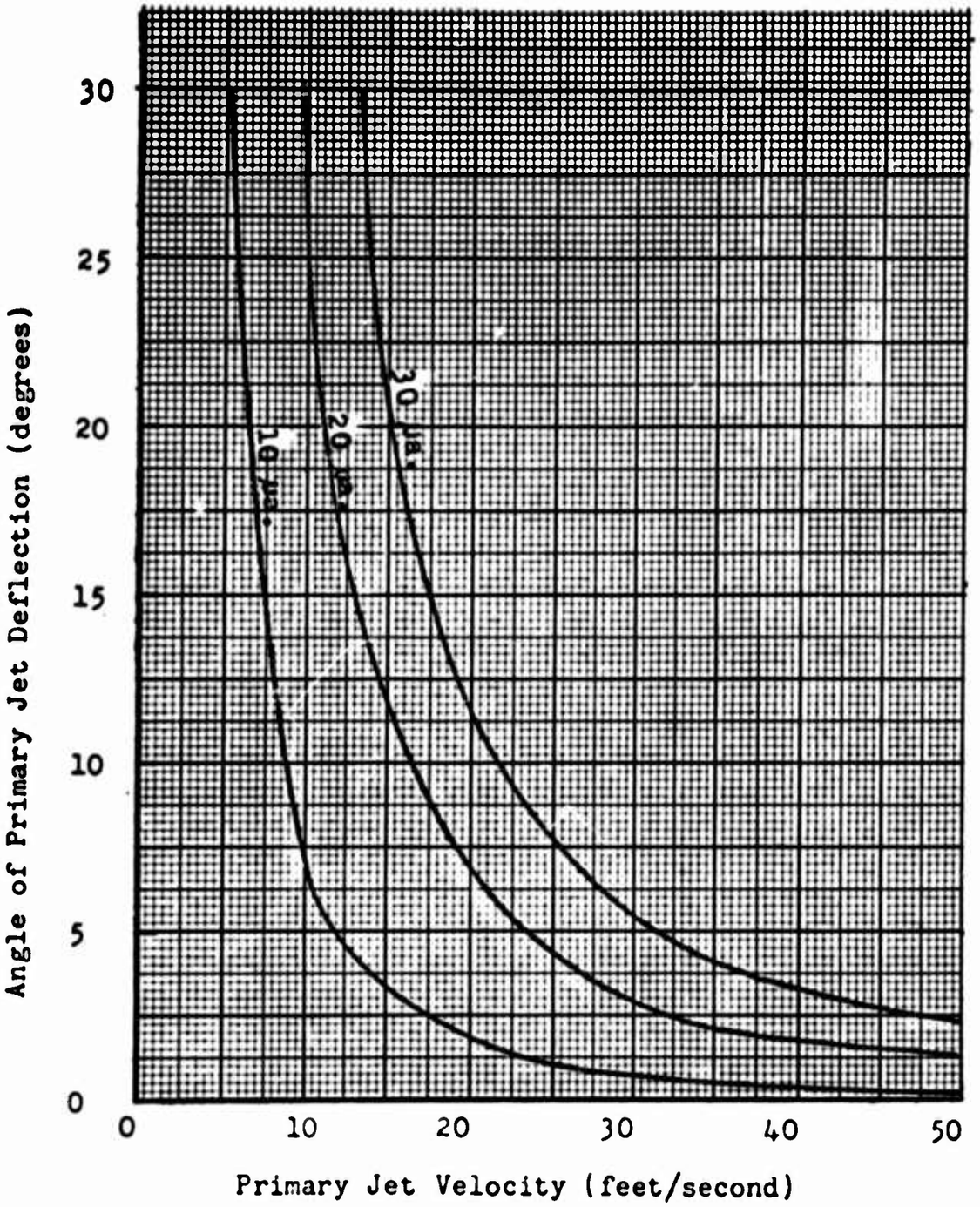

Figure 58 - Theoretical Angle of Primary Jet Deflection for Various Primary Jet Velocities and Control Jet Currents

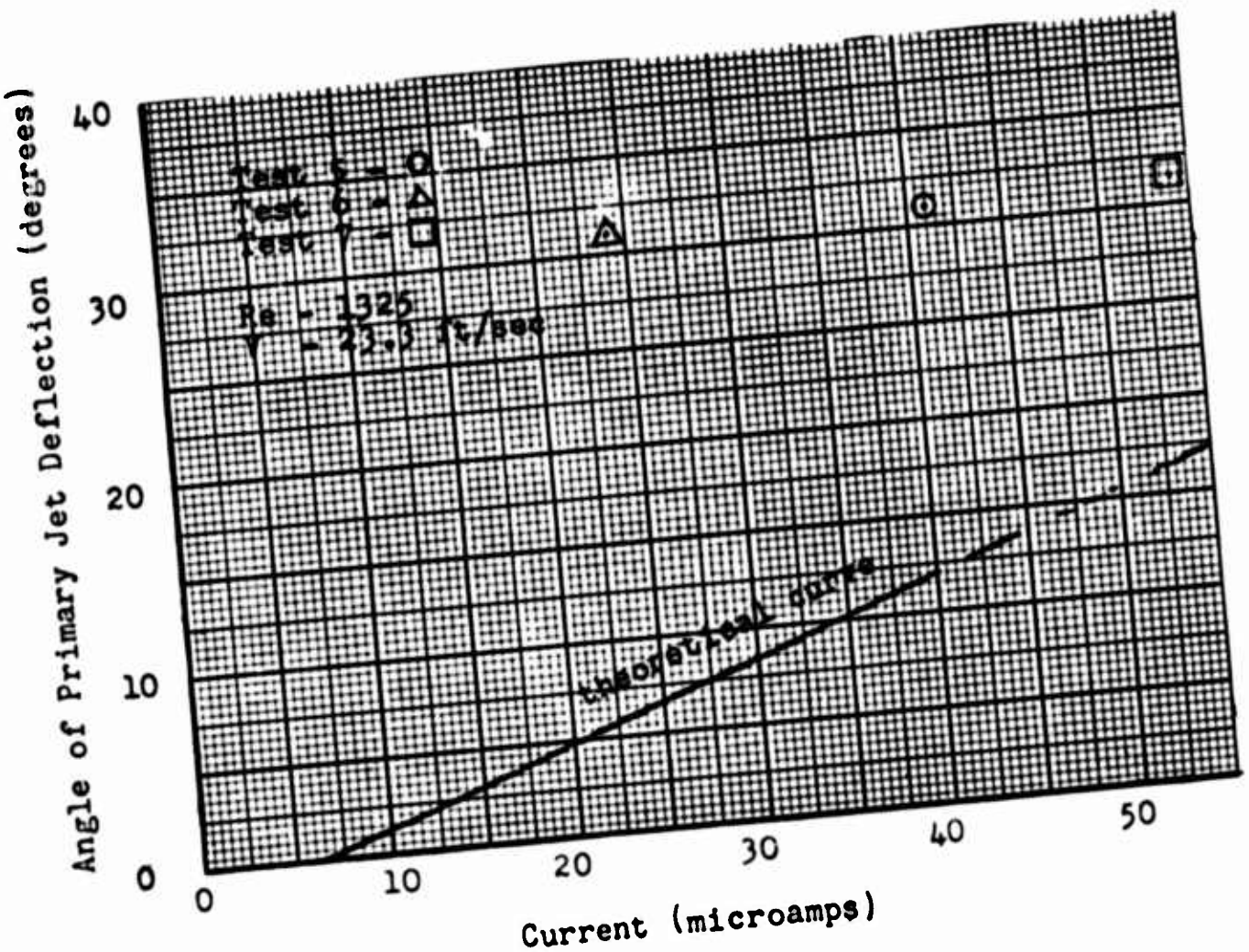

Figure 59 - Angle of Primary Jet Deflection for Various Currents at a Reynolds Number of 1325, and a Velocity of 23.3 ft/sec

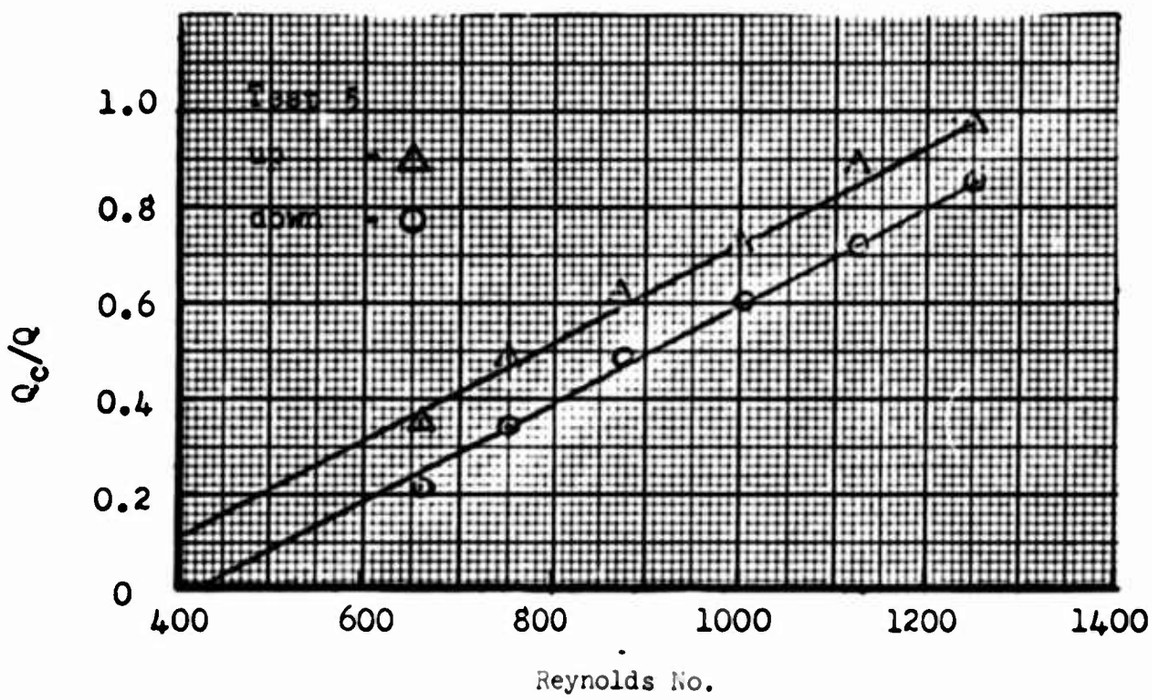

Figure 60 - Ratio of Control Jet to Primary Jet Mass Flow Rates Required to Flip Flow at Various Reynolds Numbers

Sample Calculations

Reynolds Number

From Eq. (5)

$$Re = 7710\ Kyd^2 \sqrt{\frac{hp_1}{T_1}}\ \frac{p_1 w}{RT_1 A_n \mu} \quad .$$

Making a dimensional analysis of the equation

$$q = 7710\ Kyd^2 \sqrt{\frac{hp_1}{T_1}}\ ft^3/hr \qquad \text{from Eq. (1)}$$

p_1 - $lb_f/in.^2$

w - ft

R - $lb_f\text{-}ft/lb_m\text{-}R^o$

A_n - ft^2

μ - $lb_m/sec\text{-}ft$

T_1 - R^o

$$Re = \frac{ft^3}{hr} \times \frac{lb_f}{in.^2} \times ft \times \frac{lb_m\text{-}R^o}{lb\ \text{-}ft} \times \frac{1}{R^o} \times \frac{1}{ft^2} \times \frac{ft\text{-}sec}{lb_m} \times \frac{1\ hr}{3600\ sec} \times \frac{144\ in.^2}{ft^2}$$

Re = dimensionless

The following values are known

w - 0.1095 in. = 0.0091 ft

d = 0.4375 in.

Pipe I.D. = d_p = 0.963 in.

A_n = 0.1095 x 5 in.^{2} = 0.0038 ft^2

T_1 = 530°R

R = 53.35 $lb_f\text{-}ft/lb_m\text{-}R^o$

μ at 70°F = 11.97 x 10^{-6} $lb_m/sec\text{-}ft$ (see ref. 14)

Substituting these values into the equation for Reynolds number

$$Re = \frac{144 \times 7710 \times (0.4375)^2 \times 0.0091}{3600 \times 53.35 \times 0.0038 \times 11.97 \times 10^{-6}} Ky \sqrt{h}(p_1/T_1)^{1.5}$$

$$Re = 0.222 \times 10^6 \; Ky \sqrt{h} \; (p_1/T_1)^{1.5} \quad .$$

β for orifice, Ref. 13, is equal to

$$\beta = d/\text{Pipe I.D.}$$

$$\beta = 0.4375/0.963$$

$$\beta = 0.455$$

For a pressure drop across the orifice, $h_1 = 2.5$ inches H_2O

$$p_1 = 14.7 \text{ psi} + 0.35 \text{ in. Hg}$$

$$p_1 = 14.7 \text{ psi} + 0.491 \text{ psi/in.Hg} \times 0.35 \text{ in.Hg}$$

$$p_1 = 14.7 \text{ psi} + 0.17 \text{ psi} = 14.87 \text{ psi}$$

$$h_1/p_1 = 2.5/14.87 = 0.168$$

From Ref. 13, Fig. 98, page 171, using values of h_1/p_1 and β;$Y = 0.998$.

Assuming a Reynolds number in the pipe equal to

$$Re_p = 6000$$

$K = 0.6313$ from Table 12, page 142.

$$Re = 0.222 \times 10^6 \times 0.6313 \times 0.998 \times \sqrt{2.5} \times (14.87/530)^{1.5}$$

$$Re = 1000$$

Checking the assumed Reynolds number for the pipe, Re_p

$$\text{Area pipe} = \frac{3.14 \times (0.963)^2}{4 \times 144}$$

$$= 0.00505 \text{ ft}^2$$

$$Re_p = \frac{Re\ A_n d_p}{A_p w}$$

$$Re_p = 1000 \times \frac{0.0038}{0.00505} \times \frac{0.963}{0.1095}$$

$$Re_p = 1000 \times 6.6$$

$$Re_p = 6600$$

$K_{corr.}$, Table 12 is equal to 0.6290

$$Re_{corr.} = Re \times \frac{K_{corr.}}{K}$$

$$Re_{corr.} = 1000 \times 0.6290/0.6313$$

$$Re_{corr.} \cong 1000$$

Velocity at Nozzle Outlet

$$V_n = \frac{Re\ \mu}{\rho_n w} \qquad \text{from Eq. (2)}$$

$$V_n = \frac{Re\ RT_n}{\rho_n w}$$

$$V_n \quad \frac{53.35\ lb_f\text{-}ft/lb_m\text{-}R^o \times 530^o\ R \times 11.97\ lb_m/ft\text{-}sec}{14.7\ lb\ /in.^2 \times 0.0091\ ft \times 144\ in.^2/ft^2}$$

$$V_n = (1.76 \times 10^{-2})\ Re \qquad (27)$$

For Re = 2000

$$V = (1.76 \times 10^{-2})\ 2000 = 35.2\ ft/sec \quad .$$

Channel Velocity

$$p_t - p_s = \frac{\rho V^2}{2g_c}\ , \qquad \text{from Eq. (6)}$$

For Test 3, at B = 0.50 in., Y - 0.90 in.

$$p_t = p_s = 0.0060\ in.\ H_2O$$

$$V^2 = 2(p_t - p_s)g_c/\rho$$

$$V^2 = \frac{2 \times 0.0060 \text{ in. } H_2O \times \dfrac{0.037 \text{ lb}_f}{\text{in.}^2\text{-in. } H_2O} \times \dfrac{32.2 \text{ lb}_m\text{-ft}}{\text{lb}_f\text{-sec}^2}}{\dfrac{0.075 \text{ lb}_m}{\text{ft}^3} \quad \dfrac{1 \text{ ft}^2}{144 \text{ in.}^2}}$$

$$V^2 = 0.0060 \text{ in. } H_2O \times \frac{4470 \text{ ft}^2}{\text{sec}^2\text{-in. } H_2O}$$

$$V^2 = 26.9 \text{ ft}^2/\text{sec}^2$$

$$V = 5.2 \text{ ft/sec} \quad .$$

<u>Current Required to Flip the Flow</u>

$$I - a(e)^{m \, Re} \qquad \text{from Eq. (8)}$$

$$m = \frac{\ln I_2 - \ln I_1}{Re_2 - Re_1} \qquad \text{from Eq. (10)}$$

From Fig. 48,

$$a = 1.60$$

$$I_2 = 100 \text{ microamps}$$

$$I_1 = 10 \text{ microamps}$$

$$Re_2 = 1250$$

$$Re_1 = 560$$

$$m = \frac{\ln 100 - \ln 10}{1250 - 560} \quad \frac{4.61 - 2.30}{690}$$

$$m = 0.00335$$

therefore,

$$I = 1.60 \, (e)^{0.0035 \, Re} \quad .$$

Theoretical Geometric Shape Factor, c/K_o

$$c/K_o = \frac{x_2 - x_o}{K_o \; A_c} \qquad \text{from Eqs. (21), (22)}$$

$x_2 - x_o = 0.75$ in.

$K_o = 0.216$ in.^{2}/volt-sec

$A_c = 5 \times 0.32$ in.$^2 = 1.6$ in.^{2}

$$c/K_o = \frac{0.75 \text{ in.} \times \dfrac{44.2 \text{ ft-lb}_f}{\text{min-watt}} \times \dfrac{1 \text{ min}}{60 \text{ sec}} \times \dfrac{12 \text{ in.}}{1 \text{ ft}}}{\dfrac{0.216 \text{ in.}^2}{\text{volt-sec}} \times 1.60 \text{ in.}^2 \quad \dfrac{1 \text{ amp-volt}}{1 \text{ watt}}}$$

$$c/K_o = \frac{19.0 \text{ lb}_f}{\text{in.}^2\text{-amp}}$$

Experimental Geometric Shape Factor, c/K_o

$$p = (c/K_o)I \qquad \text{from Eq. (22)}$$

From Fig. 57,

$$\text{Slope} = \frac{4 \times 10^{-3} \text{ in. } H_2O \times \dfrac{0.037 \text{ lb}_f}{\text{in.}^2\text{-in. } H_2O}}{20 \times 10^{-6} \text{ amp}}$$

$$\text{Slope} = \frac{7.40 \text{ lb}_f}{\text{in.}^2\text{-amp}} = c/K_o$$

Angle Primary Jet Deflection

$$\tan \alpha = \frac{\rho_c A_c V_c \bar{V}_c}{\rho_n \; q V_n} \qquad \text{(eq. 25)}$$

For Re = 1000

$V = (1.76 \times 10^{-5})\ Re = 17.6$ ft/sec from Eq. (27)

$q = 7710\ Kyd^2\ \frac{hp_1}{T_1}$

$K = 0.6313$

$y = 0.998$

$h = 2.50$ in. H_2O

$p_1 = 14.7$ psi + 0.35 in. Hg = 14.87 psi

$T_1 = 530^oR$

$d = 0.4373$ in.

$$q = 7710\ (0.4375)^2 \times 0.6313 \times 0.998 \times \frac{2.5 \times 14.87}{530}$$

$q = 246\ ft^3/hr$

$\rho_n = 0.075\ lb_m/ft^3$

$\rho_c = 0.075\ lb_m/ft^3$

$A_c = 5 \times 0.32\ in.^2 = 1.60\ in.^2$

V_c at I = 10 microamps, from Fig. 55

$V_c = 2.1$ ft/sec

$$\rho_c A_c = \frac{0.075\ lb_m}{ft^3} \times 1.6\ in.^2 \times \frac{1\ ft^2}{144\ in.^2} \times \frac{3600\ sec}{1\ hr}$$

$$\rho_c A_c = \frac{3.00\ lb_m\text{-sec}}{ft\text{-}hr}$$

$$\rho_c A_c V_c^2 = \frac{3.00\ lb_m\text{-sec}}{ft\text{-}hr} \times \frac{(2.1)^2\ ft^2}{sec^2} = \frac{13.2\ ft\text{-}lb_m}{sec\text{-}hr}$$

$$\rho_n q V_n = \frac{0.075\ lb_m}{ft^3} \times \frac{246\ ft^3}{hr} \times \frac{17.6\ ft}{sec} = \frac{325\ lb_m\text{-}ft}{sec\text{-}hr}$$

$$\tan \alpha = \frac{13.2}{325} = 0.0405$$

$$\alpha = 2.25^o\ .$$

Experimental Calculation of Angle of Primary Jet Deflection

Angle Channel Divergence = 5°

From Fig. 50, Test 6, channel tilted up 4°,

$$x = 0.18 \text{ inch}$$

Horizontal distance from nozzle outlet to channel inlet = 0.57 inch

Vertical distance from bottom nozzle outlet to top of bottom plate at channel inlet = 0.445 inch

$$\tan \alpha = \frac{0.445 + 0.18 \sin 1^{\circ}}{0.570 + 0.18 \cos 1^{\circ}}$$

$$\tan \alpha = 0.594$$

$$\alpha = 31.0^{\circ}$$

List of Equipment

1. High-Voltage Power Supply

   Type: D.C. Power Supply with built-in filter and transformer
   Rating: 0-30 kilovolts
   Make: Sorensen
   Model: 5030-4

2. High-Voltage Power Supply

   Type: D.C. Power Supply with external transformer and filter
   Rating: 0-50 kilovolts
   0-10 milliamps
   Make: Peschel Electronics, Inc., Patterson, N. J.
   Model: PS 50 - 10y

3. D.C. Microammeter

   Type: Px-161
   Rating: 0-200-500-1000 microamps
   Make: Westinghouse
   Model: 291874 Bal3

4. Voltmeter

Type: Electrostatic, double-pivoted moving vane
Rating: 0-10-20-30-40 kilovolts
Make: Singer Co., Bridgeport, Conn.
Model: ESH

5. Micromanometer

Make: Flow Corporation, Arlington, Mass.
Model: MM3

6. Traversing Microscope

Type: Micrometer traverse
Range: 0-4 inch travel
Make: Gartner Scientific Corporation, Chicago, Ill.
Model: 1560 P

7. Manometer

Type: Inclined
Range: 0-1 inch water
Make: Ellison Co., Chicago, Ill.

SECTION VII

REFERENCES

1. Mitral, A., "L'effect Coanda," Proceedings 5th International Congress of Applied Mechanics, 1938.

2. McMahan, K. D., "Fluidynamic Control of Fluid Flow," Proceedings 5th International Congress of Applied Mechanics, 1938.

3. Todd, K. W., "Mechanical Relay of the Fluid Jet Type," British Patent Application, May, 1940 (U.S. Patent No. 2408705, Oct., 1946).

4. Cain, D. W., "Preliminary Investigation of a Liquid Vortex Valve Having No Moving Parts," General Engineering Laboratory Report, General Electric Company.

5. Pohl, R. W., Physical Principles of Electricity and Magnetism. Van Nostrand, New York, N.Y., 1947.

6. Thompson, J. J., and Thompson, G. P., Conduction of Electricity Through Gases. 3rd Ed., Cambridge University Press, Cambridge, England, 1933.

7. Stuetzer, Otmar M., "Ion Drag Pressure Generation," Journal of Applied Physics, Vol. 30, No. 7, July, 1959, pp. 984-994.

8. Olson, R. E., "Reattachment of a Two-Dimensional Jet to an Adjacent Plate," Symposium on Fluid Jet Control Devices, ASME, 1962, pp. 23-29.

9. Cambel, Ali B., Plasma Physics and Magnetofluidmechanics, McGraw-Hill Book Company, New York, N. Y., 1963.

10. Cobine, James Dillon, Gaseous Conductors, 2nd Ed., Dover Publications, New York, New York, 1958.

11. Schlichting, Herman, Boundary Layer Theory, 4th Ed., McGraw-Hill Book Company, New York, N. Y., 1960.

12. Olsen, R. E., "Interim Report on Aerodynamic Studies of Pure Pneumatic Systems," Research Laboratories, United Aircraft Corporation, Prepared for the Diamond Ordance Fuze Laboratories, U. S. Army Contract DA-49-186-ORD-512, June 30, 1962.

13. Fluid Meters, Their Theory and Application, 5th Ed., The American Society of Mechanical Engineers, New York, N. Y., 1959.

14. Binder, Raymond C., Fluid Mechanics, 4th Ed., Prentice-Hall, Inc., Englewood Cliffs, N. J., 1962.

16. Velkoff, Henry R., "Electrofluidmechanics: A Study of Electrostatic Actions in Fluids," Technical Report No. ASD-TR-61-642, Propulsion Laboratory, Aeronautical Systems Division, Air Force Systems Command, Wright-Patterson Air Force Base, Ohio, February, 1962.

17. Velkoff, Henry R., "Electrofluidmechanics: Investigation of the Effects of Electrostatic Fields on the Heat Transfer and Boundary Layers," Technical Documentary No. ASD-TRD-62-650, Propulsion Laboratory, Aeronautical Systems Division, Air Force Systems Command, Wright-Patterson Air Force Base, Ohio, September, 1962.

18. Velkoff, Henry R., "Exploratory Study of the Influence of Electrostatic Fields on Flow Attachment," Proposal for Engineering Research as Submitted to The National Science Foundation by the Department of Mechanical Engineering, The Ohio State University, Columbus, Ohio, March, 1964.

Unclassified
Security Classification

DOCUMENT CONTROL DATA - R&D

(Security classification of title, body of abstract and indexing annotation must be entered when the overall report is classified)

1. ORIGINATING ACTIVITY (Corporate author)
The Ohio State University Research Foundation

2a. REPORT SECURITY CLASSIFICATION
Unclassified

2b. GROUP
NA

3. REPORT TITLE
AN EXPERIMENTAL INVESTIGATION OF THE INFLUENCE OF ELECTROSTATIC FIELDS ON FLOW ATTACHMENT

4. DESCRIPTIVE NOTES (Type of report and inclusive dates)
Technical Report - 15 August 1966

5. AUTHOR(S) (Last name, first name, initial)
Eiler, Gary P.

6. REPORT DATE
15 August 1966

7a. TOTAL NO. OF PAGES
98

7b. NO. OF REFS
18

8a. CONTRACT OR GRANT NO.
DA-31-124-ARO-D-246

b. PROJECT NO.
20014501B33G

c.

d.

9a. ORIGINATOR'S REPORT NUMBER(S)
RF Project 1864

9b. OTHER REPORT NO(S) (Any other numbers that may be assigned this report)
4942.1

10. AVAILABILITY/LIMITATION NOTICES
Distribution of this document is unlimited.

The findings in this report are not to be construed as an official Department of the Army position, unless so designated by other authorized documents.

11. SUPPLEMENTARY NOTES
None

12. SPONSORING MILITARY ACTIVITY
U. S. Army Research Office-Durham
Box CM, Duke Station
Durham, North Carolina 27706

13. ABSTRACT
An experimental investigation was conducted to determine whether an electrostatic field could be used to affect the attachment of an air stream to a flat surface. Tests were run using a fluid-amplifier type device in which corona wind was fed through the control ports of the device. It was found that the fluid stream could be made to detach from one wall, flip over to the opposite wall, and attach to that wall. The air stream could then be flipped back to the original wall by activating the opposite corona wind control port. Pressure distribution and velocity profile data were taken which indicated that by suitable design symmetric flip-flop of the fluid stream in the device could be achieved.

Key Words

Flow Attachment
Corona Wind Effects
Electrostatic Field Effects (flow)

DD FORM 1 JAN 64 1473

Unclassified
Security Classification